



HAL
open science

Acoustic wave propagation through a random dispersion of solid particles in a viscous fluid

Mb Mahbub Alam

► **To cite this version:**

Mb Mahbub Alam. Acoustic wave propagation through a random dispersion of solid particles in a viscous fluid. Acoustics [physics.class-ph]. Normandie Université, 2019. English. NNT : 2019NORMLH15 . tel-02312962

HAL Id: tel-02312962

<https://theses.hal.science/tel-02312962>

Submitted on 11 Oct 2019

HAL is a multi-disciplinary open access archive for the deposit and dissemination of scientific research documents, whether they are published or not. The documents may come from teaching and research institutions in France or abroad, or from public or private research centers.

L'archive ouverte pluridisciplinaire **HAL**, est destinée au dépôt et à la diffusion de documents scientifiques de niveau recherche, publiés ou non, émanant des établissements d'enseignement et de recherche français ou étrangers, des laboratoires publics ou privés.



Normandie Université

THESE

Pour obtenir le diplôme de doctorat

Spécialité Acoustique

Préparée au sein de l'Université du Havre

Acoustic wave propagation through a random dispersion of solid particles
in a viscous fluid

**Présentée et soutenue par
Md-Mahbub ALAM**

**Thèse soutenue publiquement le 12/09/2019
devant le jury composé de**

M. Thomas BRUNET	MC HDR – Université de Bordeaux	Rapporteur
M. Guy FEUILLARD	PU – INSA Centre Val de Loire	Rapporteur
Mme. Francine LUPPE	PU – Université du Havre	Directrice de thèse
M. Pierre MARECHAL	MC HDR – Université du Havre	Encadrant de thèse
Mrs Valerie J. PINFIELD	Reader – Loughborough University, UK	Codirectrice de thèse
M. Arnaud TOURIN	PU – ESPCI Paris	Examineur
M. Tony VALIER-BRASIER	MC – Université Pierre et Marie Curie, Paris 6	Examineur
M. Jérôme VASSEUR	PU – Université de Lille	Président du jury

**Thèse dirigée par Francine LUPPE, Pierre MARECHAL, laboratoire LOMC
et Valerie J. PINFIELD, Loughborough University, UK**



RESUME ETENDU EN FRANÇAIS

On considère dans ce travail une distribution aléatoire uniforme de particules solides, toutes identiques, immergées dans un liquide visqueux. On s'intéresse aux propriétés effectives de ce milieu pour une onde acoustique ultrasonore, c'est-à-dire aux propriétés d'un fluide fictif équivalent, dit fluide effectif, homogène, dans lequel une onde ultrasonore se propagerait avec les mêmes caractéristiques que celles de l'onde de compression « moyenne » (au sens statistique, en supposant une densité de probabilité de présence uniforme des particules au sein du fluide hôte) dans le milieu hétérogène réel. L'onde de compression moyenne ainsi définie, est dite onde cohérente de compression, et son nombre d'onde est le nombre d'onde effectif de compression. Enfin, et bien que l'onde incidente soit de compression, la nature visqueuse du fluide hôte et la présence des particules rend également possible la propagation d'une onde transverse « moyenne », dite onde transverse cohérente. Décrire le fluide effectif consiste donc à déterminer, soit les nombres d'onde effectifs et la masse volumique effective de ce fluide, soit sa masse volumique effective et ses modules de compression et de cisaillement effectifs, et à en déduire des coefficients effectifs de viscosité.

Bien que tous les modèles permettant d'aboutir à une expression analytique des propriétés effectives aient comme point de départ les équations exactes de la diffusion multiple, le terme de « modèle de type MST (Multiple Scattering Theory) » est employé ici pour des modèles tels que ceux des Refs. [1-5], et celui de « modèle auto-consistant » pour ceux issus de la Coherent Potential Approximation tels que ceux des Refs. [6-8]. Les premiers sont basés sur une hypothèse de faible concentration et permettent d'obtenir les nombres d'onde effectifs sous la forme de développement de Taylor, en puissance de la concentration. Dans les seconds, l'hypothèse « basse concentration » est remplacée par une hypothèse « basse fréquence ». Une présentation plus détaillée et plus complète de ces différents types de modèles, et de quelques autres, est présentée dans le chapitre 1.

Le chapitre 2 de ce manuscrit concerne l'étude des coefficients de diffusion d'une particule sphérique élastique dans un fluide visqueux. Pour une onde partielle incidente de mode n et de polarisation p ($p = C$ pour les ondes de compression, $p = S$ pour les

ondes de cisaillement dans le plan (r, θ)), associée au potentiel de déplacement $j_n(k_p r) P_n(\cos \theta) e^{im\varphi}$ en coordonnées sphériques (r, θ, φ) centrées sur le centre de la particule, et une onde diffusée de polarisation q ($q = C, S$) associée au potentiel $T_n^{(pq)} h_n^{(1)}(k_q r) P_n(\cos \theta) e^{im\varphi}$, des expressions approchées des coefficients de diffusion T_n^{pq} sont obtenues sous l'hypothèse de grandes longueurs d'onde devant le rayon a de la particule, à l'exception de la longueur d'onde transverse dans le fluide. Pour les modes $n = 0$ et $n = 1$, ces expressions sont similaires à celles déjà publiées respectivement dans la Ref. [9] et dans les Refs. [10,11] :

$$T_0^{cc} = i \frac{(B - B')(k_c a)^3}{4\mu + 3B'}$$

avec B et B' les modules d'élasticité volumiques respectifs du fluide extérieur et de la particule, $\mu = -i\omega\eta$, et η le coefficient de viscosité de cisaillement,

$$\begin{aligned} T_1^{cc} &= \frac{i\beta_h}{3Y} (\hat{\rho} - 1) (k_c a)^3 \\ T_1^{cs} &= -\frac{(k_c a)}{Y} (\hat{\rho} - 1) \\ T_1^{sc} &= -2 \frac{(\hat{\rho} - 1)}{(k_s a) Y} (k_c a)^2 \\ T_1^{ss} &= -\frac{[3\beta_{ja} + 2(\hat{\rho} - 1)\gamma_{ja}]}{Y} \end{aligned} ,$$

avec $\hat{\rho}$ le rapport des masses volumiques particule / fluide extérieur,

$$Y = 3\beta_{ha} + 2(\hat{\rho} - 1)\gamma_{ha}$$

Et

$$\begin{aligned} \beta_{ze} &= k_s a z_1'(k_s e) - z_1(k_s e) = -k_s e z_0(k_s e) \\ \gamma_{ze} &= k_s a z_1'(k_s e) + 2z_1(k_s e) = k_s e z_2(k_s e) \end{aligned} ,$$

z_n étant soit une fonction de Bessel j_n , soit une fonction de Hankel de première espèce $h_n = h_n^{(1)}$, $e = a$ dans les expressions précédentes des coefficients de diffusion et $e = b$ dans l'expression de la masse volumique effective donnée page v.

Pour $n > 1$:

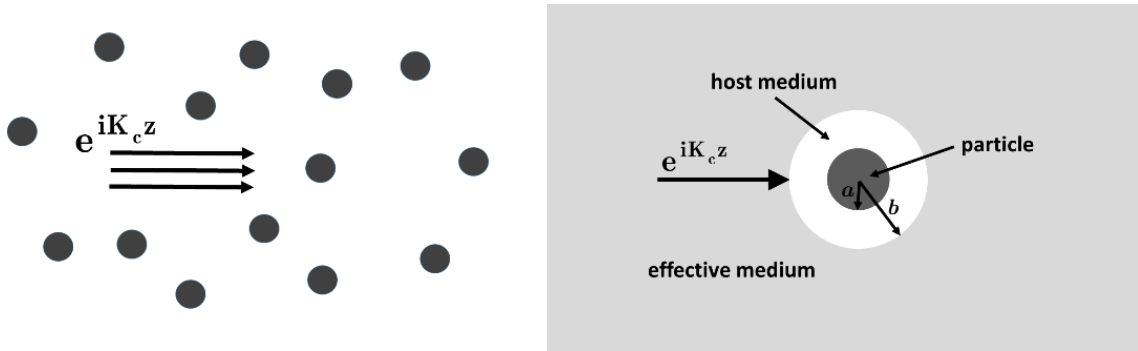
$$\begin{aligned} T_n^{cc} &= -i \frac{n}{(n+1)(1+2n)!!(2n-1)!!} \frac{-i + y_s^2 h_n(y_s) j_{n+1}(y_s)}{i + y_s^2 h_n(y_s) j_{n-1}(y_s)} (k_c a)^{2n+1} \\ T_n^{cs} &= -\frac{y_s}{(n+1)(2n-1)!!} \frac{j_n(y_s)}{i + y_s^2 h_n(y_s) j_{n-1}(y_s)} (k_c a)^n \\ T_n^{sc} &= -\frac{n}{(2n-1)!!} \frac{j_n(y_s)}{i + y_s^2 h_n(y_s) j_{n-1}(y_s)} (k_c a)^{n+1} \\ T_n^{ss} &= -\frac{y_s^2 j_n(y_s) j_{n-1}(y_s)}{i + y_s^2 h_n(y_s) j_{n-1}(y_s)} \end{aligned}$$

Ainsi, pour une onde incidente de compression, le coefficient de diffusion en onde transverse S du mode $n = 2$ est-il d'un ordre de grandeur équivalent à celui du coefficient de diffusion en onde C des modes $n = 0$ et $n = 1$, comme cela avait déjà été constaté numériquement au cours du travail de la Ref. [12] effectué au tout début de cette thèse. Nous avons choisi de ne pas présenter ici la Ref. [12] car un autre modèle [5] que celui utilisé dans le reste du manuscrit et, limité dans tous les cas à de faibles concentrations, y était utilisé, d'une façon différente de celle présentée dans la Ref. [13], ce qui pose des questions pour le moment encore sans réponse.

Les expressions obtenues pour $n > 1$ montrent que les coefficients de diffusion ne dépendent du rapport des masses volumiques des milieux solide et fluide que pour les modes monopolaire $n = 0$ et dipolaire $n = 1$, raison pour laquelle seuls ces deux modes ont été utilisés par la suite pour la détermination de la masse volumique effective.

Le chapitre 3, qui a fait l'objet de la Ref. [14], présente le modèle auto-consistant utilisé [8] pour déterminer la masse volumique effective, ainsi que l'étude de cette dernière.

Le milieu hétérogène, constitué de la concentration c de particules sphériques élastiques de rayon a dans un fluide visqueux, est modélisé par un noyau sphérique de même matériau que les particules et de même rayon, entourées d'une coque sphérique du fluide hôte, le tout immergé dans un autre fluide visqueux, comme représenté sur la figure suivante.



Le rayon b de la couche de fluide intérieure est lié au rayon a des particules et à leur concentration c par la relation :

$$\frac{a^3}{b^3} = c ,$$

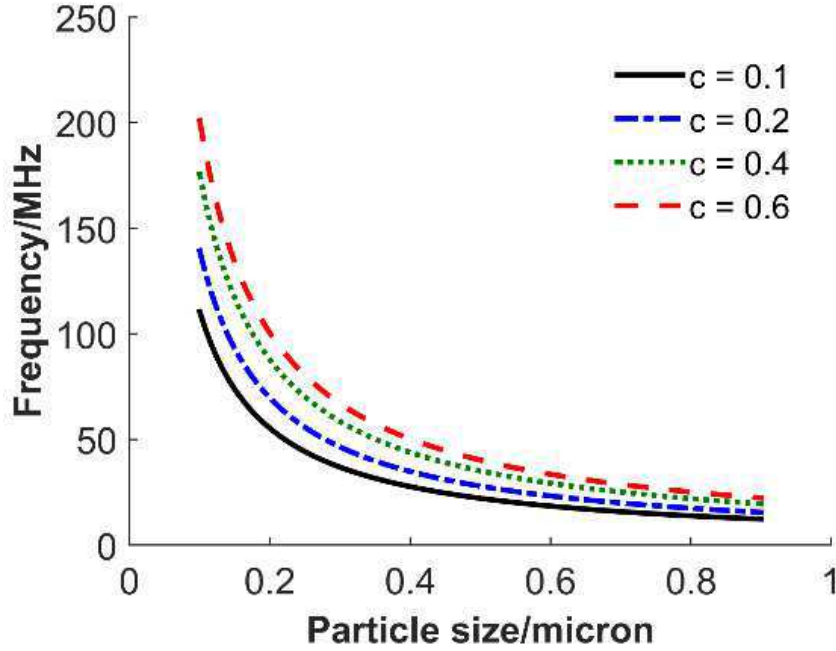
et le fluide extérieur est considéré comme le fluide effectif quand la diffusion de l'ensemble noyau-coque, dans le cas d'une onde plane de compression incidente, est minimale.

Dans le but d'obtenir des expressions analytiques des propriétés effectives, l'hypothèse de grandes longueurs d'onde est de nouveau faite, cette fois-ci par rapport au rayon b , et, de nouveau, en excluant toute hypothèse quant aux longueurs d'onde de cisaillement dans chacun des fluides. Ceci conduit à définir la fréquence f maximale de validité du modèle, considérant une valeur maximale de $|k_c b|$ (petite devant l'unité) par :

$$af < |k_c b|_{\max} \frac{v}{2\pi} c^{1/3} ,$$

où v est la vitesse de phase adiabatique des ondes de compression dans le fluide hôte intérieur.

Pour des particules de silice dans l'eau, la figure suivante présente ainsi l'évolution de cette fréquence maximale en fonction de a , pour différentes valeurs de concentration.



L'annulation des premières ondes partielles diffusées, correspondant aux modes $n = 0$ et $n = 1$, sous ces hypothèses, conduit à l'obtention du module d'élasticité volumique effectif,

$$B_{\text{eff}} = \frac{B(k_c b)^3 + 4i\mu T_0^{\text{cc}}}{(k_c b)^3 - 3iT_0^{\text{cc}}},$$

et du rapport de la masse volumique effective sur celle du fluide hôte,

$$\frac{\rho_{\text{eff}}}{\rho} = 1 + 9i \frac{\delta}{\chi},$$

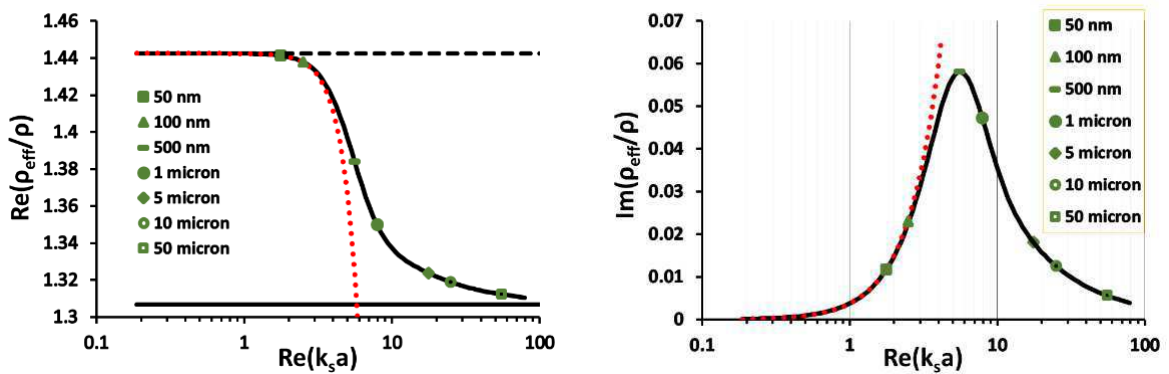
Avec

$$\begin{aligned} \delta &= (-T_1^{\text{cc}} T_1^{\text{ss}} + T_1^{\text{sc}} T_1^{\text{cs}}) \beta_{\text{hb}} - T_1^{\text{cc}} \beta_{\text{jb}} \\ \chi &= (k_c b)^3 \beta_{\text{jb}} - 3i(k_c b) T_1^{\text{sc}} + (k_c b)^3 T_1^{\text{ss}} \beta_{\text{hb}} \\ &\quad - 6i(-T_1^{\text{cc}} T_1^{\text{ss}} + T_1^{\text{sc}} T_1^{\text{cs}}) \gamma_{\text{hb}} + 6iT_1^{\text{cc}} \gamma_{\text{jb}} - 6i \frac{(k_c b)^2}{(k_s b)} T_1^{\text{cs}} \end{aligned}$$

Le développement limité du rapport entre la masse volumique effective et celle du milieu hôte, autour de $k_s a = 0$ et jusqu'à l'ordre 4 en $k_s a$, permet de vérifier que le terme dominant (ordre 0 en $k_s a$) de la masse volumique effective, quand le milieu hôte se rapproche d'un milieu élastique, est bien la moyenne volumique des masses volumiques respectives des particules et du milieu hôte. A l'opposé, pour des valeurs élevées de $|k_s a|$, correspondant à un milieu hôte se rapprochant d'un fluide idéal, la masse volumique effective se rapproche bien de son expression pour un fluide hôte de viscosité nulle,

$$\frac{\rho_{\text{eff}}}{\rho} = \frac{(\rho + 2\rho') + c(\rho' - \rho)}{(\rho + 2\rho') - 2c(\rho' - \rho)}.$$

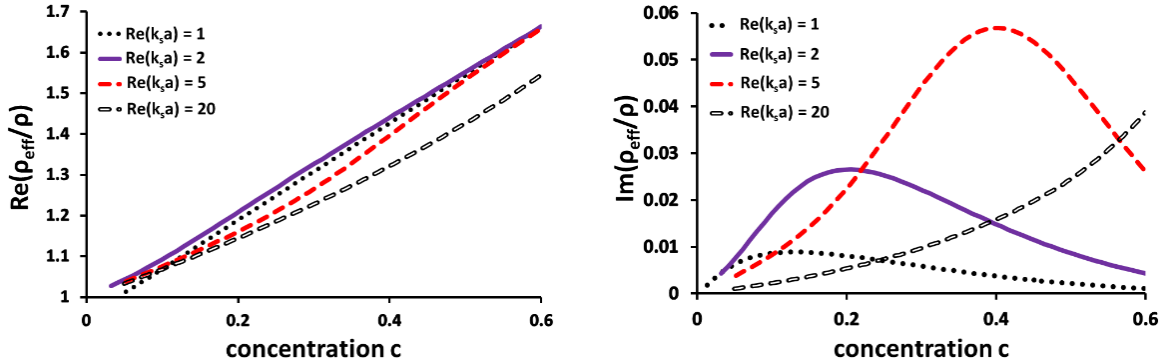
Entre ces deux extrêmes, la masse volumique effective évolue, avec $k_s a$, comme le montre la figure suivante, dans le cas de particules de silice dans l'eau.



Dans cette figure, les lignes horizontales hachurée et continue représentent les limites pour un milieu hôte respectivement élastique et fluide idéal, et les lignes rouges au développement de Taylor autour de $k_s a = 0$. Les points verts, quant à eux, représentent le rayon a minimal de particules de silice, dans l'eau et avec une concentration $c = 0,4$, compatible avec les hypothèses effectuées, c'est à dire une valeur donnée maximale (petite devant l'unité) de $|k_c b|$:

$$a_{\max} = 2 \frac{(\Re(k_s a))^2 |k_c|}{|k_c b|_{\max} |k_s^2|} c^{-1/3} .$$

Cette figure met en évidence une « fréquence de résonance », pour $\Re(k_s a) \simeq 5$, et la figure suivante montre l'augmentation de cette fréquence de résonance avec la concentration, de façon similaire à celle observée [10] auparavant sur les courbes d'atténuation et de vitesse de l'onde de compression effective.



Le chapitre 4 porte encore sur la masse volumique effective, cette fois-ci pour des sphéroïdes rigides alignés, de rayons polaire a_p et équatorial a_{eq} , d'ellipticité e_{ll} , avec

$$e_{\text{ll}} = \sqrt{1 - \frac{\min^2(a_p, a_{\text{eq}})}{\max^2(a_p, a_{\text{eq}})}} ,$$

sous l'hypothèse de faible ellipticité ou de grande longueur d'onde transverse,

$$\left| k_s (a_p^2 - a_{\text{eq}}^2)^{1/2} \right| \ll 1 .$$

La modélisation adoptée est celle développée par Ament [15] pour des sphères. Elle est basée sur l'écriture de l'équilibre entre forces inertielle et hydrodynamiques au niveau d'une particule solide, supposée soumise à des déplacements harmoniques de translation dus à une onde plane incidente de compression. Sous l'hypothèse d'écoulement incompressible, la vitesse des particules du fluide effectif y est supposée égale à la moyenne volumique des vitesses respectives des particules de fluide et de solide, et la masse volumique effective est obtenue en considérant que la quantité de mouvement effective, est, elle aussi, égale à la moyenne volumique des quantités de mouvement du fluide hôte et des particules solides. Bien qu'une étude plus récente [11] prenne en

compte la nature compressible de l'écoulement dû à l'onde acoustique, et que les particules y soient supposées rigides, le modèle d'Ament conduit, comme vu au chapitre précédent, à une expression correcte de la masse volumique effective dans le cas d'un fluide hôte non visqueux, et c'est, conjuguée à sa plus grande simplicité que celui de la Ref. [11], la raison pour laquelle il est utilisé dans ce dernier chapitre. Il est donc présenté, dans un premier temps, dans le cas de particules sphériques, afin de ré-établir la masse volumique effective trouvée par Ament,

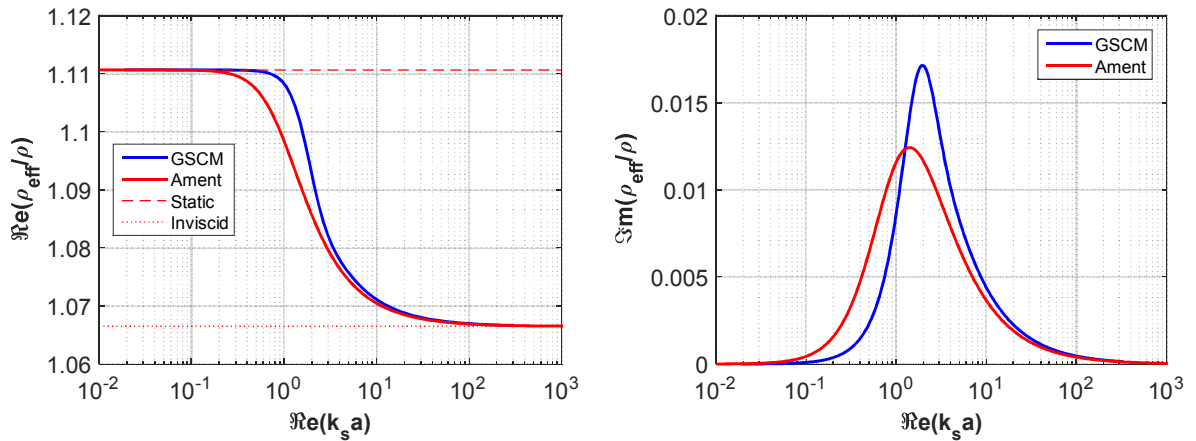
$$\frac{\rho_{\text{eff}}}{\rho} = 1 - c + \hat{c}\rho - \frac{2(\hat{\rho} - 1)^2 c(1 - c)}{W + iZ},$$

Avec

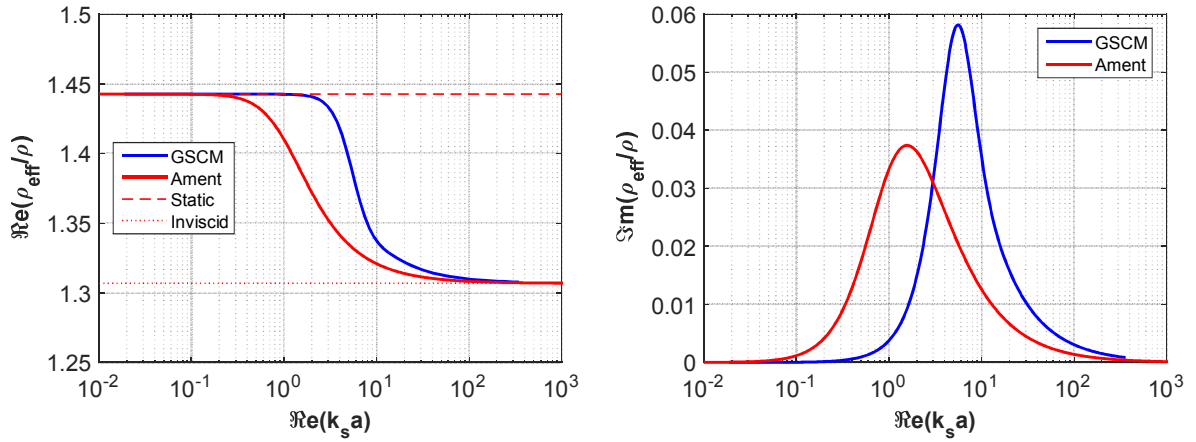
$$W = 2(1 - \hat{\rho})(1 - c) + \frac{9}{2} \frac{1}{\Re(k_s a)} + 3$$

$$Z = \frac{9}{2} \left(\frac{1}{\Re(k_s a)} + \frac{1}{\Re^2(k_s a)} \right),$$

et de la comparer avec celle obtenue dans le cadre de ce travail, comme illustré sur la figure suivante, tracée pour des particules de silice dans l'eau et une concentration $c = 0,1$:



et une concentration $c = 0,4$:



Quand la concentration augmente, le désaccord entre les deux modèles augmente : le pic de « résonance » observé sur la partie imaginaire du rapport des masses volumiques, observé à fréquence plus élevée dans le cas de notre modèle que dans celui d’Ament, est translaté vers les hautes fréquences de façon beaucoup plus marquée dans notre modèle. Le modèle d’Ament considère une viscosité du fluide indépendante de la concentration dans l’écriture de la force de traînée à laquelle chaque particule est supposée soumise, contrairement au modèle auto-consistant que nous avons utilisé, qui intègre, au travers des nombres d’onde effectifs et de la masse volumique effective, une viscosité effective dépendante de la concentration.

Le modèle d’Ament est ensuite étendu au cas de particules rigides, sphéroïdales aplaties, alignées parallèlement à la direction de l’onde incidente selon leur axe de révolution, respectivement allongées (« prolate spheroids ») ou aplaties (« oblate spheroids ») dans cette direction. Les expressions obtenues pour la masse volumique effective sont identiques dans les deux cas :

$$\frac{\rho_{\text{eff}}}{\rho} = 1 - c + \hat{c}\hat{\rho} - \frac{(1 - \hat{\rho})^2 c(1 - c)}{W'^2 + iZ'^2 + (1 - c)(\hat{\rho} - 1)},$$

avec

$$W'^2 = \frac{1}{1 - \left(\frac{1}{\varepsilon^2} - 1\right) Q_1\left(\frac{1}{\varepsilon}\right)} + 4 \frac{\varepsilon^2 a_p}{\kappa^2 a_{eq}} \frac{1}{\Re(k_s a_{eq})}$$

$$Z'^2 = 4 \frac{\varepsilon^2 a_p}{\kappa^2 a_{eq}} \frac{1}{\Re(k_s a_{eq})} + 3 \frac{\varepsilon}{\kappa} \frac{1}{\Re^2(k_s a_{eq})} \quad ,$$

$$\kappa = \frac{1}{2} \left(1 + \frac{1}{\varepsilon^2}\right) \ln\left(\frac{1 + \varepsilon}{1 - \varepsilon}\right) - \frac{1}{\varepsilon}$$

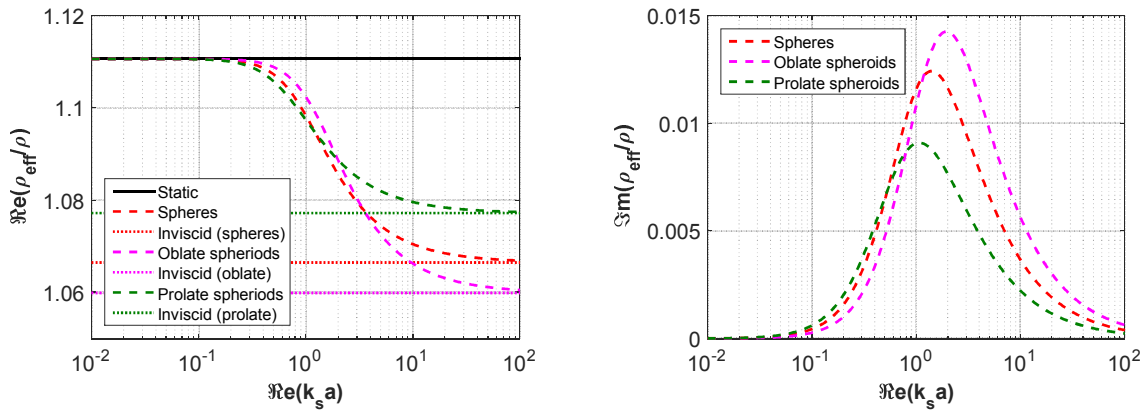
et Q_1 la fonction de Legendre de 2^{nde} espèce, telle que :

$$Q_1(x) = \frac{x}{2} \ln\left(\frac{x+1}{x-1}\right) - 1 \quad , \quad \text{et } \varepsilon = \frac{\max(a_p, a_{eq})}{a_p} e_{ll} \quad .$$

A concentration c , volume des particules $a^3 = 1 \mu\text{m}^3$, et ellipticité $e_{ll} = 0,9$ donnés, tels

que $\left|k_s (a_p^2 - a_{eq}^2)^{1/2}\right|_{\max} < 2.10^{-4}$, la figure suivante présente la comparaison entre les

cas des sphères et des sphéroïdes, oblongues comme aplaties, pour des particules de silice (considérées comme rigides) dans l'eau et une concentration de 0,1.



Les courbes correspondant à des sphéroïdes allongées sont situées de part et d'autre de celles correspondant à des sphères. A fréquence donnée, la masse volumique effective est plus proche de celle qui correspondrait à un fluide non-visqueux pour les sphéroïdes allongés dans le sens de la propagation de l'onde, en raison de leur opposition moindre au mouvement du fluide environnant sous l'effet de l'onde incidente.

Enfin le manuscrit se clôt par une conclusion dans laquelle sont rappelés les principaux résultats obtenus et des perspectives de recherche future avancées :

- Calcul des coefficients de diffusion de l'ensemble noyau-coque
- Calcul des coefficients de diffusion de sphéroïdes oblongues ou aplaties
- Essai d'utilisation du modèle auto-consistant pour calculer les nombres d'onde effectifs et une viscosité transverse effective
- Calcul d'une viscosité effective à partir du modèle d'Ament en établissant une relation entre la force de traînée et la concentration
- Essai d'établissement d'un modèle hydrodynamique pour calculer le nombre d'onde effectif de compression dans le cas de particules sphéroïdales oblongues ou aplaties

RÉFÉRENCES

- [1] J. G. Fikioris, and P.C. Waterman, "Multiple scattering of waves II 'Hole corrections' in the scalar case", *J. Math. Phys.*, vol. 5, pp. 1413–1420, 1964.
- [2] C. M. Linton, and P. A. Martin, "Multiple scattering by random configurations of circular cylinders: Second-order corrections for the effective wavenumber", *J. Acous. Soc. Am.*, vol. 117, pp. 3413–3423, 2005.
- [3] J.-M. Conoir, and A. N. Norris, "Effective wavenumbers and reflection coefficients for an elastic medium containing random configurations of cylindrical scatterers", *Wave Motion*, vol. 47, pp. 183–197, 2010.
- [4] A. N. Norris, J.-M. Conoir, "Multiple scattering by cylinders immersed in fluid: High order approximations for the effective wavenumbers", *J. Acous. Soc. Am.*, vol. 129, no 1, pp. 104–113, 2011.
- [5] F. Luppé, J.-M. Conoir, and A. N. Norris, "Effective wave numbers for thermo-viscoelastic media containing random configurations of spherical scatterers", *J. Acous. Soc. Am.*, vol. 131, pp. 1113–1120, 2012.
- [6] G. C. Gaunard, and H. Überall, "Resonance effects and the ultrasonic effective properties of particulate composites", *J. Acous. Soc. Am.*, vol. 74, pp. 305–313, 1983.
- [7] C. Jin, "On the estimation of dynamic mass density of random composites", *J. Acous. Soc. Am.*, vol. 132, pp. 615–620, 2012.
- [8] J. Mei, Z. Liu, W. Wen, and P. Sheng, "Effective dynamic mass density of composites", *Phys. Rev. B*, vol. 76, no. 13, pp. 134205 1-20, 2007.
- [9] J. R. Allegra, and S. A. Hawley, "Attenuation of Sound in Suspensions and Emulsions: Theory and Experiments," *J. Acous. Soc. Am.*, 51, 1545–1564, 1972.
- [10] V. J. Pinfield, and D. M. Forrester, "Multiple scattering in random dispersions of spherical scatterers: Effects of shear-acoustic interactions", *J. Acous. Soc. Am.*, vol. 141, pp. 649–660, 2017.

- [11] T. Valier-Brasier, J.-M. Conoir, F. Coulouvrat, J.-L. Thomas, “Sound propagation in dilute suspensions of spheres : Analytical comparison between coupled phase model and multiple scattering theory”, *J. Acous. Soc. Am.*, vol. 138, no 4, pp. 2598-2612, 2015.
- [12] M. M. Alam, F. Luppé, V.J. Pinfield, P. Marechal, “The coherent shear wave in suspensions”, *J. Phys : Conf. Ser.*, vol. 1017, no 1, pp. 012003 1-8, 2018.
- [13] T. Valier-Brasier, J.-M. Conoir, “Propagation of coherent transverse waves : Influence of the translational and rotational subwavelength resonances », *J. Acous. Soc. Am.*, vol. 142, pp. 512-522, 2017.
- [14] M.M. Alam, V.J. Pinfield, F. Luppé, P. Maréchal, “Effective dynamic properties of random complex media with spherical particles”, *J. Acous. Soc. Am.*, vol. 145, no 6, pp. 3727-3740, 2019.
- [15] W. S. Ament, “Sound propagation in gross mixtures”, *J. Acous. Soc. Am.*, vol. 25, no 4, pp. 638-641, 1953.

ACKNOWLEDGEMENTS

I would like to begin by giving my deepest gratitude to my principal advisor Pr. Francine Luppé for giving me the opportunity of conducting doctoral research under her supervision at this wonderful laboratory.

I would like to express my special appreciation and thanks to my co-supervisor Dr. Pierre Maréchal for his constant help, advice, and guidance that has made my PhD research productive. I have learned a lot from working with him.

I would like to thank sincerely Dr. Valerie Pinfield for co-supervising my dissertation from Loughborough through emails and regular Skype meetings. I also thank her for hosting me at University of Loughborough for a three-month research visit during my PhD.

I sincerely appreciate all the administrative support that I have received from Pr. Pascal Pareige during my PhD work.

I would like to thank all the members of the laboratory who work at 4th floor, especially Pr. Mounsif Ech-Cherif El Kettani for all the parties he threw at the laboratory.

I also thank Dr. Thomas Brunet, Pr. Guy Geuillard, Pr. Arnaud Tourin, Pr. Jérôme Vasseur and Dr. Tony Valier-Brasier for being the jurors of my thesis.

I acknowledge the financial support that I have received throughout my PhD study from the University of Le Havre.

I cannot finish without thanking my family. I would like to thank my parents for their undying love and support, and my brothers Saiful, Shamsul, and Srijohn for always cheering me up and for always being there.

LIST OF SYMBOLS

Roman letters

a	particle radius
A	vector potential
b	shell radius
B	bulk modulus
c	particle volume fraction
d	particle dimension
<i>D</i>	drag on a particle
e_{11}	ellipticity
f	frequency
i	square root of -1
k_c	compressional wavenumber
k_s	shear wavenumber
K_c	effective compressional wavenumber
K_s	effective shear wavenumber
n	partial wave mode
N	number of particles per unit volume
r	radius (at any position)
x_c	$= k_c b$, dimensionless compressional wavenumber
x_s	$= k_s b$, dimensionless shear wavenumber
X_c	$= K_c b$, effective dimensionless compressional wavenumber
X_s	$= K_s b$, effective dimensionless shear wavenumber

y_c	= $k_c a$, dimensionless compressional wavenumber
y_s	= $k_s a$, dimensionless shear wavenumber
Y_c	= $K_c a$, effective dimensionless compressional wavenumber
Y_s	= $K_s a$, effective dimensionless shear wavenumber
V	volume of a particle
v_{eff}	effective wave speed

Greek letters

α	attenuation
β	real part of the shear wavenumber
δ	viscous skin depth
Δ	density contrast
ε	function of equatorial and polar radius
δ_{ij}	Kronecker delta: $\delta_{ij} = 1$, for $i = j$; $\delta_{ij} = 0$, for $i \neq j$
η	shear viscosity
λ	Lamé parameter
μ	shear modulus/ Lamé parameter
ρ	density
σ_{ij}	stress tensor
θ	spherical coordinate
ϕ	spherical coordinate
ψ	Debye potential
χ	Debye potential
Φ	scalar potential
ω	circular frequency

TABLE OF CONTENTS

INTRODUCTION.....	1
CHAPTER ONE.....	5
BACKGROUND.....	5
1.1 INTRODUCTION.....	5
1.2 REVIEW OF EXISTING THEORIES.....	6
1.2.1 Phenomenological Approach.....	6
1.2.2 Multiple Scattering Theory.....	8
1.2.3 Self-Consistent Theory.....	10
CHAPTER TWO.....	17
SINGLE-SPHERE SCATTERING.....	17
2.1 INTRODUCTION.....	17
2.2 LITERATURE REVIEW.....	19
2.3 FORMULATION OF THE PROBLEM.....	23
2.3.1 Wave Equation.....	23
2.3.2 Symmetry and Solutions of Wave Equations.....	25
2.3.3 Displacement and Stress Expressions.....	27
2.3.4 Boundary Condition Equations.....	29
2.4 SCATTERING COEFFICIENTS.....	31
2.4.1 Monopole-Scattering Coefficient.....	31
2.4.2 Dipole-Scattering Coefficients.....	32
2.4.3 Nth-order Scattering Coefficients.....	36
2.4.4 Normalised Scattering Coefficients.....	48
2.5 NUMERICAL RESULTS.....	49
2.5.1 Dipole scattering coefficients.....	50
2.5.2 Quadrupole scattering coefficients.....	53
2.5.3 Dependence of Coefficients on Orders.....	55
2.6 CONCLUSION.....	56

CHAPTER THREE	61
EFFECTIVE DYNAMIC PROPERTIES WITH SPHERES	61
3.1 INTRODUCTION	61
3.2 MODEL	62
3.2.1 Core-Shell System for Effective Medium	62
3.2.2 Core-Shell Boundary Equations	64
3.2.3 Effective Bulk Modulus.....	66
3.2.4 Effective Dynamic Mass Density	69
3.3 RESULTS OF NUMERICAL CALCULATIONS	77
3.3.1 Dependence on Frequency at Different Particle Sizes.....	80
3.3.2 Dependence on Frequency at Different Concentrations	81
3.3.3 Dependence on Concentration at Fixed y_s	83
3.3.4 Dependence on Frequency with Different Viscosities.....	85
3.4 CONCLUSION	86
CHAPTER FOUR	89
EFFECTIVE DENSITY WITH SPHEROIDS.....	89
4.1 INTRODUCTION	89
4.2 SPHERICAL PARTICLES	90
4.2.1 Drag force	90
4.2.2 Effective Mass Density.....	92
4.2.3 Inviscid Limit	94
4.3 SPHEROIDAL PARTICLES	95
4.3.1 Prolate Spheroids.....	96
4.3.2 Oblate Spheroids.....	101
4.4 NUMERICAL RESULTS AND DISCUSSION.....	103
4.5 CONCLUSION	107
CONCLUSION AND FUTURE PROSPECTS	109
APPENDIX	111

INTRODUCTION

Estimating the effective properties of complex media is of interest from both a theoretical and an experimental point of view owing to their numerous applications; these include the mechanical properties of solid composite structures, the sound-absorbing properties of porous materials and the dynamic properties of fluid-suspended particle systems. A proper understanding of the dynamic properties of suspensions is of great significance, for example in the determination of particle mass or density by oscillatory methods, or in resonant acoustic mixing.

Acoustic propagation in dispersions of particles in fluids has drawn plenty of attention and has found many important applications in science and engineering, as discussed in Ref. [1]. Although many workers have conducted an extensive amount of research on acoustic characterisation of the physical properties of suspensions for nearly a century, they usually either consider inviscid host fluid cases or include viscosity without taking particle-particle interactions into account. There is a very little research on the inclusion of fluid viscosity through inter-particle interactions in modelling acoustic wave propagation in suspensions. However, it has been demonstrated recently, both theoretically and experimentally, that the viscous nature of the host fluid does indeed play an important part in determining the effective properties of a suspension [2]–[6].

The question motivating the work reported in this thesis is this: what are the appropriate effective properties for propagation in a suspension of particles in a viscous liquid? Luppé *et al.*[3] applied the multiple scattering model of Conoir *et al.*[7], devoted to cylinders in an elastic matrix, to solid spheres in a thermo-viscous fluid. The application of this model to suspensions of silica particles [5] showed that the additional effects of mode conversion owing to fluid viscosity have increasing impact on the effective properties at higher concentrations. Hence, the work reported in this thesis began with the use of the multiple scattering model of Ref. [3] in order to obtain the effective shear wave number [8].

The effective shear viscosity is studied through the use of its relation to the effective wavenumber and mass density, taking the latter as the volume average of the fluid and respective particles densities as it would be if the host was an elastic solid. Later, Valier-Brasier et al. [9] reported a different expression for the effective shear wavenumber, using the same model [3], but under different assumptions. Questions remained, therefore, as to the appropriate effective properties in the case of a viscous liquid host.

The multiple scattering models (reviewed in Chapter 1) on which this model ([3]) is built, provide the effective wavenumbers as solutions of an implicit dispersion equation. Under the low concentration assumption, the effective wavenumbers are given explicitly as series in integer powers of the concentration. Hence these multiple scattering models are useful at low concentration, but are limited in their application to systems of high concentration. This is the reason why we use here a different method, a core-shell model, restricted to “low frequency”, but not to low concentration, based on Mei’s work [10]. It is applied in Ref. [10] to solid cylinders in an elastic matrix, and we extend it in this work to solid spheres in a viscous fluid to obtain the effective mass density [11] by incorporating mode conversion phenomena.

The assumptions made throughout this thesis are as follows. We consider linear acoustics: the incident wave field amplitude is supposed to be small enough such that nonlinear effects like generation of subharmonics do not occur. The host medium is assumed to be a Newtonian viscous liquid, and thermal effects are neglected [4]. This thesis also deals with the so-called *Rayleigh scattering regime* for the compressional waves: the wavelength of compressional wave in the continuous phase, and that of compressional and shear waves in dispersed phase are considered to be much larger than the dimension of the particle. However, no restriction has been placed on the magnitude of the shear wavelength in the background fluid. The particles are assumed to be spherical and all identical, and to be linear elastic solids. The spheres are assumed to be randomly distributed, so that the effective properties are isotropic in the long wavelength regime.

The rest of the thesis is organized as follows. In Chapter One we briefly discuss and review different types of models that are used to determine the effective properties of discrete random media. Chapter Two deals with the scattering of an acoustic wave by an elastic spherical object immersed in a viscous fluid. We first formulate the scattering problem and then calculate the scattering coefficients for the sphere for general partial wave orders, taking the fluid viscosity into account through the inherent coupling between compressional and shear waves. We present approximate formulas for those scattering coefficients in the Rayleigh scattering regime for compressional waves. In Chapter Three, we present the core-shell model and extend it for viscous host fluid and derive the effective bulk modulus and mass density of the system. Chapter Four deals with spheroidal particles in a viscous fluid. We extend the existing Ament model from spherical particles to spheroidal ones so as to investigate the dynamic behavior of the effective mass density for suspensions of both prolate and oblate spheroids. A summary of our main results and perspectives for future work are given in the Conclusion.

REFERENCES

- [1] R. E. Challis, M. J. W. Povey, M. L. Mather, and A. K. Holmes, "Ultrasound techniques for characterizing colloidal dispersions," *Reports Prog. Phys.*, vol. 68, no. 7, pp. 1541–1637, 2005.
- [2] F. Luppé, T. Valier-Brasier, J. M. Conoir, and P. Pareige, "Coherent wave propagation in viscoelastic media with mode conversions and pair-correlated scatterers," *Wave Motion*, vol. 72, pp. 244-259, 2017.
- [3] F. Luppé, J.-M. Conoir, and A. N. Norris, "Effective wave numbers for thermo-viscoelastic media containing random configurations of spherical scatterers," *J. Acoust. Soc. Am.*, vol. 131, no. 2, pp. 1113–1120, 2012.
- [4] V. J. Pinfield and D. M. Forrester, "Multiple scattering in random dispersions of spherical scatterers: Effects of shear-acoustic interactions," *J. Acoust. Soc. Am.*, vol. 141, no. 1, pp. 649–660, 2017.
- [5] D. M. Forrester, J. Huang, V. J. Pinfield, and F. Luppé, "Experimental verification of nanofluid shear-wave reconversion in ultrasonic fields," *Nanoscale*, vol. 8, no. 10, pp. 5497–5506, 2016.
- [6] D. M. Forrester, J. Huang, and V. J. Pinfield, "Characterisation of colloidal dispersions using ultrasound spectroscopy and multiple-scattering theory inclusive of shear-wave effects," *Chem. Eng. Res. Des.*, vol. 114, pp. 69–78, 2016.

- [7] J. M. Conoir and A. N. Norris, “Effective wavenumbers and reflection coefficients for an elastic medium containing random configurations of cylindrical scatterers,” *Wave Motion*, vol. 47, pp. 183–197, 2010.
- [8] M. Alam, F. Luppé, V. J. Pinfield and P. Maréchal P., “The coherent shear wave in suspensions,” *J. Phys. Conf. Ser.*, vol. 1017, pp. 012003 1-8, 2018.
- [9] T. Valier-Brasier and J-M. Conoir, “Propagation of coherent transverse waves: Influence of the translational and rotational subwavelength resonances,” *J. Acoust. Soc. Am.*, vol. 142, no. 2, pp. 512-522, 2017.
- [10] J. Mei, Z. Liu, W. Wen and P. Shen, “Effective dynamic mass density of composites,” *Phys. Rev. B*, vol. 76, no. 13, pp. 134205:1-20, 2007.
- [11] M. M. Alam, V. J. Pinfield, F. Luppé and P. Maréchal, “Effective dynamic properties of random complex media with spherical particles,” *J. Acoust. Soc. Am.*, vol. 145, no. 6, pp. 3727-3740, 2019.

CHAPTER ONE

BACKGROUND

1.1 INTRODUCTION

A plane acoustic/elastic wave, which may be characterized by a frequency and a propagation direction, can freely propagate in an infinite homogeneous medium. However, a wave undergoes scatterings while travelling in a complex random material. Since waves can carry information about a system in which they propagate, it is of particular interest to investigate and understand the scattering occurring in the system. As an example, we can think of a plane wave propagating through a finite scattering region, which consists of a finite number N of inhomogeneities (e.g. inclusions, voids, cracks) but is otherwise homogeneous. The total displacement field $\mathbf{u}(\mathbf{r})$ at an observation point \mathbf{r} located outside the scatterers can be written as:

$$\mathbf{u}(\mathbf{r}) = \mathbf{u}_{\text{inc}}(\mathbf{r}) + \sum_{i=1}^N \mathbf{u}_s(\mathbf{r}, \mathbf{r}_i) \quad (1.1)$$

$\mathbf{u}_{\text{inc}}(\mathbf{r})$ is the displacement at \mathbf{r} caused by the incident wave and $\mathbf{u}_s(\mathbf{r}, \mathbf{r}_i)$ the displacement at \mathbf{r} produced by the wave scattered by the i -th scatterer. The latter is in turn produced by the primary (incident) wave and also by the rescattering (i.e. secondary and higher-order scatterings) of the primary waves from the other particles. Therefore, one has to solve a multiple scattering problem in order to calculate $\mathbf{u}(\mathbf{r})$ exactly, which requires the knowledge of the exact location of all the particles in order to account for the continuity of the displacements and stresses across the boundary of each particle. However, in general, it is not feasible to obtain this kind of exact information about a disordered medium, and thus one has to make some approximation.

In a disordered medium, the positions of the particles, and, eventually, their physical parameters, are treated as random variables, and the statistical average of the

propagating fields defines the coherent waves, whose complex wavenumbers are the effective wavenumbers. The effective medium is defined as the (fictitious) homogeneous medium in which waves would propagate with those same complex wavenumbers. Obviously, the coherent fields depend upon the multiple scattering events the original incident wave has undergone; the effective properties, i.e. those of the effective medium, depend thus on the particles size to the wavelengths ratios. The imaginary parts of the effective wavenumbers describe the attenuation the coherent waves undergo, due to multiple scattering and intrinsic visco-elasticity of the host medium, and mean free paths may be defined [1]. When propagation in the disordered medium is studied over distances smaller or the order of one elastic mean free path, the description of the disordered medium as an effective one makes sense [2-3]. When it is larger than a few mean free paths, then it is more relevant to study the energy diffusion rather than the amplitude propagation. This work focuses on the first case, where defining an effective medium makes sense.

The modelling of composite materials and the concept of effective medium date back to the late nineteenth and early twentieth century with the works of Maxwell, Rayleigh and Einstein [4]. Maxwell obtained the effective conductivity of a composite medium [5]. Rayleigh developed a multipole method to find the effective electrical conductivity of a periodic medium composed of cylinders [6]. Einstein found an expression for the effective viscosity of a dilute suspension of rigid spherical particles in a viscous fluid [7].

In what follows, we review and discuss different approaches to estimating the effective properties of a discrete random medium.

1.2 REVIEW OF EXISTING THEORIES

1.2.1 Phenomenological Approach

The phenomenological approach is an effective medium approach [8]. The velocity of sound v through a homogeneous medium is given by the Newton-Laplace formula:

$$v = (\rho \kappa)^{-1/2} \tag{1.2}$$

where ρ and κ are respectively the density and compressibility of the medium. When a compressional wave propagates through a suspension, there will be a well-defined phase velocity V such that one can define an effective density ρ_{eff} and compressibility κ_{eff} , which are related by the following simple equation:

$$v_{\text{eff}} = (\rho_{\text{eff}}\kappa_{\text{eff}})^{-1/2} \quad (1.3)$$

Wood first applied this equation to fluid mixtures [9], and Urick generalised it to dispersions of solid particles [10]. If a two-phase mixture composed of a volume fraction c of a phase with density ρ' and compressibility κ' , suspended in another phase of density ρ and compressibility κ , then the Urick assumptions are:

$$\rho_{\text{eff}} = (1 - c)\rho + c\rho' \quad (1.4)$$

$$\kappa_{\text{eff}} = (1 - c)\kappa + c\kappa' \quad (1.5)$$

The assumption behind the Urick equation is that the particles are infinitesimally small compared to the wavelength of the wave, and hence the scattering can be ignored. Although the Urick equation works for many systems where the above assumptions are approximated, it cannot always make a satisfactory prediction. As particles increase in size compared to the wavelength of the wave, the assumption based on the Urick equation is no longer valid and hence significant deviations between theoretical prediction and experimental data occur.

In order to calculate a value for the phase velocity in a suspension, Ament derived an expression for the effective dynamic mass density using an elementary physics approach [11]. Combining equations of incompressible flow, conservation of momentum, and equilibrium between the viscous drag (which includes the inertial and viscous terms) and the buoyant force on the suspended particle, Ament obtained an expression for the effective density of a suspension:

$$\rho_{\text{eff}} = (1 - c)\rho + c\rho' - \frac{2(\rho' - \rho)^2 c(1 - c)W}{W^2 + Z^2} \quad (1.7)$$

$$\text{with } W = 2(\rho' - \rho)(1 - c) + \frac{9}{2} \frac{1}{\beta a} \rho + 3\rho, \quad \beta = \sqrt{\frac{\rho\omega}{2\eta}}, \quad \text{and } Z = \frac{9}{2} \rho \left[\frac{1}{\beta a} + \left(\frac{1}{\beta a} \right)^2 \right],$$

where a is the particle radius, η the shear viscosity of the host fluid and ω the circular frequency. Therefore, with Eqns. (1.5) and (1.7), equation (1.3) gives the phase speed in the suspension. The Ament expression is based on the assumption that the particles are spherical, rigid and small compared with the compression wavelength but is comparable in size to the shear wavelength in the host fluid. The Ament equation tends to the Urick equation in the limit of very small particles (i.e. $\beta a \ll 1$). Although the Ament formula has not been employed much in the literature, it has been found to be in good agreements with experimental measurements of phase velocity when employed [11, 12]. Since the Ament effective density formula contains several textual errors, it requires to be rederived which has been done in the fourth chapter.

1.2.2 Multiple Scattering Theory

Another approach to estimating effective dynamic properties of random distributions of particles is Multiple Scattering Theories (MSTs). When a wave propagates in a random medium, it undergoes several scattering events. This process is called multiple scattering, in contrast to single scattering, where the wave is scattered only once. Waves scattered from one inclusion can encounter a neighbouring inclusion which rescatters some of the original incident wave back onto the first inclusion. The incident and scattered waves from all the scatterers combine on the average to produce a new wave, known as the *coherent wave*, propagating at a different phase velocity and with attenuation [13]. MSTs mainly focus on calculating the coherent wavenumber of a random distribution of scatterers as a perturbation of the wavenumber of the host matrix.

MST was initiated by Foldy in 1945; he derived a dispersion relation for an acoustic wave in a system of isotropic scatterers by introducing a configurational averaging procedure [13]. Lax later extended the theory of Foldy to obtain a new dispersion relation for anisotropic scatterers and applied the Quasi-Crystalline Approximation (QCA) to determine the effective field [14]. In both Foldy's and Lax's works the effective wave number was expressed in terms of the particle concentration and the

forward far field scattering amplitude taken from the solution of the single particle wave scattering problem. Waterman and Truell improved these two models by adding the effect of far-field backscattering to the multiple scattering process [15], which acted as the basis for large number of multiple scattering models.

In order to consider higher concentration in the MSTs, Fikioris and Waterman introduced the pair correlation function in the form of “hole correction” to make sure that inclusions do not overlap during the averaging process [16].

Lloyd and Berry [17] applied the multiple scattering method of Lloyd [18], developed for the treatment of the electronic structure of liquids and disordered alloys, to the propagation of waves through a random dispersion of spherical particles. Lloyd and Berry also demonstrated that there is an implicit assumption of a superposition of thin slabs behind the Waterman and Truell model.

Varadan *et al.* formulated an MST for randomly distributed spherical [19] and cylindrical [20] inclusions in an elastic matrix using QCA and a pair-correlation function to estimate effective phase velocity and coherent attenuation. More recently, Linton and Martin validated Lloyd-Berry’s formula and have given a new derivation for cylindrical [21] and spherical scatterers [22]. Identification of effective density and elastic properties based on multiple scattering models has also been carried out, to second order in concentration and therefore limited to low concentration [23–26].

Although Multiple Scattering Models are therefore well-established for obtaining effective properties, they have mainly focused on *ideal* (inviscid) host fluids and are valid only up to a limited concentration. This is due to the assumption made in MSTs that concentration is low, and effective properties are typically expressed as series in orders of the concentration, in contrast to the effective medium models where high concentrations are not constrained. However, an additional factor is the effect of thermal and shear wave modes produced by scattering of the acoustic waves by the particles; although the thickness of the thermal and viscous boundary layers are typically very small, they can affect other particles when the concentration is high and inter-particle separations consequently small. These effects have been neglected in MSTs until relatively recently, when Conoir and Norris generalised Linton and Martin’s formula for cylindrical particles in elastic media [27], providing the framework to include all effective wave modes (acoustic, thermal and shear) in the complex medium. The model

was extended to three dimensions (spherical particles) at second order in concentration by Luppé, Conoir and Norris (LCN) [28], and later to higher concentrations (third order), accounting for weak pair-correlations [29].

Alam *et al.* conducted a numerical study of the LCN model for a random dispersion of silica particles in viscous water and studied the effective shear wavenumber [30]. Using the coherent shear wavenumber from the LCN model and assuming a volume average mass density, the effective viscosity was defined and studied numerically.

The previously-neglected multi-mode conversions have been demonstrated to be significant in nanoparticle suspensions and the new model applied to such systems [31] presents a greatly improved agreement with experimental data [32-33]. Further experimental evidence of the need for the determination of improved effective properties is provided by a number of other workers studying acoustic propagation in liquid suspensions of particles [34-35].

1.2.3 Self-Consistent Theory

1.2.3.1 Static Theory

One approach used to determine the effective properties of random composites is to use *self-consistent* theories. A single inclusion is embedded within an effective homogeneous medium and self-consistency is imposed such that the physical properties (e.g. strain, stress) in the embedding medium surrounding this single inclusion are the same as those in the effective medium as a whole. While the early models, such as the static self-consistent method of Hill [36] and Budiansky [37], treated each inclusion as embedded directly in the infinite, homogeneous, effective medium, Christensen and Lo [38] proposed a *Generalised Self Consistent Model* (GSCM), originally developed by Kerner [39]. The GSCM introduced a layer of the host matrix material into the equivalence model; the inclusion was treated as though embedded within a shell of host material, which was then embedded within the infinite effective medium (as illustrated in Figure 1.1). Christensen [40] investigated several theoretical models and concluded that the only one of these that produced acceptable results and improved agreement with experimental data was the GSCM model; it thus received much attention and was

exploited by many authors [41–45]. However, these schemes were purely static, focussing on the averaging or homogenisation of physical quantities such as stress, strain and displacement [46]. For dynamic, wave-based problems such as acoustics, an extension of the models to include wave phenomena is necessary.

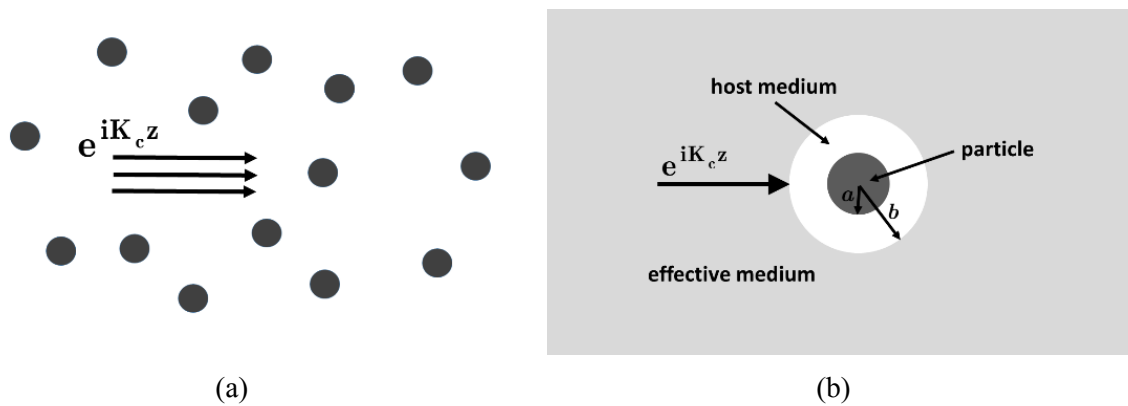


Figure 1.1 shows (a) the propagation of the average wavenumber through a random dispersion of particles (b) how the system can be modelled using the Generalised Self Consistent Method.

1.2.3.2 Dynamic Theory

Although there are a variety of dynamic effective medium models, the most widely adopted is based on the following two hypotheses [47-48]:

- (i) a single inclusion (coated with a shell of the host medium) behaves as if isolated and embedded in the corresponding effective medium,
- (ii) the mean wave field in the composite medium coincides with the wave field propagating in the homogeneous effective medium.

The first hypothesis reduces the many-particle problem to a single-particle one in the same way as the static self-consistent models, and the second one is the *self-consistency* condition applied to the wave field.

Any wave propagating in a composite material can be thought of as the sum of two wave fields: a mean (coherent) wave propagating in a medium having the dynamic effective properties of the composite and a number of fluctuating waves arising from the multiple scattering of the mean wave due to the spatial randomness in the elastic

parameters of the composite material. The fluctuating field, which, in an effective medium, on average, requires to be zero [49].

This wave-based generalised self-consistent theory has been applied by many investigators. For solid inhomogeneous systems, models include the self-consistent approach of Kanaun *et al.* [48], Sabina and Willis [50], the quasi-static-limit approximations of Berryman [51-52], Kuster and Toksöz [53], Jin [54] and Mei *et al.* [55], the dynamic approach of Gaunard [56], investigating solid in solid composites at low concentration (no multiple scattering) to obtain static shear modulus and density, extended by Kerr [57] to obtain frequency-dependent parameters for spherical solid inclusions, and by Kim [49] to obtain frequency-dependent elastic parameters. For complex fluids, i.e. liquid suspensions of particles, the effective medium method has been studied by Hemar *et al.* [58] and McClements *et al.* [59] to determine acoustic properties with thermal effects, Cowan *et al.* [60], and Hipp *et al.* [61] for acoustic systems with both thermal and shear phenomena. These workers were motivated by the characterisation of particles in suspensions using acoustic spectroscopy and the need to account for thermal and shear phenomena which were not accounted for in existing multiple scattering models.

1.2.3.3 Dynamic Generalised Method

Since MSTs are limited to low volume concentrations, Yang and Mal combined the GSCM with Waterman and Truell's MST in order to obtain a Dynamic Generalised Self Consistent Method (DGSCM) [62], whereby they calculated the effective wavenumber of a fibre-reinforced composite (a 2D cylindrical problem) in a self-consistent manner; they showed that the effective wave speed calculated was in good agreement with experimental data. Yang [63] and Kim [64] used the same methodology for spherical inclusions. Other workers have also combined the two approaches, to determine effective properties at higher concentrations, but retaining the wave-nature of the problem. McClements *et al.* applied this approach for thermal interactions [59], and Hipp combined the two methods for a thermal-viscous-acoustic system of spherical particles although assumptions were made regarding effective properties rather than deriving them [61].

REFERENCES

- [1] P. Sheng and Z. Q. Zhang, “Scalar-wave localization in a two-component composite,” *Phys. Rev. Lett.*, vol. 57, no. 15, pp. 1879–1882, 1986.
- [2] D. Sornette, “Acoustic Waves in Random Media. I. Weak Disorder Regime,” *Acta Acust. united with Acust.*, vol. 67, no. 3, pp. 199–215, 1989.
- [3] D. Sornette, “Acoustic Waves in Random Media. II. Coherent Effects and Strong Disorder Regime,” *Acta Acust. united with Acust.*, vol. 67, no. 4, pp. 251–265, 1989.
- [4] G. W. Milton, *The Theory of Composites*. 2009.
- [5] G. Chrystal, “A Treatise on Electricity and Magnetism An Elementary Treatise on Electricity,” *Nature*, vol. 25, no. 637, pp. 237–240, 2008.
- [6] Lord Rayleigh, “LVI. *On the influence of obstacles arranged in rectangular order upon the properties of a medium*,” *London, Edinburgh, Dublin Philos. Mag. J. Sci.*, vol. 34, no. 211, pp. 481–502, Dec. 1892.
- [7] A. Einstein, “Eine neue bestimmung der molekul-dimension (A new determination of the molecular dimensions),” *Ann. Phys.*, vol. 19, pp. 289–306, 1906.
- [8] A. H. Harker and J. A. G. Temple, “Velocity and attenuation of ultrasound in suspensions of particles in fluids,” *J. Phys. D. Appl. Phys.*, vol. 21, no. 11, pp. 1576–1588, 1988.
- [9] A. B. Wood, “A Textbook of Sound,” *Nature*, 1956.
- [10] R. J. Urick, “A sound velocity method for determining the compressibility of finely divided substances,” *J. Appl. Phys.*, vol. 18, no. 11, pp. 983–987, 1947.
- [11] W. S. Ament, “Sound Propagation in Gross Mixtures,” *J. Acoust. Soc. Am.*, vol. 25, no. 4, pp. 638–641, 2005.
- [12] L. D. Hampton, “Acoustic Properties of Sediments,” *J. Acoust. Soc. Am.*, vol. 36, no. 10, pp. 1993–1993, 2005.
- [13] L. L. Foldy, “The multiple scattering of waves. I. General theory of isotropic scattering by randomly distributed scatterers,” *Phys. Rev.*, vol. 67, no. 3–4, pp. 107–119, 1945.
- [14] P. C. Waterman and R. Truell, “Multiple scattering of waves,” *Journal of Mathematical Physics*, vol. 2, no. 4, pp. 512–537, 1961.
- [15] P. C. Waterman and R. Truell, “Multiple scattering of waves,” *J. Math. Phys.*, vol. 2, no. 4, pp. 512–537, 1961.
- [16] J. G. Fikioris and P. C. Waterman, “Multiple scattering of waves. II. ‘Hole corrections’ in the scalar case,” *J. Math. Phys.*, vol. 5, no. 10, pp. 1413–1420, 1964.
- [17] P. Lloyd and M. V. Berry, “Wave propagation through an assembly of spheres: IV. Relations between different multiple scattering theories,” *Proc. Phys. Soc.*, vol. 91, no. 3, pp. 678–688, 1967.
- [18] P. Lloyd, “Wave propagation through an assembly of spheres: II. The density of single-particle eigenstates,” *Proc. Phys. Soc.*, vol. 90, no. 1, pp. 207–216, 1967.

- [19] V. K. Varadan, Y. Ma, and V. V. Varadan, “A multiple scattering theory for elastic wave propagation in discrete random media,” *J. Acoust. Soc. Am.*, vol. 77, no. 2, pp. 375–385, 2005.
- [20] V. K. Varadan, V. V. Varadan, and Y. Ma, “Multiple scattering of elastic waves by cylinders of arbitrary cross section. II. Pair-correlated cylinders,” *J. Acoust. Soc. Am.*, vol. 78, no. 5, pp. 1874–1878, 2005.
- [21] C. M. Linton and P. A. Martin, “Multiple scattering by random configurations of circular cylinders: Second-order corrections for the effective wavenumber,” *J. Acoust. Soc. Am.*, vol. 117, no. 6, pp. 3413–3423, 2005.
- [22] C. M. Linton and P. A. Martin, “Multiple Scattering by Multiple Spheres: A New Proof of the Lloyd–Berry Formula for the Effective Wavenumber,” *SIAM J. Appl. Math.*, vol. 66, no. 5, pp. 1649–1668, 2006.
- [23] W. J. Parnell and I. D. Abrahams, “Multiple point scattering to determine the effective wavenumber and effective material properties of an inhomogeneous slab,” *Waves in Random and Complex Media*, vol. 20, no. 4, pp. 678–701, 2010.
- [24] M. Caleap, B. W. Drinkwater, and P. D. Wilcox, “Coherent acoustic wave propagation in media with pair-correlated spheres,” *J. Acoust. Soc. Am.*, vol. 131, no. 3, pp. 2036–2047, 2012.
- [25] P. A. Martin, A. Maurel, and W. J. Parnell, “Estimating the dynamic effective mass density of random composites,” *J. Acoust. Soc. Am.*, vol. 128, no. 2, pp. 571–577, 2010.
- [26] C. Aristégui and Y. C. Angel, “Effective mass density and stiffness derived from P-wave multiple scattering,” *Wave Motion*, vol. 44, no. 3, pp. 153–164, 2007.
- [27] A. N. Norris and J.-M. Conoir, “Multiple scattering by cylinders immersed in fluid: High order approximations for the effective wavenumbers,” *J. Acoust. Soc. Am.*, vol. 129, no. 1, pp. 104–113, 2011.
- [28] F. Luppé, J.-M. Conoir, and A. N. Norris, “Effective wave numbers for thermo-viscoelastic media containing random configurations of spherical scatterers,” *J. Acoust. Soc. Am.*, vol. 131, no. 2, pp. 1113–1120, 2012.
- [29] F. Luppé, T. Valier-Brasier, J. M. Conoir, and P. Pareige, “Coherent wave propagation in viscoelastic media with mode conversions and pair-correlated scatterers,” *Wave Motion*, vol. 72, pp. 244–259, 2017.
- [30] M. Alam, F. Luppé, V. J. Pinfield, and P. Maréchal, “The coherent shear wave in suspensions,” in *Journal of Physics: Conference Series*, 2018.
- [31] V. J. Pinfield and D. M. Forrester, “Multiple scattering in random dispersions of spherical scatterers: Effects of shear-acoustic interactions,” *J. Acoust. Soc. Am.*, vol. 141, no. 1, pp. 649–660, 2017.
- [32] D. M. Forrester, J. Huang, V. J. Pinfield, and F. Luppé, “Experimental verification of nanofluid shear-wave reconversion in ultrasonic fields,” *Nanoscale*, vol. 8, no. 10, pp. 5497–5506, 2016.
- [33] D. M. Forrester, J. Huang, and V. J. Pinfield, “Characterisation of colloidal dispersions using ultrasound spectroscopy and multiple-scattering theory inclusive of shear-wave effects,” *Chem. Eng. Res. Des.*, vol. 114, pp. 69–78, Oct. 2016.

- [34] R. E. Challis and V. J. Pinfield, “Ultrasonic wave propagation in concentrated slurries - The modelling problem We dedicate this paper to the memory of our much respected friend and colleague, the late Dr. Bernard Hosten of the University of Bordeaux.,” *Ultrasonics*, vol. 54, no. 7, pp. 1737–1744, 2014.
- [35] J. Dubois, C. Aristégui, O. Poncelet, and A. L. Shuvalov, “Coherent acoustic response of a screen containing a random distribution of scatterers: Comparison between different approaches,” in *Journal of Physics: Conference Series*, 2011, vol. 269, no. 1.
- [36] R. Hill, “A self-consistent mechanics of composite materials,” *J. Mech. Phys. Solids*, vol. 13, no. 4, pp. 213–222, 1965.
- [37] B. Budiansky, “On the elastic moduli of some heterogeneous materials,” *J. Mech. Phys. Solids*, vol. 13, no. 4, pp. 223–227, 1965.
- [38] R. M. Christensen and K. H. Lo, “Solutions for effective shear properties in three phase sphere and cylinder models,” *J. Mech. Phys. Solids*, vol. 27, no. 4, pp. 315–330, 1979.
- [39] E. H. Kerner, “The elastic and Thermo-elastic properties of composite media,” *Proc. Phys. Soc. Sect. B*, vol. 69, no. 8, pp. 808–813, 1956.
- [40] R. M. Christensen, “A critical evaluation for a class of micro-mechanics models,” *J. Mech. Phys. Solids*, vol. 38, no. 3, pp. 379–404, 1990.
- [41] Y. Benveniste, “The effective mechanical behaviour of composite materials with imperfect contact between the constituents,” *Mech. Mater.*, vol. 4, no. 2, pp. 197–208, 1985.
- [42] H. A. Luo and G. J. Weng, “On Eshelby’s inclusion problem in a three-phase spherically concentric solid, and a modification of Mori-Tanaka’s method,” *Mech. Mater.*, vol. 6, no. 4, pp. 347–361, 1987.
- [43] G. Siboni and Y. Benveniste, “A micromechanics model for the effective thermomechanical behaviour of multiphase composite media,” *Mech. Mater.*, vol. 11, no. 2, pp. 107–122, 1991.
- [44] Y. Huang, K. X. Hu, X. Wei, and A. Chandra, “A generalized self-consistent mechanics method for composite materials with multiphase inclusions,” *J. Mech. Phys. Solids*, vol. 42, no. 3, pp. 491–504, 1994.
- [45] S. Biwa, N. Ito, and N. Ohno, “Elastic properties of rubber particles in toughened PMMA: Ultrasonic and micromechanical evaluation,” *Mech. Mater.*, vol. 33, no. 12, pp. 717–728, 2001.
- [46] S. Nemat-Nasser, M. Lori, and S. K. Datta, “Micromechanics: Overall Properties of Heterogeneous Materials,” *J. Appl. Mech.*, vol. 63, no. 2, p. 561, 2008.
- [47] S. K. Kanaun and V. M. Levin, “Effective medium method in the problem of axial elastic shear wave propagation through fiber composites,” *Int. J. Solids Struct.*, vol. 40, no. 18, pp. 4859–4878, 2003.
- [48] S. K. Kanaun, V. M. Levin, and F. J. Sabina, “Propagation of elastic waves in composites with random set of spherical inclusions (effective medium approach),” *Wave Motion*, vol. 40, no. 1, pp. 69–88, 2004.
- [49] J. Kim, J. Ih, and B. Lee, “Dispersion of elastic waves in random particulate composites,” *J. Acoust. Soc. Am.*, vol. 97, no. 3, pp. 1380–1388, 2005.

- [50] F. J. Sabina and J. R. Willis, “A simple self-consistent analysis of wave propagation in particulate composites,” *Wave Motion*, vol. 10, no. 2, pp. 127–142, 1988.
- [51] J. G. Berryman, “Long-wavelength propagation in composite elastic media I. Spherical inclusions,” *J. Acoust. Soc. Am.*, vol. 68, no. 6, pp. 1809–1819, 1980.
- [52] J. G. Berryman, “Long-wavelength propagation in composite elastic media II. Ellipsoidal inclusions,” *J. Acoust. Soc. Am.*, vol. 68, no. 6, pp. 1820–1831, 1980.
- [53] G. T. Kuster and M. N. Toksöz, “Velocity and Attenuation of Seismic Waves in Two-Phase Media: Part I. Theoretical Formulations,” *Geophysics*, vol. 39, no. 5, pp. 587–606, 2002.
- [54] C. Jin, “On the estimation of dynamic mass density of random composites,” *J. Acoust. Soc. Am.*, vol. 132, no. 2, pp. 615–620, 2012.
- [55] J. Mei, Z. Liu, W. Wen, and P. Sheng, “Effective dynamic mass density of composites,” *Phys. Rev. B - Condens. Matter Mater. Phys.*, vol. 76, no. 13, 2007.
- [56] G. C. Gaunard and H. Überall, “Resonance theory of the effective properties of perforated solids,” *J. Acoust. Soc. Am.*, vol. 71, no. 2, p. 282, 1982.
- [57] F. H. Kerr, “An effective medium approach to the study of plane wave propagation in an elastic matrix with spherical elastic inclusions,” *Int. J. Eng. Sci.*, vol. 30, no. 2, pp. 187–198, 1992.
- [58] Y. Hemar, N. Herrmann, P. Lemaréchal, R. Hocquart, and F. Lequeux, “Effective Medium Model for Ultrasonic Attenuation Due to the Thermo-Elastic Effect in Concentrated Emulsions,” *J. Phys. II*, vol. 7, no. 4, pp. 637–647, 1997.
- [59] D. J. McClements, Y. Hemar, and N. Herrmann, “Incorporation of thermal overlap effects into multiple scattering theory,” *J. Acoust. Soc. Am.*, vol. 105, no. 2, pp. 915–918, 2002.
- [60] M. L. Cowan, K. Beaty, J. H. Page, Z. Liu, and P. Sheng, “Group velocity of acoustic waves in strongly scattering media: Dependence on the volume fraction of scatterers,” *Phys. Rev. E - Stat. Physics, Plasmas, Fluids, Relat. Interdiscip. Top.*, vol. 58, no. 5, pp. 6626–6636, 1998.
- [61] A. K. Hipp, G. Storti, and M. Morbidelli, “Acoustic characterization of concentrated suspensions and emulsions. 2. Experimental validation,” *Langmuir*, vol. 18, no. 2, pp. 405–412, 2002.
- [62] R. Bin Yang and A. K. Mal, “Multiple scattering of elastic waves in a fiber-reinforced composite,” *J. Mech. Phys. Solids*, vol. 42, no. 12, pp. 1945–1968, 1994.
- [63] R.-B. Yang, “A Dynamic Generalized Self-Consistent Model for Wave Propagation in Particulate Composites,” *J. Appl. Mech.*, vol. 70, no. 4, p. 575, 2003.
- [64] J. Y. Kim, “On the generalized self-consistent model for elastic wave propagation in composite materials,” *Int. J. Solids Struct.*, vol. 41, no. 16–17, pp. 4349–4360, 2004.

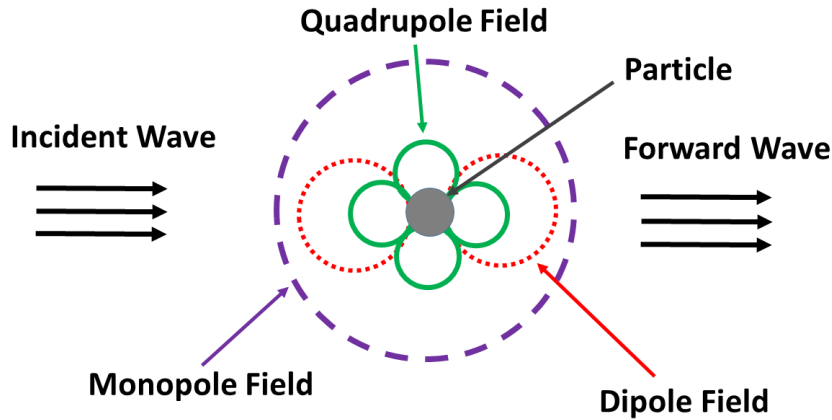
CHAPTER TWO

SINGLE-SPHERE SCATTERING

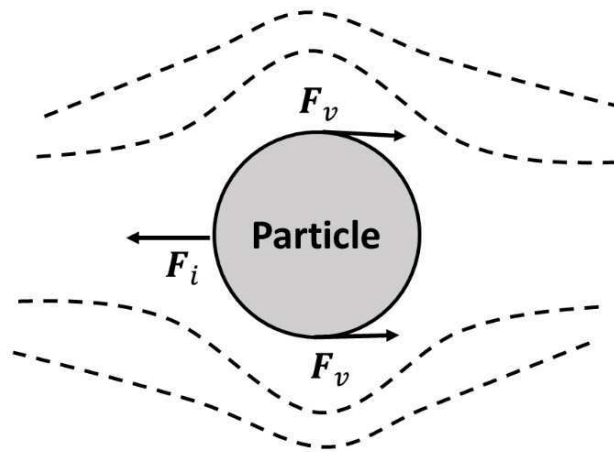
2.1 INTRODUCTION

The scattering of an acoustic wave by a single inclusion is an underpinning scattering problem, which has been investigated for almost one and a half centuries, dating back to the work of Lord Rayleigh (John William Strutt) [1]. Single sphere scattering, being a fundamental physical problem, still retains a position of importance in scattering theory. This problem is often studied because it is less complicated in nature than other geometrical configurations, and, as such, can be described by a minimum number of parameters. Knowledge of the scattering characteristics of a single spherical particle, though not directly related to many applications, has far-reaching implications in single particle models [2-3], multiple scattering models [4–11] and effective medium models [7, 12–15].

A spherical particle subject to an acoustic field pulsates (radial expansions and contractions) and oscillates (translatory to-and-fro motion) relative to the surrounding liquid. The pulsation and oscillation the particle undergoes act as a source of the scattered waves. If there is a density contrast between the particle and the liquid, an inertial force exists; if the liquid has a viscosity, there exists a viscous force as well, which opposes the inertial force, thereby damping the oscillation of the particle. If the particle's density is close to its surrounding fluid, thermal effects, due to the differences between the thermal properties of the particle and of the continuous phase, becomes dominant and hence the inertial effects are negligible. However, in situations where the density contrast between the particle and its surrounding fluid is high, the dominant form of scattering is visco-inertial, while thermal scattering becomes insignificant [3].



(a)



(b)

Figure 2.1 (a) shows the scattering profile of a single spherical particle immersed in a viscous fluid and subject to an acoustic compressional wave field in the long wavelength (Rayleigh) limit. Figure 2.1 (b) shows the inertial force F_i and the viscous force F_v acting on the particle as the acoustic wave sets the particle into vibratory motion.

The total wave field, which is expressed as an infinite sum of partial wave orders, can be approximated to a sum of the first few orders in the long wavelength region. Figure 2.1 (a) shows the first few multipole components for an incident compressional wave: a monopole component due to the particle pulsation originating from the compressibility contrast, a dipole component due to the particle oscillation stemming from the density contrast, and a quadrupole component arising from the shear modulus contrast. At higher frequencies, more and more partial wave modes are required to calculate the total wave field, which entails the determination of higher order scattering coefficients.

In this chapter we calculate analytical expressions for scattering coefficients for an elastic spherical particle embedded in a viscous liquid for arbitrary partial wave orders by taking account of the inherent coupling between compressional and shear wave modes. We start with a brief review of single-sphere scattering and then discuss the essential theory to study scattering by a sphere in order to facilitate the derivations of scattering coefficients. At the end of this chapter we present the numerical results for scattering coefficients.

2.2 LITERATURE REVIEW

Early work was mainly focused on the scattering of scalar (sound) wave by a single inclusion embedded in an inviscid fluid because of less mathematical complexity. Lord Rayleigh first theoretically investigated the scattering of sound by a spherical inclusion in an ideal fluid in 1872. He obtained the exact solution to the problem in terms of an infinite series involving products of Bessel functions and Legendre polynomials, known as the Rayleigh partial wave method. For the case of a rigid particle, he performed the calculation for a particle of size comparable to the wavelength, but in the case of a fluid scatterer, he confined himself on account of mathematical difficulty to the case when the dimension of the fluid scatterer is much smaller than the wavelength, also known as *Rayleigh scattering* $k_c a \ll 1$, where k_c is the compressional wavenumber and a the radius of the particle [16]. Rayleigh's solution, being in the form of an infinite series, does not pose any difficulty for $k_c a \ll 1$, because only the first few terms of the series contribute significantly.

The work of Rayleigh - which opened the door to acoustic scattering theory - was built on by a number of workers over the years. Since Rayleigh in his treatment assumed the spherical obstacle to be either liquid or perfectly rigid, Herzfeld extended Rayleigh's theory for an elastic spherical inclusion with finite elastic constants, but he focused attention on a small-sphere limit as did Rayleigh for the fluid inclusion [17]. Faran conducted a similar investigation to that of Herzfeld; he derived an exact analytical solution for the scattering phase angle for an arbitrary partial wave order by taking both the transmitted compressional and shear wave in the sphere as well as the scattered compressional wave in the fluid [18]. Since important contributions to the acoustic scattering arise when the dimension of a scatterer is comparable to the wavelength, Anderson, neglecting both viscous and thermal

effects, analytically calculated the reflectivity coefficient for a sphere of diameter up to several wavelength; the coefficient reduced to that obtained by Rayleigh in the limit of small acoustic-radius [19]. Hart reported formulas for the reflectivity and total cross section for scattering of sound wave from a sphere of arbitrary size when the acoustic properties of the sphere are close to those of the host fluid [20].

For the case of an elastic sphere embedded in another elastic medium, the situation is more complicated because when an elastic wave of either the compressional or shear type interacts with an elastic scatterer, waves of both types are generated in the scattered field and inside the scatterer. Since developing full elastic wave treatments is difficult, most studies employ various approximations to tackle the problem. Ying and Truell first reported on a theoretical study of the scattering of elastic waves from a spherical inhomogeneity embedded in an elastic solid matrix for an incident plane compressional wave; they considered three different types of spherical inclusions: an elastic sphere, a spherical cavity, and a rigid sphere [21]. They dealt with each type of inclusion separately instead of obtaining them from the elastic sphere case because some terms in their general solution become ambiguous when taking the limiting value of the density of the particle. Pao and Mow improved Ying and Truell's results by redefining the boundary conditions for a rigid sphere assuming that the rigid sphere undergoes translational motion in its surrounding elastic solid, and then demonstrated that the result of the elastic sphere reduced to all three types of spheres, i.e. rigid, fluid, and cavity, by taking their corresponding limits [22]. Einspruch and Truell adopted the method of Ying and Truell to study the scattering of a plane compressional wave by a fluid-filled spherical cavity and obtained explicit expressions for the scattering coefficients [23]. Knopoff published two articles in 1959 where he explored the scattering of a plane compressional wave [24] and of a shear wave [25] by a perfectly rigid sphere imbedded in an elastic solid medium and calculated the directivity pattern in the far field for both types of waves.

Einspruch and his co-workers published a paper in 1960 where they investigated the scattering of a plane transverse (shear) wave by four different types of spherical obstacle in an elastic solid matrix [26]. Kraft and his co-workers, in the light of Einspruch *et al.*'s analytical results, carried out a numerical study on the transverse scattering cross section for a wide range of shear wavenumber-radius values for a spherical cavity [27], and an elastic sphere [28]. One of the results of Ying and Truell's, and Einspruch *et al.*'s work was

that the scattering cross section for a rigid sphere was independent of the wavelength in the Rayleigh limit. They considered the rigid sphere to be immovable in the solid matrix, meaning that the resultant displacement due to the combined incident and scattered waves vanishes at the surface of the sphere. Iwashimizu, on the contrary, while working on the same problem, treated the rigid sphere as movable and demonstrated that the scattering cross-section depends on the inverse of the fourth power of the wavelength in the Rayleigh limit as it does for other types of spherical obstacles [29]. Iwashimizu pointed out that Einspruch *et al.*'s expression of the scattering cross section of an elastic sphere diverges in the limit of rigid sphere, and calculated a modified expression which reduces to the rigid sphere case in the limit of infinite shear modulus of the particle.

Waterman developed a matrix theory to study the scattering of elastic (and electromagnetic) waves by an elastic inclusion of general shape embedded in an elastic solid [30]. Waterman scattering theory was based only on the compressional wave mode, which is governed by a single scalar wave equation. Varathrajulu and Pao extended Waterman's matrix theory to full elastic wave scattering by taking account of the coupling between longitudinal and transverse waves [31]. Hinders undertook a study on the scattering from an elastic obstacle of arbitrary size for the case of a planar incident compressional or shear wave, and derived exact solutions for the scattered waves; he also analytically obtained expressions for the scattering cross section and extinction coefficients [32]. Sessarego *et al.* conducted an experiment to measure the scattering of a compressional wave by an aluminium sphere embedded in Plexiglas, which validated their own analytical results [33].

Scattering of acoustic waves from a single inclusion in a viscous fluid has also drawn much attention in the literature. Viscous fluids support shear waves just like elastic solids do, but in viscous fluids they are lossy. Sewell was the first to calculate the loss of energy due to scattering from an incident sound wave in the presence of a rigid, infinitely heavy (immovable) particle by taking account of the viscous nature of the host fluid (gas) [34]. Epstein and Carhart treated the scattering of acoustic waves from a fluid sphere in viscous and thermally conducting fluids with a view to calculating attenuation due to sound propagation in a random dispersion of fluid particles in another fluid phase [2]. A similar approach was followed by Allegra and Hawley, in which they extended the work of Epstein and Carhart to an elastic sphere [3]. More recently, Pinfield and Challis obtained an analytical solution for the long-wavelength zero-order scattering coefficient for a fluid

sphere suspended in a fluid medium by taking viscous and thermal effects into consideration [35]. They expressed the zero-order scattering coefficient as a sum of thermal and non-thermal contributions and improved each term in accuracy by retaining terms of order $(k_c a)^2$ which had been neglected by previous workers. Pinfield and Forrester presented analytical expressions for the first-order scattering coefficients of an elastic sphere immersed in a viscous fluid for both incident compressional and shear waves [10]. Although the expressions have been derived under the assumption of long compressional wavelength, the shear wavelength in the host fluid is regarded as general.

Kuster and Toksoz have obtained solutions of scattering coefficients of a solid particle in a solid matrix for an arbitrary mode when the scattering takes place in the Rayleigh region [12]. Since, as a general rule, the compressional and shear wavelengths are of the same order of magnitude in most solids, the problem can be reasonably simplified in the Rayleigh regime, since both compressional and shear wavelengths are long compared with the particle size. In a viscous fluid, on the other hand, the situation is different. As the wavelength of a shear wave can be one or more orders of magnitude smaller than that of the compressional wave in a viscous fluid, or of the compressional and shear waves in the solid, the problem becomes comparatively complicated when addressed under the long compressional wavelength approximation while at the same time imposing no restriction on the shear wavelength. For this situation, Pinfield and Forrester have obtained analytical solutions for scattering coefficients for the dipole-scattering mode as just mentioned above. Nonetheless, no analytical expressions for the scattering coefficients for general partial wave orders for this problem have been reported as yet. This chapter concentrates on the interaction of planar compressional and viscous shear waves with an elastic sphere embedded in a viscous fluid with a particular focus on obtaining analytical approximations for scattering coefficients from the boundary-value problems. The purpose of this study is to investigate the effect of fluid viscosity on acoustic wave scattering through the inherent coupling between compressional and viscous wave modes. Under particular conditions the general expressions obtained are shown to coincide with the earlier results available in the literature.

2.3 FORMULATION OF THE PROBLEM

2.3.1 Wave Equation

From the equation of motion of an elastic solid and the linear stress-strain relations for a homogenous isotropic elastic medium, we obtain the following equation:

$$(\lambda + \mu) \nabla (\nabla \cdot \mathbf{u}) + \mu \nabla^2 \mathbf{u} = \rho \frac{\partial^2 \mathbf{u}}{\partial t^2} \quad (2.1)$$

where $\mathbf{u}(\mathbf{r}, t)$ is the displacement field, ∇ the vector differential operator, t the time, ρ the mass density. λ and μ are so-called Lamé parameters which characterise the medium and can also take complex values to represent lossy materials [36].

The well-known Helmholtz decomposition [37] allows us to resolve \mathbf{u} into the sum of an irrotational vector field and a solenoidal vector field:

$$\mathbf{u} = \nabla \Phi + \nabla \times \mathbf{A} \quad (2.2)$$

where $\Phi(\mathbf{r}, t)$ and $\mathbf{A}(\mathbf{r}, t)$ are scalar and vector potentials. It should be noted that Eqn. (2.2) relates the three components of the displacement vector to four other functions: the scalar potential and the three components of the vector potentials. This indicates that Φ and the components of \mathbf{A} should be subjected to an additional constraint condition, usually taken as $\nabla \cdot \mathbf{A} = 0$ [38].

Upon insertion of Eqn. (2.2) into Eqn. (2.1) and after some algebra we obtain:

$$\nabla \left[(\lambda + 2\mu) \Delta \Phi - \rho \frac{\partial^2 \Phi}{\partial t^2} \right] + \nabla \times \left[\mu \Delta \mathbf{A} - \rho \frac{\partial^2 \mathbf{A}}{\partial t^2} \right] = \mathbf{0} \quad (2.3)$$

Equation (2.3) can be split into two homogeneous wave equations: one scalar and one vector,

$$(\lambda + 2\mu) \Delta \Phi - \rho \frac{\partial^2 \Phi}{\partial t^2} = 0 \quad (2.4)$$

$$\mu \Delta \mathbf{A} - \rho \frac{\partial^2 \mathbf{A}}{\partial t^2} = \mathbf{0} \quad (2.5)$$

Although the wave equations are separated, the two potentials are usually coupled by the boundary conditions, provided that the physical domain is infinite. We assume that the potentials are time harmonic plane waves with angular frequency ω such that the time-dependence is $\exp(-i\omega t)$, which implies that $\partial/\partial t \rightarrow -i\omega$.

Applying Fourier Transforms, the time dependent wave equations (2.4) and (2.5) reduce to Helmholtz wave equations

$$(\Delta + k_c^2)\Phi = 0 \quad (2.6)$$

$$(\Delta + k_s^2)\mathbf{A} = \mathbf{0} \quad (2.7)$$

$$\text{where } k_c^2 = \frac{\rho}{\lambda + 2\mu}\omega^2 \quad (2.8)$$

$$\text{and } k_s^2 = \frac{\rho}{\mu}\omega^2. \quad (2.9)$$

Here k_c and k_s are the longitudinal (compressional) and transverse (shear) wavenumbers respectively. The compressional and shear wavenumbers for a viscous fluid can be written as:

$$k_c = \frac{\omega}{v_c} + i\alpha(\omega) \quad (2.10)$$

$$\text{and } k_s = \sqrt{\frac{\rho\omega}{2\eta}}(1 + i) \quad (2.11)$$

where v_c is the adiabatic sound speed, $\alpha(\omega)$ is the attenuation parameter and η is the shear viscosity. It is generally the practice to add a small imaginary parameter $i\alpha$ to the wavenumber in order to account for the attenuation.

By reason of the decoupling of Eqn. (2.3) into two separate wave equations, it is evident that both plane compressional and shear waves can independently propagate in an infinite homogeneous isotropic medium retaining their individuality and with their respective characteristic velocities. The waves, however, cannot propagate independently of each other if the medium contains discontinuities in elastic properties. If a wave of either kind

encounters a scattering obstacle, waves of both kinds are produced at the surface of the particle. If the scatterer is an elastic solid or a viscous fluid, waves of both kinds are generated inside the scatterer as well. The process in which the energy redistributes at the boundary of the scatterer from a given type of elastic/acoustic wave to a wave of the other type is known as *wave mode conversion*.

2.3.2 Symmetry and Solutions of Wave Equations

We use a spherical coordinate (r, θ, ϕ) , with $r \geq 0$, $0 \leq \theta \leq \pi$, $0 \leq \phi < 2\pi$, located at the centre of a spherical particle of radius a . We consider the propagation case where the plane incident wave (compression/shear) propagates in the $+z$ -direction.

The vector potential \mathbf{A} can be expressed in terms of two scalar potentials, known as Debye potentials [39]:

$$\mathbf{A} = \nabla \times (\mathbf{r}\psi) + \nabla \times \nabla \times (\mathbf{r}\chi) \quad (2.12)$$

such that $(\Delta + k_s^2)(\psi, \chi) = 0$, where \mathbf{r} is the radial vector.

The rigorous mathematical proof of Eqn. (2.12) can be found in the Ref. [40]. The two Debye potentials ψ and χ represent two polarizations of the transverse (shear) wave [37, 42]. The Φ potential is coupled with the ψ and vice versa, while χ is decoupled from both Φ and ψ . Since the χ potential only interacts with itself and is not related to mode-conversion, it will not appear any further in our discussion. From here on in we use the ψ potential to refer to “shear wave or s -wave” throughout the thesis for convenience.

Let us consider that an incident plane compressional wave, impinging on the particle, has the form $\Phi = \Phi_0 \exp(\mathbf{i}\mathbf{k}_c \cdot \mathbf{r}) = \Phi_0 \exp(\mathbf{i}\mathbf{k}_c \cdot r\hat{\mathbf{z}})$. Henceforth, for convenience, the time dependence factor $\exp(-i\omega t)$ will be omitted from all expressions representing waves throughout the thesis.

The Helmholtz equation (2.6) admits a general solution of the following form:

$$(\Phi, \psi) = \sum_{n=0}^{\infty} \sum_{m=-n}^n Q_{mn} z_n(k_p r) P_n^m(\cos \theta) \exp(im\phi). \quad (p = c \text{ or } s). \quad (2.13)$$

where Q_{mm} are the expansion coefficients, $z_n(k_q r)$ are the spherical Bessel functions of order n , $P_n^m(\cos\theta)$ are Legendre functions, and the indexes c and s stand for ‘compression’ and ‘shear’ respectively. The Bessel functions, depending on the medium in which a wave exists, need to be chosen accordingly. In the infinite embedding medium, the solution must be defined at large distances, while within the spherical particle, the solution must be regular (continuous) at the origin.

In the next chapter, we shall study the scattering of a shell consisting of a core solid particle of radius a , surrounded by a spherical shell of a viscous fluid, when the whole is submitted to an incident harmonic compressional plane wave. For an incident compressional wave (c) propagating in the z direction, by virtue of the azimuthal symmetry, the angular dependence of the plane wave is just $P_n(\cos\theta)$, and one can write:

$$\Phi_{\text{inc}} = \sum_{n=0}^{\infty} i^n (2n+1) j_n(k_c r) P_n(\cos\theta) \quad (2.14)$$

This incident plane wave on the shell will give rise to two incident waves onto the core, a compressional of the same form as in equation (2.14) and a shear wave (s) of a similar form:

$$\psi_{\text{inc}} = \sum_{n=0}^{\infty} i^n (2n+1) j_n(k_s r) P_n(\cos\theta) \quad (2.15)$$

The incident compressional wave (p) scatters into both c and s waves outside the particle with the potentials:

$$\Phi_c = \sum_{n=0}^{\infty} i^n (2n+1) T_n^{cc} h_n(k_c r) P_n(\cos\theta) \quad (2.16)$$

$$\psi_s = \sum_{n=0}^{\infty} i^n (2n+1) T_n^{cs} h_n(k_s r) P_n(\cos\theta) \quad (2.17)$$

Here $h_n(u)$ are spherical Hankel functions of the first kind of the order n . These $h_n(u)$ functions have asymptotic behaviour as $i^{-(n+1)} \exp(iu) / u$ and hence represent a scattered (outgoing) wave.

The incident s wave mode likewise scatters into both c and s waves with the potentials:

$$\Phi_s = \sum_{n=0}^{\infty} i^n (2n+1) T_n^{sc} h_n(k_c r) P_n(\cos \theta) \quad (2.18)$$

$$\psi_s = \sum_{n=0}^{\infty} i^n (2n+1) T_n^{ss} h_n(k_s r) P_n(\cos \theta) \quad (2.19)$$

The refracted c and s waves inside the particle due to the incident p have the potentials,

$$\Phi'_c = \sum_{n=0}^{\infty} i^n (2n+1) A_n^{cc} j_n(k'_c r) P_n(\cos \theta) \quad (2.20)$$

$$\psi'_s = \sum_{n=0}^{\infty} i^n (2n+1) A_n^{cs} j_n(k'_s r) P_n(\cos \theta) \quad (2.21)$$

and for the case of an incident s wave mode,

$$\Phi'_s = \sum_{n=0}^{\infty} i^n (2n+1) A_n^{sc} j_n(k'_c r) P_n(\cos \theta) \quad (2.22)$$

$$\psi'_s = \sum_{n=0}^{\infty} i^n (2n+1) A_n^{ss} j_n(k'_s r) P_n(\cos \theta) \quad (2.23)$$

where k'_c and k'_s are wavenumbers of c and s waves inside the particle. The set of expansion coefficients T_n^{cc} to A_n^{ss} are the amplitudes of the partial wave modes and are determined from the interface condition at the particle surface $r = a$.

2.3.3 Displacement and Stress Expressions

The displacement and stress components are continuous at the surface of the particle. The continuity of the displacement vector ensures that the particle always remains in intimate

contact with its surrounding material, while the continuity of the traction guarantees that the acceleration at the boundary does not go infinite [28].

For a single particle, the boundary conditions prescribed at the interface between the particle and the continuous phase are as follows:

$$u_r^+(r = a) = u_r^-(r = a) \quad (\text{radial displacement}) \quad (2.24)$$

$$u_\theta^+(r = a) = u_\theta^-(r = a) \quad (\text{tangential displacement}) \quad (2.25)$$

$$\sigma_{rr}^+(r = a) = \sigma_{rr}^-(r = a) \quad (\text{normal stress}) \quad (2.26)$$

$$\sigma_{r\theta}^+(r = a) = \sigma_{r\theta}^-(r = a) \quad (\text{tangential stress}) \quad (2.27)$$

u_ϕ and $\sigma_{r\phi}$ vanish due to the azimuthal symmetry.

To obtain the boundary condition equations, physical quantities such as displacement and stress require that they be expressed in terms of potentials. The displacement and stress components entering into the above boundary conditions can be expressed in terms of potentials in spherical coordinates as:

$$u_r = \frac{\partial \Phi}{\partial r} - \frac{1}{r} \left(\frac{\partial^2 \psi}{\partial \theta^2} + \cot \theta \frac{\partial \psi}{\partial \theta} \right) \quad (2.28)$$

$$u_\theta = \frac{1}{r} \frac{\partial}{\partial \theta} (\Phi + \psi) + \frac{\partial^2 \psi}{\partial r \partial \theta} \quad (2.29)$$

$$\sigma_{rr} = \frac{\rho \omega^2}{k_s^2} \left[(2k_c^2 - k_s^2) \Phi + 2 \frac{\partial^2 \Phi}{\partial r^2} \right] + \frac{2\rho \omega^2}{k_s^2} \frac{\partial}{\partial r} \left[-\frac{1}{r} \left(\frac{\partial^2 \psi}{\partial \theta^2} + \cot \theta \frac{\partial \psi}{\partial \theta} \right) \right] \quad (2.30)$$

$$\begin{aligned} \sigma_{r\theta} = & \frac{\rho \omega^2}{k_s^2} \left\{ \frac{1}{r} \frac{\partial}{\partial \theta} \left[-\frac{1}{r} \left(\frac{\partial^2 \psi}{\partial \theta^2} + \cot \theta \frac{\partial \psi}{\partial \theta} \right) \right] + \frac{\partial}{\partial r} \left(\frac{\partial^2 \psi}{\partial r \partial \theta} + \frac{1}{r} \frac{\partial \psi}{\partial \theta} \right) - \frac{1}{r} \left(\frac{\partial^2 \psi}{\partial r \partial \theta} + \frac{1}{r} \frac{\partial \psi}{\partial \theta} \right) \right\} \\ & + \frac{\rho \omega^2}{k_s^2} \left[\frac{1}{r} \frac{\partial^2 \Phi}{\partial r^2} + \frac{\partial}{\partial r} \left(\frac{1}{r} \frac{\partial \Phi}{\partial \theta} \right) - \frac{1}{r^2} \frac{\partial \Phi}{\partial \theta} \right] \end{aligned} \quad (2.31)$$

2.3.4 Boundary Condition Equations

For the sake of compactness, let us define the dimensionless longitudinal and shear wavenumbers in the host medium as $y_c := k_c a$ and $y_s := k_s a$ respectively, and in the spherical particle as $y'_c := k'_c a$ and $y'_s := k'_s a$ respectively. Terms of equal orders in the series expansion are equated thanks to the orthogonal property of the Legendre polynomials, producing the following four equations from the boundary conditions in the order of radial displacement, tangential displacement, radial stress component and tangential stress component, respectively for an incident compressional wave:

$$\begin{aligned} & y_c j'_n(y_c) + T_n^{cc} y_c h'_n(y_c) + T_n^{cs} n(n+1) h_n(y_s) \\ &= A_n^{cc} y'_c j'_n(y'_c) + A_n^{cs} n(n+1) j_n(y'_s) \end{aligned} \quad (2.32)$$

$$\begin{aligned} & j_n(y_c) + T_n^{cc} h_n(y_c) + T_n^{cs} [y_s h'_n(y_s) + h_n(y_s)] \\ &= A_n^{cc} j_n(y'_c) + A_n^{cs} [y'_s j'_n(y'_s) + j_n(y'_s)] \end{aligned} \quad (2.33)$$

$$\begin{aligned} & \frac{\rho}{y_s^2} \left\{ (y_s^2 - 2n(n+1)) j_n(y_c) + 4y_c j'_n(y_c) \right\} \\ & + T_n^{cc} \frac{\rho}{y_s^2} \left\{ (y_s^2 - 2n(n+1)) h_n(y_c) + 4y_c h'_n(y_c) \right\} \\ & + 2T_n^{cs} \frac{\rho}{y_s^2} n(n+1) [h_n(y_s) - y_s h'_n(y_s)] \\ &= A_n^{cc} \frac{\rho'}{y_s'^2} \left\{ [y_s'^2 - 2n(n+1)] j_n(y'_c) + 4y'_c j'_n(y'_c) \right\} \\ & + 2A_n^{cs} \frac{\rho'}{y_s'^2} n(n+1) [j_n(y'_s) - y'_s j'_n(y'_s)] \end{aligned} \quad (2.34)$$

$$\begin{aligned}
& 2 \frac{\rho}{y_s^2} [j_n(y_c) - y_c j_n'(y_c)] + 2T_n^{cc} \frac{\rho}{y_s^2} [h_n(y_c) - y_c h_n'(y_c)] \\
& + T_n^{cs} \frac{\rho}{y_s^2} \{2y_s h_n' + [y_s^2 - 2n(n+1) + 2] h_n(y_s)\} \\
& = 2A_n^{cc} \frac{\rho'}{y_s'^2} [j_n(y_c') - y_c' j_n'(y_c')] \\
& + A_n^{cs} \frac{\rho'}{y_s'^2} \{2y_s' j_n' + [y_s'^2 - 2n(n+1) + 2] j_n(y_s')\}
\end{aligned} \tag{2.35}$$

The scattering coefficients are obtained as a solution to these four linear algebraic equations. In a similar fashion, for an incident shear wave, one can readily write the following boundary equations:

$$\begin{aligned}
& y_s j_n'(y_s) + j_n(y_s) + T_n^{sc} h_n(y_c) + T_n^{ss} [y_s h_n'(y_s) + h_n(y_s)] \\
& = A_n^{sc} j_n(y_c') + A_n^{ss} [y_s' j_n'(y_s') + j_n(y_s')]
\end{aligned} \tag{2.36}$$

$$\begin{aligned}
& n(n+1) j_n(y_s) + T_n^{sc} y_c h_n'(y_c) + T_n^{ss} n(n+1) h_n(y_s) \\
& = A_n^{sc} y_c' j_n'(y_c') + A_n^{ss} n(n+1) j_n(y_s')
\end{aligned} \tag{2.37}$$

$$\begin{aligned}
& 2 \frac{\rho}{y_s^2} n(n+1) [j_n(y_s) - y_s j_n'(y_s)] \\
& + T_n^{sc} \frac{\rho}{y_s^2} \{(y_s^2 - 2n(n+1)) h_n(y_c) + 4y_c h_n'(y_c)\} \\
& + 2T_n^{ss} \frac{\rho}{y_s^2} n(n+1) [h_n(y_s) - y_s h_n'(y_s)] \\
& = A_n^{sc} \frac{\rho'}{y_s'^2} \{[y_s'^2 - 2n(n+1)] j_n(y_c') + 4y_c' j_n'(y_c')\} \\
& + 2A_n^{ss} \frac{\rho'}{y_s'^2} n(n+1) [j_n(y_s') - y_s' j_n'(y_s')]
\end{aligned} \tag{2.38}$$

$$\begin{aligned}
& \frac{\rho}{y_s^2} \left\{ 2y_s j'_n + \left[y_s^2 - 2n(n+1) + 2 \right] j_n(y_s) \right\} \\
& + 2T_n^{sc} \frac{\rho}{y_s^2} \left[h_n(y_c) - y_c h'_n(y_c) \right] \\
& + T_n^{ss} \frac{\rho}{y_s^2} \left\{ 2y_s h'_n + \left[y_s^2 - 2n(n+1) + 2 \right] h_n(y_s) \right\} \\
& = 2A_n^{sc} \frac{\rho'}{y_s'^2} \left[j_n(y'_c) - y'_c j'_n(y'_c) \right] \\
& + A_n^{ss} \frac{\rho'}{y_s'^2} \left\{ 2y'_s j'_n + \left[y_s'^2 - 2n(n+1) + 2 \right] j_n(y'_s) \right\}
\end{aligned} \tag{2.39}$$

2.4 SCATTERING COEFFICIENTS

The expansion coefficients T_n^{pq} in the above boundary equations are the scattering coefficients, each representing the scattering process and mode conversion at a single particle for a wave of mode q mode-converted from an incident wave of mode p for a partial wave of order n . Scattering coefficients characterise how a scatterer scatters waves, and as a general rule, depend on the geometry, the frequency and the properties of component phases (i.e. density, compressibility). Although analytical approximations for the monopole and dipole scattering coefficients have already been reported in the literature, we derive them in the next sections for the purpose of using them in the next chapter. We then go on to obtain analytical solutions for scattering coefficients for general partial wave orders.

2.4.1 Monopole-Scattering Coefficient

The zeroth-order mode is the monopole mode, which is characterised by an axisymmetric contraction and expansion of the particle and its surrounding medium, with no translatory motion - shear waves are absent. The equations for the polar displacement and stress components are identically zero, and therefore the system reduces to the following two boundary equations:

$$\begin{aligned}
& y_c j'_0(y_c) + T_0^{cc} y_c h'_0(y_c) \\
& = A_0^{cc} y'_c j'_0(y'_c)
\end{aligned} \tag{2.40}$$

$$\begin{aligned}
& -(\lambda + 2\mu)y_c^2 j_0(y_c) - 4\mu y_c j_0'(y_c) \\
& + T_0^{\text{cc}} \left[-(\lambda + 2\mu)y_c^2 h_0(y_c) - 4\mu y_c h_0'(y_c) \right] \\
& = A_0^{\text{cc}} \left[-(\lambda' + 2\mu')y_c'^2 j_0(y_c') - 4\mu' y_c' j_0'(y_c') \right]
\end{aligned} \tag{2.41}$$

We express the stress components in terms of (complex) Lamé parameters for reasons that will become apparent in the next chapter. Since $y_c, y_c' \ll 1$, we retain only the leading-order terms in the power-series expansions of the Bessel and Hankel functions, and obtain:

$$T_0^{\text{cc}} = \frac{3(\lambda - \lambda') + 2(\mu - \mu')}{3(4\mu + 3\lambda + 2\mu')} y_c^3, \tag{2.42}$$

or in terms of bulk modulus:

$$T_0^{\text{cc}} = i \frac{(B - B')}{4\mu + 3B'} y_c^3, \tag{2.43}$$

where $B = \lambda + (2/3)\mu$ and $B' = \lambda' + (2/3)\mu'$ are the bulk moduli in the host fluid and in the sphere respectively. This expression agrees with the Refs. [14, 22] for an elastic solid host and the Ref. [2] for a viscous host fluid.

2.4.2 Dipole-Scattering Coefficients

The boundary condition equations for the dipole scattering for an incident compression wave are obtained by setting $n=1$ in Eqns. (2.32) to (2.35).

$$T_1^{\text{cc}} y_c h_1'(y_c) + 2T_1^{\text{cs}} h_1(y_s) - A_1^{\text{cc}} y_c' j_1'(y_c') - 2A_1^{\text{cs}} j_1(y_s') = -y_c j_1'(y_c) \tag{2.44}$$

$$\begin{aligned}
& T_1^{\text{cc}} h_1(y_c) + T_1^{\text{cs}} \left[y_s h_1'(y_s) + h_1(y_s) \right] - A_1^{\text{cc}} j_1(y_c') \\
& - A_1^{\text{cs}} \left[y_s' j_1'(y_s') + j_1(y_s') \right] = -j_1(y_c)
\end{aligned} \tag{2.45}$$

$$\begin{aligned}
& T_1^{\text{cc}} \frac{\rho}{y_s^2} \left\{ y_s^2 h_1(y_c) - 4[h_1(y_c) - y_c h_1'(y_c)] \right\} \\
& + 4T_1^{\text{cs}} \frac{\rho}{y_s^2} [h_1(y_s) - y_s h_1'(y_s)] \\
& - A_1^{\text{cc}} \frac{\rho'}{y_s'^2} \left\{ y_s'^2 j_1(y_c') - 4[j_1(y_c') - y_c' j_1'(y_c')] \right\} \\
& - 4A_1^{\text{cs}} \frac{\rho'}{y_s'^2} [j_1(y_s') - y_s' j_1'(y_s')] \\
& = -\frac{\rho}{y_s^2} \left\{ y_s^2 j_1(y_c) - 4[j_1(y_c) - y_c j_1'(y_c)] \right\}
\end{aligned} \tag{2.46}$$

$$\begin{aligned}
& 2T_1^{\text{cc}} \frac{\rho}{y_s^2} [h_1(y_c) - y_c h_1'(y_c)] \\
& + T_1^{\text{cs}} \frac{\rho}{y_s^2} \left[-2[h_1(y_s) - y_s h_1'(y_s)] + y_s^2 h_1(y_s) \right] \\
& - 2A_1^{\text{cc}} \frac{\rho'}{y_s'^2} [j_1(y_c') - y_c' j_1'(y_c')] \\
& - A_1^{\text{cs}} \frac{\rho'}{y_s'^2} \left\{ -2[j_1(y_s') - y_s' j_1'(y_s')] + y_s'^2 j_1(y_s') \right\} \\
& = -\frac{2\rho}{y_s^2} [j_1(y_c) - y_c j_1'(y_c)]
\end{aligned} \tag{2.47}$$

Multiplying Eqn. (2.47) by 2 and then adding it to (2.46) yields:

$$T_1^{\text{cc}} \frac{\rho}{\rho'} h_1(y_c) + 2T_1^{\text{cs}} \frac{\rho}{\rho'} h_1(y_s) - A_1^{\text{cc}} j_1(y_c') - 2A_1^{\text{cs}} j_1(y_s') = -\frac{\rho}{\rho'} j_1(y_c) \tag{2.48}$$

We now subtract Eqn. (2.45) from Eqn. (2.44) and Eqn. (2.48) from (2.45). The particle in question is a solid in which both y_c' and y_s' are about the same order of magnitude and hence are small in the Rayleigh regime. This helps us simplify the calculation by taking advantage of their smallness and hence keeping only the leading-order terms of Bessel functions of arguments y_c' and y_s' . Carrying out all the operations results in the following two simplified equations:

$$[y_c h_1'(y_c) - h_1(y_c)] T_1^{\text{cc}} + [-y_s h_1'(y_s) + h_1(y_s)] T_1^{\text{cs}} = j_1(y_c) - y_c j_1'(y_c) \tag{2.49}$$

$$(\hat{\rho} - 1) h_1(y_c) T_1^{\text{cc}} + [\hat{\rho} y_s h_1'(y_s) - (2 - \hat{\rho}) h_1(y_s)] T_1^{\text{cs}} = (1 - \hat{\rho}) j_1(y_c) \tag{2.50}$$

Solving the system of equations gives:

$$T_1^{cc} = \frac{h_1(y_s)[(2\hat{\rho}-3)j_1(y_c) - (\hat{\rho}-2)y_c j_1'(y_c)] + y_s h_1'(y_s)[j_1(y_c) - \hat{\rho}y_c j_1'(y_c)]}{-h_1(y_c)[(2\hat{\rho}-3)h_1(y_s) + y_s h_1'(y_s)] + y_c h_1'(y_c)[(\hat{\rho}-2)h_1(y_s) + \hat{\rho}y_s h_1'(y_s)]} \quad (2.51)$$

$$T_1^{cs} = \frac{(\hat{\rho}-1)y_c [h_1(y_c)j_1'(y_c) - j_1(y_c)h_1'(y_c)]}{-h_1(y_c)[(2\hat{\rho}-3)h_1(y_s) + y_s h_1'(y_s)] + y_c h_1'(y_c)[(\hat{\rho}-2)h_1(y_s) + \hat{\rho}y_s h_1'(y_s)]} \quad (2.52)$$

Taking series expansions of the Bessel and Hankel functions of small arguments produce:

$$T_1^{cc} = -\frac{iy_c^3 [h_1(y_s) - y_s h_1'(y_s)](\hat{\rho}-1)}{3[(4\hat{\rho}-7)h_1(y_s) + (1+2\hat{\rho})y_s h_1'(y_s)]}, \quad (2.53)$$

and
$$T_1^{cs} = -\frac{(\hat{\rho}-1)y_c}{(4\hat{\rho}-7)h_1(y_s) + (1+2\hat{\rho})y_s h_1'(y_s)} \quad (2.54)$$

which are exactly the same as those derived in Ref. [7].

Using the recurrence relations (A9) and (A10), one can show that:

$$T_1^{cc} = \frac{iy_c^3 (\hat{\rho}-1)h_2(y_s)}{3[3h_2(y_s) - 2(\hat{\rho}-1)h_0(y_s)]} \quad (2.55)$$

$$T_1^{cs} = \frac{(\hat{\rho}-1)y_c}{3h_2(y_s) - 2(\hat{\rho}-1)h_0(y_s)} \quad (2.56)$$

Equation (2.55) agrees with Ref. [3].

Employing the same technique, one can solve the problem straightforwardly for the shear incident case. For an incident shear wave, we have the follow system of equations:

$$T_1^{sc} y_c h_1'(y_c) + 2T_1^{ss} h_1(y_s) - A_1^{sc} y_c' j_1'(y_c') - 2A_1^{ss} j_1(y_s') = -2j_1(y_s) \quad (2.57)$$

$$\begin{aligned}
& T_1^{\text{sc}} h_1(y_c) + T_1^{\text{ss}} [y_s h_1'(y_s) + h_1(y_s)] \\
& - A_1^{\text{sc}} j_1(y'_c) - A_1^{\text{ss}} [y'_s j_1'(y'_s) + j_1(y'_s)] \\
& = -[y_s j_1'(y_s) + j_1(y_s)]
\end{aligned} \tag{2.58}$$

$$\begin{aligned}
& T_1^{\text{sc}} \frac{\rho}{y_s} \{y_s^2 h_1(y_c) - 4[h_1(y_c) - y_c h_1'(y_c)]\} \\
& + 4T_1^{\text{ss}} \frac{\rho}{y_s^2} [h_1(y_s) - y_s h_1'(y_s)] \\
& - A_1^{\text{sc}} \frac{\rho'}{y_s'^2} \{y_s'^2 j_1(y'_c) - 4[j_1(y'_c) - y'_c j_1'(y'_c)]\} \\
& - 4A_1^{\text{ss}} \frac{\rho'}{y_s'^2} [j_1(y'_s) - y'_s j_1'(y'_s)] \\
& = -4 \frac{\rho}{y_s^2} [j_1(y_s) - y_s j_1'(y_s)]
\end{aligned} \tag{2.59}$$

$$\begin{aligned}
& 2T_1^{\text{sc}} \frac{\rho}{y_s} [h_1(y_c) - y_c h_1'(y_c)] \\
& + T_1^{\text{ss}} \frac{\rho}{y_s^2} [-2[h_1(y_s) - y_s h_1'(y_s)] + y_s^2 h_1(y_s)] \\
& - 2A_1^{\text{sc}} \frac{\rho'}{y_s'^2} [j_1(y'_c) - y'_c j_1'(y'_c)] \\
& - A_1^{\text{ss}} \frac{\rho'}{y_s'^2} \{-2[j_1(y'_s) - y'_s j_1'(y'_s)] + y_s'^2 j_1(y'_s)\} \\
& = -\frac{\rho}{y_s^2} [-2[j_1(y_s) - y_s j_1'(y_s)] + y_s^2 j_1(y_s)]
\end{aligned} \tag{2.60}$$

Executing all the steps as mentioned above for the incident compressional wave yields the two simplified equations:

$$[y_c h_1'(y_c) - h_1(y_c)] T_1^{\text{sc}} + [h_1(y_s) - y_s h_1'(y_s)] T_1^{\text{ss}} = y_s j_1'(y_s) - j_1(y_s) \tag{2.61}$$

$$(\hat{\rho} - 1) h_1(y_c) T_1^{\text{sc}} + [\hat{\rho} y_s h_1'(y_s) - (2 - \hat{\rho}) h_1(y_s)] T_1^{\text{ss}} = -\hat{\rho} y_s j_1'(y_s) + (2 - \hat{\rho}) j_1(y_s) \tag{2.62}$$

Solving them for T_1^{sc} and T_1^{ss} , we get:

$$T_1^{\text{sc}} = \frac{2(\hat{\rho} - 1)y_s y_c^2 [j_1(y_s)h_1'(y_s) - j_1'(y_s)h_1(y_s)]}{h_1(y_s)[i(2\hat{\rho} - 3) + (\hat{\rho} - 2)y_c^3 h_1'(y_c)] + [i + \hat{\rho} y_c^3 h_1'(y_c)]y_s h_1'(y_s)} \quad (2.63)$$

$$T_1^{\text{ss}} = -\frac{j_1(y_s)[i(2\hat{\rho} - 3) + (\hat{\rho} - 2)y_c^3 h_1'(y_c)] + [i + \hat{\rho} y_c^3 h_1'(y_c)]y_s j_1'(y_s)}{h_1(y_s)[i(2\hat{\rho} - 3) + (\hat{\rho} - 2)y_c^3 h_1'(y_c)] + [i + \hat{\rho} y_c^3 h_1'(y_c)]y_s h_1'(y_s)} \quad (2.64)$$

After expanding and retaining the leading-order terms of $h_1(y_c)$ and $h_1'(y_c)$, these equations simplify to:

$$T_1^{\text{sc}} = \frac{2(\hat{\rho} - 1)y_c^2}{y_s [(4\hat{\rho} - 7)h_1(y_s) + (2\hat{\rho} + 1)y_s h_1'(y_s)]} \quad (2.65)$$

and
$$T_1^{\text{ss}} = -\frac{(4\hat{\rho} - 7)j_1(y_s) + (2\hat{\rho} + 1)y_s j_1'(y_s)}{(4\hat{\rho} - 7)h_1(y_s) + (2\hat{\rho} + 1)y_s h_1'(y_s)} \quad (2.66)$$

2.4.3 Nth-order Scattering Coefficients

Having derived expressions for the dipole-scattering coefficients, we can now proceed to extend the solution to higher order partial waves. However, the procedure for solving nth-order scattering coefficients is more complicated than that for the dipole case, yet simplification can be achieved thanks to y_c , y_c' and y_s' being small and roughly the same order of magnitude in the long-wavelength regime. We have retained the leading-order terms for Bessel functions with arguments y_c , y_c' and y_s' .

The solution for both incident compressional and shear wave cases proceeds through the following steps:

- $\sigma_{\text{rr}} - n \sigma_{\text{r}\theta}$: All incident wave and internal wave expressions are simplified by retaining the dominant term only since other terms are higher order in y_c , y_c' or y_s . Equation (A) retains all coefficients.

- Equation (A)/ $\rho' - u_\theta$ eliminates compressional wave inside the particle to express the shear wave coefficients inside in terms of the two outer coefficients. It results in equation (B).
- Substitute equation (B) into u_θ (producing equation (C)) relates compressional wave inside to the two outside coefficients.
- Substitute equation (B) and equation (C) into σ_{rr} equation – gives equation (D) – two outside coefficients only
- $n u_\theta - u_r$: Uses recurrence relation to result in Bessel and Hankel functions of order $n + 1$.
 - for incident compressional wave: we neglect the following terms: $O(y_c^{n+1})$ (incident wave), $A_n^{cc} \times O(y_c'^{n+1})$, $A_n^{cs} \times O(y_s'^n)$ relative to the retained terms in $T_n^{cc} \times O(y_c^{-(n+1)})$ and $T_n^{cs} \times O(y_c^0)$. We will later establish (once the order of the scattering coefficients is known) that the neglected terms are of order $O(y_c^{n+1})$, $O(y_c^{n+1})$ and $O(y_c^{2n})$ respectively whereas the retained terms are both $O(y_c^n)$, therefore justifying the approximations. The resulting equation (E) therefore only has the outer scattering coefficients.
 - for incident shear wave: Neglect the following terms: $A_n^{sc} \times O(y_c'^{n+1})$, $A_n^{ss} \times O(y_s'^n)$ relative to the retained terms in $T_n^{sc} \times O(y_c^{-(n+1)})$ and $T_n^{ss} \times O(y_c^0)$. We will later establish (once the order of the scattering coefficients is known) that the neglected terms are of order $O(y_c)$ and $O(y_c^n)$ respectively whereas the retained terms are both $O(y_c^0)$, therefore justifying the approximations. The resulting equation (E) therefore only has the outer scattering coefficients.
- Equations (D) and (E) determine the two outside coefficients.
- We express solution as leading order in y_c using j_n and h_n for small arguments.

With these steps, we now derive the scattering coefficients for incident compressional and shear waves.

Case 1: Compression Incident

On multiplication of Eqn. (2.32) by n and then subtracting it from Eqn. (2.33) yields:

$$T_n^{cc} [n h_n (y_c) - y_c h'_n (y_c)] + T_n^{cs} n [y_s h'_n (y_s) - n h_n (y_s)] = 0 \quad (2.67)$$

Now multiplying Eqn. (2.35) by n and then subtracting it from Eqn. (2.34) gives:

$$\begin{aligned} & \bar{\rho} j_n (y_c) + T_n^{cc} \frac{\bar{\rho}}{y_s^2} \left\{ y_s^2 h_n (y_c) - 2(n+2) [n h_n (y_c) - y_c h'_n (y_c)] \right\} \\ & + T_n^{cs} \frac{\bar{\rho}}{y_s^2} \left\{ 2n(n+2) [n h_n (y_s) - y_s h'_n (y_s)] - n y_s^2 h_n (y_s) \right\} \\ & = A_n^{cc} j_n (y'_c) - A_n^{cs} n j_n (y'_s) \end{aligned} \quad (2.68)$$

where $\bar{\rho} := \frac{\rho}{\rho'}$

Subtracting Eqn. (2.33) from (2.68) and then solving for A_n^{cs} yields:

$$A_n^{cs} = - \frac{(\bar{\rho} - 1) j_n (y_c) + a_1 T_n^{cc} + b_1 T_n^{cs}}{y'_s j'_n (y'_s) + (n+1) j_n (y'_s)} \quad (2.69)$$

where $b_1 = \frac{\bar{\rho}}{y_s^2} [2n(n+2) [n h_n (y_s) - y_s h'_n (y_s)] - n y_s^2 h_n (y_s)] - [y_s h'_n (y_s) + h_n (y_s)]$

$$a_1 = \frac{\bar{\rho}}{y_s^2} \left\{ y_s^2 h_n (y_c) - 2(n+2) [n h_n (y_c) - y_c h'_n (y_c)] \right\} - h_n (y_c)$$

Inserting Eqn. (2.69) in Eqn. (2.33) gives A_n^{cc} in terms of T_n^{cc} and T_n^{cs} .

$$\begin{aligned} & j_n (y_c) + T_n^{cc} h_n (y_c) + T_n^{cs} [y_s h'_n (y_s) + h_n (y_s)] \\ & + \frac{(\bar{\rho} - 1) j_n (y_c) + a_1 T_n^{cc} + b_1 T_n^{cs}}{[y'_s j'_n (y'_s) + (n+1) j_n (y'_s)]} [y'_s j'_n (y'_s) + j_n (y'_s)] \\ & = A_n^{cc} j_n (y'_c) \end{aligned} \quad (2.70)$$

We substitute A_n^{cc} and A_n^{cs} into Eqn. (2.34) and then perform some algebraic manipulation, which produces:

$$\begin{aligned}
& \left[\frac{n}{2n+1} - \frac{1}{y_s'^2} 2n(n-1) \right] \left\{ T_n^{\text{cc}} h_n(y_c) + T_n^{\text{cs}} [y_s h_n'(y_s) + h_n(y_s)] \right\} \\
& + \frac{(n+1)}{(2n+1)} T_n^{\text{cc}} \frac{\bar{\rho}}{y_s^2} \left\{ y_s^2 h_n(y_c) - 2(n+2)[n h_n(y_c) - y_c h_n'(y_c)] \right\} \\
& + \frac{(n+1)}{(2n+1)} T_n^{\text{cs}} \frac{\bar{\rho}}{y_s^2} \left\{ 2n(n+2)[n h_n(y_s) - y_s h_n'(y_s)] - n y_s^2 h_n(y_s) \right\} \\
& - T_n^{\text{cc}} \frac{\bar{\rho}}{y_s^2} \left\{ [y_s^2 - 2n(n+1)] h_n(y_c) + 4y_c h_n'(y_c) \right\} \\
& - T_n^{\text{cs}} \frac{\bar{\rho}}{y_s^2} 2n(n+1) [h_n(y_s) - y_s h_n'(y_s)] \\
& = \frac{n}{2n+1} (\bar{\rho} - 1) j_n(y_c) - \frac{\bar{\rho}}{y_s^2} 2n(n-1) j_n(y_c) + \frac{1}{y_s'^2} 2n(n-1) j_n(y_c)
\end{aligned} \tag{2.71}$$

Now we collect like terms and then simplify:

$$\begin{aligned}
& \frac{n}{2n+1} (1 - \bar{\rho}) h_n(y_c) T_n^{\text{cc}} - \frac{1}{y_s'^2} 2n(n-1) T_n^{\text{cc}} h_n(y_c) \\
& + T_n^{\text{cc}} \frac{\bar{\rho}}{y_s^2} \frac{2n(n-1)}{(2n+1)} [(n+1) h_n(y_c) + y_c h_n'(y_c)] \\
& + \left[\frac{n}{2n+1} - \frac{1}{y_s'^2} 2n(n-1) \right] T_n^{\text{cs}} [y_s h_n'(y_s) + h_n(y_s)] \\
& - \frac{(n+1)}{(2n+1)} \bar{\rho} n h_n(y_s) T_n^{\text{cs}} \\
& + T_n^{\text{cs}} \frac{\bar{\rho}}{y_s^2} \frac{2n(n^2-1)}{(2n+1)} [(n+1) h_n(y_s) + y_s h_n'(y_s)] \\
& = \frac{n}{2n+1} (\bar{\rho} - 1) j_n(y_c) - \frac{\bar{\rho}}{y_s^2} 2n(n-1) j_n(y_c) + \frac{1}{y_s'^2} 2n(n-1) j_n(y_c)
\end{aligned} \tag{2.72}$$

We rewrite Eqn. (2.67) as:

$$T_n^{\text{cs}} = -i \frac{(2n+1)!!}{y_c^{n+1}} \frac{1}{n [n h_n(y_s) - y_s h_n'(y_s)]} T_n^{\text{cc}} = D_n T_n^{\text{cc}} \tag{2.73}$$

where $D_n := -i \frac{(2n+1)!!}{y_c^{n+1}} \frac{1}{n [n h_n(y_s) - y_s h_n'(y_s)]}$

We substitute Eqn. (2.73) into Eqn. (2.72) and perform some algebra and then divide the resulting equation through $\bar{\rho}$:

$$\begin{aligned}
& \left[\frac{n}{2n+1}(1-\bar{\rho}) - \frac{1}{y_s'^2} 2n(n-1) + \frac{\bar{\rho}}{y_s^2} \frac{2n(n^2-1)}{(2n+1)} \right] h_n(y_c) T_n^{\text{cc}} \\
& + \frac{\bar{\rho}}{y_s^2} \frac{2n(n-1)}{(2n+1)} y_c h_n'(y_c) T_n^{\text{cc}} \\
& + \left[\frac{n}{2n+1} - \frac{1}{y_s'^2} 2n(n-1) + \frac{\bar{\rho}}{y_s^2} \frac{2n(n^2-1)}{(2n+1)} \right] [y_s h_n'(y_s) + h_n(y_s)] D_n T_n^{\text{cc}} \\
& + \frac{\bar{\rho} n(n+1)}{(2n+1)} \left[\frac{2n(n-1)}{y_s^2} - 1 \right] h_n(y_s) D_n T_n^{\text{cc}} \\
& = \left[\frac{n}{2n+1}(\bar{\rho}-1) + \left(\frac{1}{y_s'^2} - \frac{\bar{\rho}}{y_s^2} \right) 2n(n-1) \right] j_n(y_c)
\end{aligned} \tag{2.74}$$

with $\hat{\rho} := \frac{1}{\bar{\rho}} = \frac{\rho'}{\rho}$.

Keeping the leading-order terms of Hankel functions with argument y_c and solving for T_n^{cc} give:

$$T_n^{\text{cc}} = \frac{\left[\frac{n}{2n+1}(1-\hat{\rho}) + \left(\frac{\hat{\rho}}{y_s'^2} - \frac{1}{y_s^2} \right) 2n(n-1) \right]}{M_n + N_n E_n} \frac{y_c^{2n+1}}{(2n-1)!!(2n+1)!!} \tag{2.75}$$

with $M_n := -i \left[\frac{n}{2n+1}(\hat{\rho}-1) - \frac{\hat{\rho}}{y_s'^2} 2n(n-1) \right]$

$$E_n := -i \frac{(2n+1)}{n[nh_n(y_s) - y_s h_n'(y_s)]}$$

$$\begin{aligned}
N_n := & \left[\frac{\hat{\rho} n}{2n+1} - \frac{\hat{\rho}}{y_s'^2} 2n(n-1) + \frac{1}{y_s^2} \frac{2n(n^2-1)}{(2n+1)} \right] [y_s h_n'(y_s) + h_n(y_s)] \\
& + \frac{n(n+1)}{(2n+1)} \left[\frac{2n(n-1)}{y_s^2} - 1 \right] h_n(y_s)
\end{aligned}$$

Case 2: Shear Incident

The calculation of scattering coefficients for an incident shear wave is more complicated than for the incident compressional case in that the Bessel function with argument for the incident wave is no longer small.

Multiplying Eqn. (2.36) by n and subtracting it from (2.37) produces:

$$\begin{aligned}
 & -n y_s j_n(y_s) + n^2 j_n(y_s) \\
 & + T_n^{\text{sc}} [y_c h_n'(y_c) - n h_n(y_c)] \\
 & + T_n^{\text{ss}} n [n h_n(y_s) - y_s h_n'(y_s)] = 0
 \end{aligned} \tag{2.76}$$

Now multiplying Eqn. (2.39) by n and then subtracting the resulting equation from Eqn. (2.38) gives:

$$\begin{aligned}
 & \frac{\bar{\rho}}{y_s^2} \{2n(n+2)[n j_n(y_s) - y_s j_n'(y_s)] - n y_s^2 j_n(y_s)\} \\
 & + T_n^{\text{sc}} \frac{\bar{\rho}}{y_s^2} \{y_s^2 h_n(y_c) - 2(n+2)[n h_n(y_c) - y_c h_n'(y_c)]\} \\
 & + T_n^{\text{ss}} \frac{\bar{\rho}}{y_s^2} \{2n(n+2)[n h_n(y_s) - y_s h_n'(y_s)] - n y_s^2 h_n(y_s)\} \\
 & = A_n^{\text{sc}} j_n(y_c') - A_n^{\text{ss}} n j_n(y_s')
 \end{aligned} \tag{2.77}$$

Subtracting Eqn. (2.36) from (2.77) yields:

$$\begin{aligned}
 & \frac{\bar{\rho}}{y_s^2} [2n(n+2)[n j_n(y_s) - y_s j_n'(y_s)] - n y_s^2 j_n(y_s)] \\
 & - y_s j_n'(y_s) - j_n(y_s) \\
 & + T_n^{\text{sc}} \frac{\bar{\rho}}{y_s^2} [y_s^2 h_n(y_c) - 2(n+2)(n h_n(y_c) - y_c h_n'(y_c))] \\
 & - T_n^{\text{sc}} h_n(y_c) - T_n^{\text{ss}} [y_s h_n'(y_s) + h_n(y_s)] \\
 & + T_n^{\text{ss}} \frac{\bar{\rho}}{y_s^2} [2n(n+2)(n h_n(y_s) - y_s h_n'(y_s)) - n y_s^2 h_n(y_s)] \\
 & = -A_n^{\text{ss}} [y_s' j_n'(y_s') + (n+1) j_n(y_s')]
 \end{aligned} \tag{2.78}$$

Solving Eqn. (2.78) for A_n^{ss} :

$$A_n^{ss} = - \frac{2n(n+2) \frac{\bar{\rho}}{y_s^2} [nj_n(y_s) - y_s j_n'(y_s)] - y_s j_n'(y_s) - (\bar{\rho} + 1) j_n(y_s) + a_2 T_n^{sc} + b_2 T_n^{ss}}{[y_s' j_n'(y_s') + (n+1) j_n(y_s')]} \quad (2.79)$$

where

$$b_2 := \frac{\bar{\rho}}{y_s^2} \left\{ 2n(n+2) [nh_n(y_s) - y_s h_n'(y_s)] - y_s^2 h_n(y_s) \right\} - [y_s h_n'(y_s) + h_n(y_s)]$$

$$a_2 := \frac{\bar{\rho}}{y_s^2} \left\{ y_s^2 h_n(y_c) - 2(n+2) [nh_n(y_c) - y_c h_n'(y_c)] \right\} - h_n(y_c)$$

Inserting Eqn. (2.79) in Eqn. (2.36) gives A_n^{sc} in terms of T_n^{sc} and T_n^{ss} gives:

$$\begin{aligned} & y_s j_n'(y_s) + j_n(y_s) + T_n^{sc} h_n(y_c) + T_n^{ss} [y_s h_n'(y_s) + h_n(y_s)] \\ & + \frac{y_s' j_n'(y_s') + j_n(y_s')}{y_s' j_n'(y_s') + (n+1) j_n(y_s')} \left[\frac{\bar{\rho}}{y_s^2} 2n(n+2) [nj_n(y_s) - y_s j_n'(y_s)] \right] \\ & + \frac{y_s' j_n'(y_s') + j_n(y_s')}{y_s' j_n'(y_s') + (n+1) j_n(y_s')} \left[-y_s j_n'(y_s) - (\bar{\rho} + 1) j_n(y_s) + a_2 T_n^{sc} + b_2 T_n^{ss} \right] \\ & = A_n^{sc} j_n(y_c') \end{aligned} \quad (2.80)$$

Substituting A_n^{sc} and A_n^{ss} into Eqn. (2.38) gives:

$$\begin{aligned}
& \frac{2\bar{\rho}}{y_s^2} n(n+1) [j_n(y_s) - y_s j_n'(y_s)] + T_n^{sc} \frac{\bar{\rho}}{y_s^2} \left\{ [y_s^2 - 2n(n+1)] h_n(y_c) + 4y_c h_n'(y_c) \right\} \\
& + 2T_n^{ss} \frac{\bar{\rho}}{y_s^2} n(n+1) [h_n(y_s) - y_s h_n'(y_s)] \\
& = \frac{1}{y_s^2} [y_s'^2 - 2n(n-1)] \left\{ \frac{[y_s' j_n'(y_s') + j_n(y_s')]}{[y_s' j_n'(y_s') + (n+1) j_n(y_s')]} \left\{ \frac{\bar{\rho}}{y_s^2} 2n(n+2) [nj_n(y_s) - y_s j_n'(y_s)] \right\} \right. \\
& + \frac{1}{y_s'^2} [y_s'^2 - 2n(n-1)] \left\{ \frac{[y_s' j_n'(y_s') + j_n(y_s')]}{[y_s' j_n'(y_s') + (n+1) j_n(y_s')]} \left[-y_s j_n'(y_s) - (\bar{\rho} + 1) j_n(y_s) + a_2 T_n^{sc} + b_2 T_n^{ss} \right] \right. \\
& + \frac{1}{y_s'^2} [y_s'^2 - 2n(n-1)] \left\{ y_s j_n'(y_s) + j_n(y_s) + T_n^{sc} h_n(y_c) + T_n^{ss} [y_s h_n'(y_s) + h_n(y_s)] \right\} + \\
& \left. \frac{1}{y_s^2} \frac{2n(n^2-1)}{(2n+1)} \left\{ \frac{\bar{\rho}}{y_s^2} [2n(n+2) [nj_n(y_s) - y_s j_n'(y_s)]] - y_s j_n'(y_s) - (\bar{\rho} + 1) j_n(y_s) + a_2 T_n^{sc} + b_2 T_n^{ss} \right\} \right. \\
& \left. \right\} \tag{2.81}
\end{aligned}$$

We substitute the values of a_2 and b_2 back and perform some algebra and then the resulting equation divide through $\bar{\rho}$, which produces:

$$\begin{aligned}
& \frac{2n(n-1)}{y_s'^2} \hat{\rho} h_n(y_c) T_n^{sc} - \frac{1}{y_s^2} \frac{2n(n-1)}{(2n+1)} [(n+1) h_n(y_c) + y_c h_n'(y_c)] T_n^{sc} \\
& + \left(\frac{n}{2n+1} \right) (1 - \hat{\rho}) T_n^{sc} h_n(y_c) + \left(\frac{n+1}{2n+1} \right) h_n(y_s) T_n^{ss} \\
& - \frac{1}{y_s^2} \frac{2n(n^2-1)}{(2n+1)} [(n+1) h_n(y_s) + y_s h_n'(y_s)] T_n^{ss} \\
& + \hat{\rho} \left[\frac{2n(n-1)}{y_s'^2} - \left(\frac{n}{2n+1} \right) \right] [h_n(y_s) + y_s h_n'(y_s)] T_n^{ss} \\
& = \left[\hat{\rho} \left(\frac{n}{2n+1} \right) - \hat{\rho} \frac{2n(n-1)}{y_s'^2} + \frac{1}{y_s^2} \frac{2n(n^2-1)}{(2n+1)} \right] [y_s j_n'(y_s) + j_n(y_s)] \\
& + \left(\frac{n+1}{2n+1} \right) \left[\frac{2}{y_s^2} n^2(n-1) - 1 \right] j_n(y_s) \tag{2.82}
\end{aligned}$$

where $\hat{\rho} := \frac{1}{\rho}$. Equation (2.82) further simplifies to:

$$\begin{aligned}
& -i \frac{(2n-1)!!}{y_c^{n+1}} \left[\frac{2n(n-1)}{y_s'^2} \hat{\rho} + \left(\frac{n}{2n+1} \right) (1-\hat{\rho}) \right] T_n^{\text{sc}} \\
& + \left[\left(\frac{n+1}{2n+1} \right) - \frac{1}{y_s^2} \frac{2n^2(n^2-1)}{(2n+1)} \right] h_n(y_s) T_n^{\text{ss}} \\
& + \hat{\rho} \left[\frac{2n(n-1)}{y_s'^2} - \left(\frac{n}{2n+1} \right) - \frac{1}{y_s^2} \frac{2n(n^2-1)}{(2n+1)} \right] [h_n(y_s) + y_s h_n'(y_s)] T_n^{\text{ss}} \\
& = \left[\hat{\rho} \left(\frac{n}{2n+1} \right) - \hat{\rho} \frac{2n(n-1)}{y_s'^2} + \frac{1}{y_s^2} \frac{2n(n^2-1)}{(2n+1)} \right] [y_s j_n'(y_s) + j_n(y_s)] \\
& + \left(\frac{n+1}{2n+1} \right) \left[\frac{2}{y_s^2} n^2(n-1) - 1 \right] j_n(y_s)
\end{aligned} \tag{2.83}$$

Now we rewrite Eqn. (2.76) as:

$$\begin{aligned}
T_n^{\text{sc}} &= i \frac{ny_c^{n+1}}{(2n+1)!!} [nh_n(y_s) - y_s h_n'(y_s)] T_n^{\text{ss}} \\
& - i \frac{ny_c^{n+1}}{(2n+1)!!} [y_s j_n'(y_s) - nj_n(y_s)]
\end{aligned} \tag{2.84}$$

Upon substitution of Eqn. (2.84) into Eqn. (2.83) eliminates T_n^{sc} :

$$\begin{aligned}
& \left(\frac{n}{2n+1} \right) \left[\frac{2n(n-1)}{y_s'^2} \hat{\rho} + \left(\frac{n}{2n+1} \right) (1-\hat{\rho}) \right] [nh_n(y_s) - y_s h_n'(y_s)] T_n^{\text{ss}} \\
& + \left[\left(\frac{n+1}{2n+1} \right) - \frac{1}{y_s^2} \frac{2n^2(n^2-1)}{(2n+1)} \right] h_n(y_s) T_n^{\text{ss}} \\
& + \hat{\rho} \left[\frac{2n(n-1)}{y_s'^2} - \left(\frac{n}{2n+1} \right) - \frac{1}{y_s^2} \frac{2n(n^2-1)}{(2n+1)} \right] [h_n(y_s) + y_s h_n'(y_s)] T_n^{\text{ss}} \\
& = \left[\hat{\rho} \left(\frac{n}{2n+1} \right) - \hat{\rho} \frac{2n(n-1)}{y_s'^2} + \frac{1}{y_s^2} \frac{2n(n^2-1)}{(2n+1)} \right] [y_s j_n'(y_s) + j_n(y_s)] \\
& + \left(\frac{n}{2n+1} \right) \left[\frac{2n(n-1)}{y_s'^2} \hat{\rho} + \left(\frac{n}{2n+1} \right) (1-\hat{\rho}) \right] [y_s j_n'(y_s) - nj_n(y_s)] \\
& + \left(\frac{n+1}{2n+1} \right) \left[\frac{2}{y_s^2} n^2(n-1) - 1 \right] j_n(y_s)
\end{aligned} \tag{2.85}$$

Solving Eqn. (2.85) for T_n^{ss} gives

$$T_n^{ss} = \frac{C_n}{S_n + L_n + U_n} \quad (2.86)$$

with

$$S_n := \left(\frac{n}{2n+1} \right) \left[\frac{2n(n-1)}{y_s'^2} \hat{\rho} + \left(\frac{n}{2n+1} \right) (1 - \hat{\rho}) \right] [nh_n(y_s) - y_s h_n'(y_s)]$$

$$L_n := \left[\left(\frac{n+1}{2n+1} \right) - \frac{1}{y_s^2} \frac{2n^2(n^2-1)}{(2n+1)} \right] h_n(y_s)$$

$$U_n := \hat{\rho} \left[\frac{2n(n-1)}{y_s'^2} - \left(\frac{n}{2n+1} \right) - \frac{1}{y_s^2} \frac{2n(n^2-1)}{(2n+1)} \right] [h_n(y_s) + y_s h_n'(y_s)]$$

$$\begin{aligned} C_n := & \left[\hat{\rho} \left(\frac{n}{2n+1} \right) - \hat{\rho} \frac{2n(n-1)}{y_s'^2} + \frac{1}{y_s^2} \frac{2n(n^2-1)}{(2n+1)} \right] [y_s j_n'(y_s) + j_n(y_s)] \\ & + \left(\frac{n}{2n+1} \right) \left[\frac{2n(n-1)}{y_s'^2} \hat{\rho} + \left(\frac{n}{2n+1} \right) (1 - \hat{\rho}) \right] [y_s j_n'(y_s) - n j_n(y_s)] \\ & + \left(\frac{n+1}{2n+1} \right) \left[\frac{2}{y_s^2} n^2(n-1) - 1 \right] j_n(y_s) \end{aligned}$$

Special Case 1: Dipole Scattering Coefficients

The dipole scattering coefficients are obtained by setting $n = 1$ to the general expressions.

From Eqn. (2.75) we get:

$$T_1^{\text{cc}} = \frac{(1 - \hat{\rho})y_c}{\frac{1}{3}(\hat{\rho} - 1)h_1(y_c) + \left\{ [y_s h_1'(y_s) + h_1(y_s)] \frac{\hat{\rho}}{3} - \frac{2}{3} h_1(y_s) \right\} \left[\frac{1}{h_1(y_s) - y_s h_1'(y_s)} \left(\frac{-3i}{y_c^2} \right) \right]}$$

which simplifies to:

$$T_1^{\text{cc}} = -\frac{iy_c^3 [h_1(y_s) - y_s h_1'(y_s)] (\hat{\rho} - 1)}{3[-7h_1(y_s) + y_s h_1'(y_s) + 4\hat{\rho}h_1(y_s) + 2\hat{\rho}y_s h_1'(y_s)]} \quad (2.87)$$

Equation (2.73) gives:

$$T_1^{\text{cs}} = D_1 T_1^{\text{cc}} = \left(\frac{-3i}{y_c^2} \right) \frac{1}{[h_1(y_s) - y_s h_1'(y_s)]} T_1^{\text{cc}}$$

$$T_1^{\text{cs}} = \frac{(\hat{\rho} - 1)y_c}{7h_1(y_s) - y_s h_1'(y_s) - 4\hat{\rho}h_1(y_s) - 2\hat{\rho}y_s h_1'(y_s)} \quad (2.88)$$

For $n = 1$ Eqns. (2.86) and (2.84) respectively reduce to:

$$T_1^{\text{ss}} = \frac{C_1}{S_1 + L_1 + U_1} = -\frac{(4\hat{\rho} - 7)j_1(y_s) + (2\hat{\rho} + 1)y_s j_1'(y_s)}{(4\hat{\rho} - 7)h_1(y_s) + (2\hat{\rho} + 1)y_s h_1'(y_s)} \quad (2.89)$$

and $T_1^{\text{sc}} = \frac{2(\hat{\rho} - 1)y_c^2}{y_s [(4\hat{\rho} - 7)h_1(y_s) + (2\hat{\rho} + 1)y_s h_1'(y_s)]} \quad (2.90)$

Equations (2.87) to (2.90) are exactly the same expressions that we have already derived for the dipole scattering coefficients in Sec. 2.4.2.

Special Case 2: Quadrupole Scattering Coefficients

For $n = 2$, Eqn. (2.75) reduces to:

$$T_2^{\text{cc}} = \frac{\left[\frac{2}{5}(1 - \hat{\rho}) + 4 \left(\frac{\hat{\rho}}{y_s'^2} - \frac{1}{y_s^2} \right) \right] \left(\frac{y_c^2}{15} \right)}{M_2 + N_2 D_2} \quad (2.91)$$

where $M_2 = -i \left(\frac{3}{y_c^3} \right) \left[\frac{2}{5}(\hat{\rho} - 1) - \frac{4\hat{\rho}}{y_s'^2} \right]$

$$N_2 = \left[\frac{2\hat{\rho}}{5} - \frac{4\hat{\rho}}{y_s'^2} + \frac{12}{5} \frac{1}{y_s^2} \right] [y_s h_2'(y_s) + h_2(y_s)] + \frac{6}{5} \left[\frac{4}{y_s^2} - 1 \right] h_2(y_s)$$

$$D_2 = -i \left(\frac{15}{y_c^3} \right) \frac{1}{2[2h_2(y_s) - y_s h_2'(y_s)]}$$

y_s' being small, T_2^{cc} can be further simplified to:

$$T_2^{\text{cc}} = \frac{2iy_c^5 [y_s h_2'(y_s) - 2h_2(y_s)]}{135 [3h_2(y_s) + y_s h_2'(y_s)]} \quad (2.92)$$

From Eqn. (2.73) we get:

$$T_2^{\text{cs}} = -\frac{y_c^2}{9 [3h_2(y_s) + y_s h_2'(y_s)]} \quad (2.93)$$

For $n = 2$, Eqns. (2.86) and (2.84) respectively reduce to:

$$T_2^{\text{ss}} = \frac{C_2}{S_2 + L_2 + U_2} = -\frac{3j_2(y_s) + y_s j_2'(y_s)}{[3h_2(y_s) + y_s h_2'(y_s)]} \quad (2.94)$$

and $T_2^{\text{sc}} = -\frac{2y_c^3}{3y_s [3h_2(y_s) + y_s h_2'(y_s)]} \quad (2.95)$

Generalisation of those two cases and using equations (2.75), (2.73), (2.86), (2.84), lead to a unified form of all scattering coefficients:

$$T_n^{\text{pq}} = \frac{\hat{\rho} N_n^{\text{pq}} (1 - \delta_{n1}) + y_s'^2 N_1^{\text{pq}} \delta_{n1}}{\hat{\rho} D_n^{\text{pq}} (1 - \delta_{n1}) + y_s'^2 D_1^{\text{pq}} \delta_{n1}},$$

and using equations (A7), (A8) and (A12) leading to, for $n > 1$,

$$\begin{aligned} T_n^{\text{cc}} &= -i \frac{n}{(n+1)(1+2n)!!(2n-1)!!} \frac{-i + y_s^2 h_n(y_s) j_{n+1}(y_s)}{i + y_s^2 h_n(y_s) j_{n-1}(y_s)} y_c^{2n+1} \\ T_n^{\text{cs}} &= -\frac{y_s}{(n+1)(2n-1)!!} \frac{j_n(y_s)}{i + y_s^2 h_n(y_s) j_{n-1}(y_s)} y_c^n \\ T_n^{\text{sc}} &= -\frac{n}{(2n-1)!!} \frac{j_n(y_s)}{i + y_s^2 h_n(y_s) j_{n-1}(y_s)} y_c^{n+1} \\ T_n^{\text{ss}} &= -\frac{y_s^2 j_n(y_s) j_{n-1}(y_s)}{i + y_s^2 h_n(y_s) j_{n-1}(y_s)} \end{aligned}$$

These formulas do not involve the mass density ratio. This is the reason why we shall consider only $n = 1$ when looking for the effective mass density in the next chapter.

2.4.4 Normalised Scattering Coefficients

The set of boundary equations used to derive analytical solutions for the scattering coefficients are not easy to obtain numerical solution. This is because each element of the boundary equations contains either a Bessel or a Hankel function, which can differ wildly in magnitude, one becoming very small and the other very large with the increase in argument. Hence, the matrix equation that the set of boundary equations form becomes ill-conditioned due to the condition number being much greater than one, thereby making matrix inversion inaccurate. Another difficulty is the determination of Bessel functions which become inaccurate for large arguments.

Pinfield proposed a method to tackle these two problems [42]. The idea is to express the radial dependence of the wave potentials as ratios of the Bessel and Hankel function value at the boundary. Anson and Chivers also used a similar technique to obtain numerical stability in their shell scattering problem [43].

The analytical solutions of the scattering coefficients can be defined in a normalised form:

$$T_{nN}^{cc} = \frac{T_n^{cc}}{y_c^{2n+1}} \quad (2.96)$$

$$T_{nN}^{cs} = \frac{T_n^{cs} h_n(y_s)}{y_c^n} \quad (2.97)$$

$$T_{nN}^{sc} = \frac{T_n^{sc}}{j_n(y_s) y_c^{n+1}} \quad (2.98)$$

$$T_{nN}^{ss} = \frac{T_n^{ss} h_n(y_s)}{j_n(y_s)} \quad (2.99)$$

2.5 NUMERICAL RESULTS

Numerical calculations of the analytical results of scattering coefficients have been performed for a silica particle in water system at 25⁰C over a frequency span of 0.01 to 10 MHz. The physical parameters used in the simulations are listed in Table 2.1. The density of silica being greater than twice that of water, thermal dissipation in the system is guaranteed to be negligible compared to viscous loss [3]. Here numerical studies are conducted for the dipole and quadrupole scattering modes. So as to assess the validity of general results of scattering coefficients, their variations with orders are compared with exact solutions, obtained from numerical matrix inversion of the boundary equations.

Table 2.1: Physical properties of silica and water used in the numerical illustrations.

Parameters	Water	Silica
Sound speed (m.s ⁻¹)	1497	5968
Density (kg.m ⁻³)	997	2100
Shear viscosity (Pa.s)	8.91×10^{-4}	0
Shear modulus (GPa)	0	30.9
Attenuation factor (Np.m ⁻¹ .MHz ⁻²)	2.3×10^{-2}	2.6×10^{-10}

2.5.1 Dipole scattering coefficients

Figures 2.2 (a) and (b) show how the normalised shear-acoustic scattering coefficients vary with the real part $\Re(y_s)$ of the dimensionless shear wavenumber. The scattering coefficients are normalised using the appropriate Bessel or Hankel functions and also eliminating y_c dependence. Hence the normalised scattering coefficients have only y_s functional dependence. Both Figures 2.2 (a) and (b) have been drawn for a large particle of radius $a = 300 \mu\text{m}$ and on large $\Re(y_s)$ intervals:

- $[10^{-3}, 10^{+3}]$, corresponding to $\Re(y_c) \in [1.7 \times 10^{-7}, 1.4]$ for Figure 2.2 (a)
- $[10^{-2}, 10^{+2}]$, corresponding to $\Re(y_c) \in [2.9 \times 10^{-6}, 0.12]$ for Figure 2.2 (b).

Figure 2.2 (a) shows the limits of both our numerical code at $\Re(y_s) < 10^{-2}$ leading to non-physical oscillations, and of the scattering coefficients approximations at $\Re(y_c) > 1$. This latter discrepancy occurs for $\Re(y_s) > 10^{+2}$. This is the reason why all other figures in this chapter will be limited to $\Re(y_s) \in [10^{-2}, 10^{+2}]$. In this range, each of the curves fits accurately with its exact counterpart, obtained by solving the boundary equations numerically.

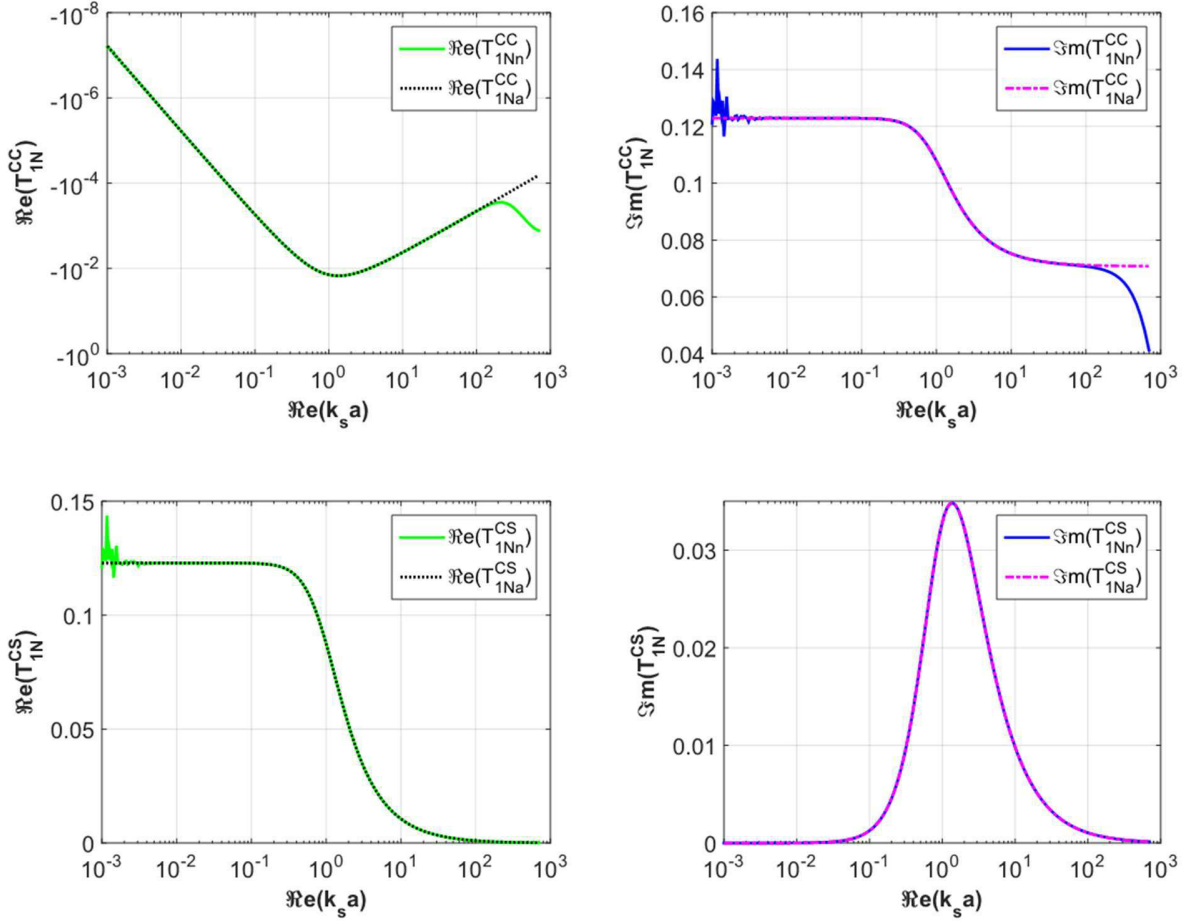


Figure 2.2: (a) shows how the real and imaginary parts of the normalised dipole scattering coefficients T_{1N}^{CC} and T_{1N}^{CS} vary with the real part of non-dimensional shear wavenumber for a silica-sphere-in-water system. The T_{1Nn}^{pq} and T_{1Na}^{qp} represent normalised numerical and normalised analytical scattering coefficients respectively.

All the curves have one feature in common: they all seem to approach a constant value at the lower and upper limits of $\Re(y_s)$ and experience marked changes near $\Re(y_s) \sim 1$. The real part of T_{1N}^{SS} looks very similar to the imaginary part of T_{1N}^{SC} , while the imaginary part of T_{1N}^{SS} looks the reflection [about the $\Re(y_s)$ -axis] of the real part of T_{1N}^{SC} .

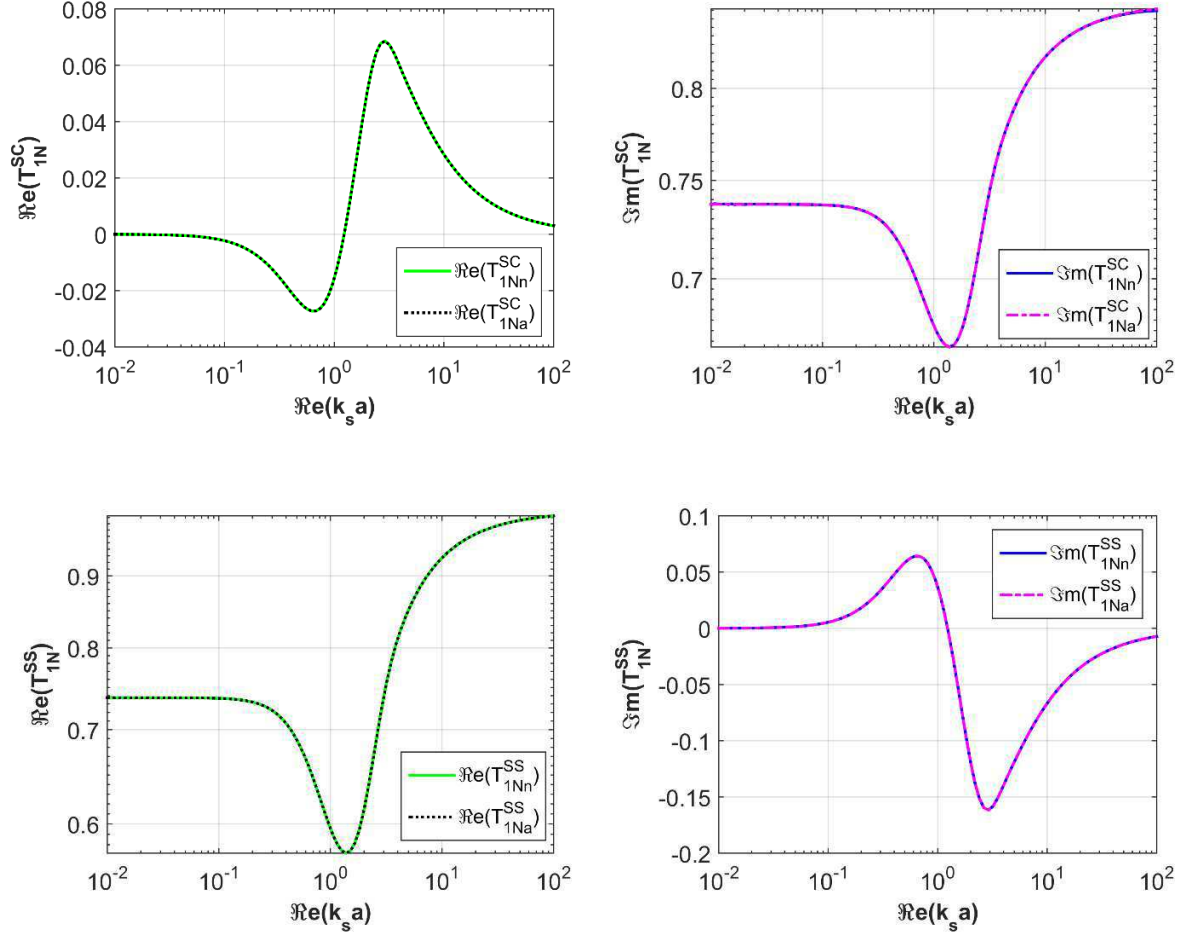


Figure 2.2: (b) shows the variation of the real and imaginary parts of the normalised dipole scattering coefficients T_{1N}^{SC} and T_{1N}^{SS} as a function of the real part of non-dimensional shear wavenumber for a silica-sphere-in-water system.

As regards to T_{1N}^{CS} , its imaginary part exhibits a pronounced peak, that can be explained using the parameter $\delta = \sqrt{2\eta / (\rho\omega)}$, which is related to the length of the unsteady viscous boundary layer that exists around the particle. The thickness of δ compared to the dimension of the particle gives a measure of viscous effects. When the thickness of the viscous boundary layer becomes comparable to the dimension of the particle, i.e. $\delta \sim a$, the particle experiences a maximum viscous loss, which manifests itself as a resonance peak; at this point the relative motion between the particle and its surrounding fluid is also maximum [3]. At low $\Re(y_s)$, the real part of T_{1N}^{CS} looks flat because of the steady (Stokes)

drag acting on the particle. The viscous boundary layer becomes thinner with increasing frequency. At sufficiently elevated frequencies, the viscous regime gives way to the inertial regime, the fluid being physically tantamount to an inviscid one, which is why the real part of T_{1N}^{CS} asymptotically approaches zero.

2.5.2 Quadrupole scattering coefficients

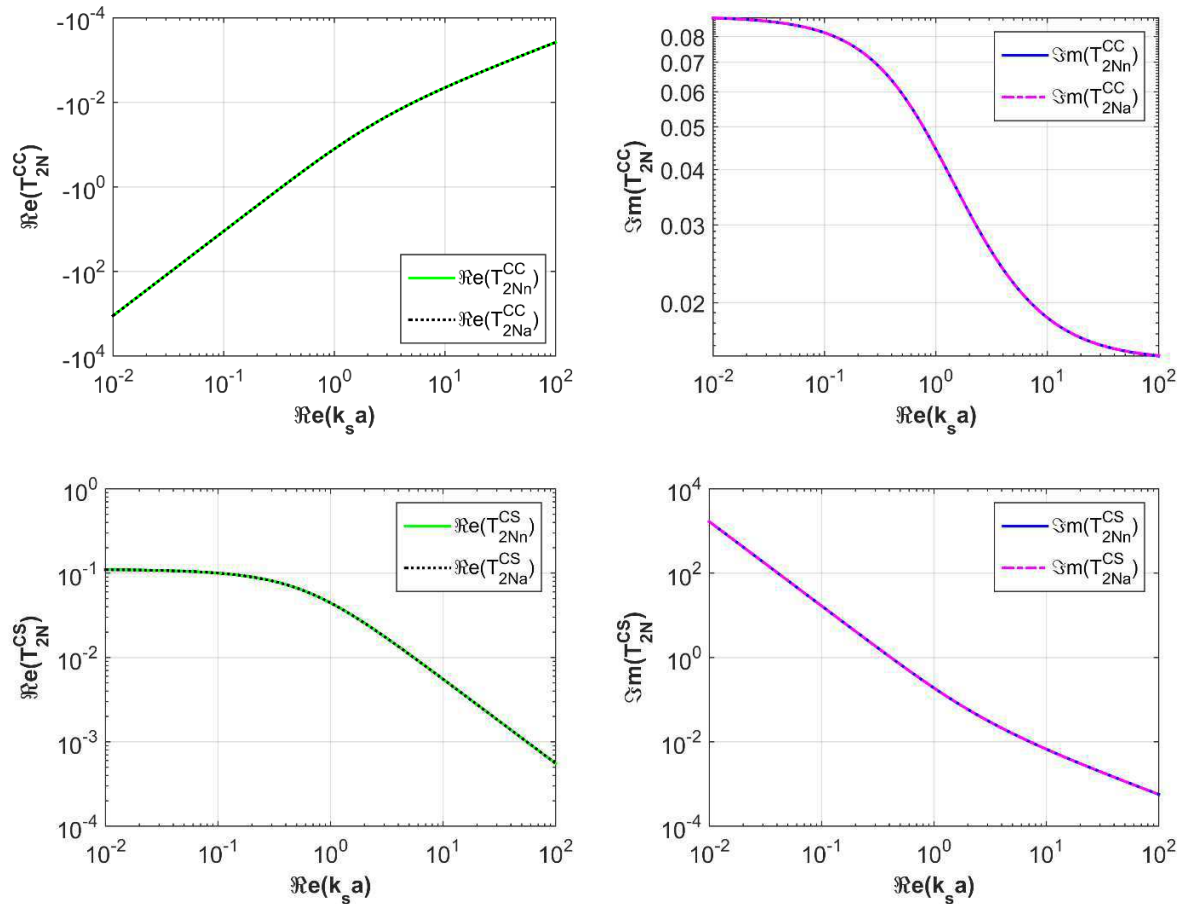


Figure 2.3: (a) shows how the real and imaginary parts of the normalised quadrupole scattering coefficients T_{2N}^{CC} and T_{2N}^{CS} vary with the real part of non-dimensional shear wavenumber for a silica-sphere-in-water system. The T_{2Nn}^{pq} and T_{2Na}^{pq} represent normalised numerical and normalised analytical scattering coefficients respectively.

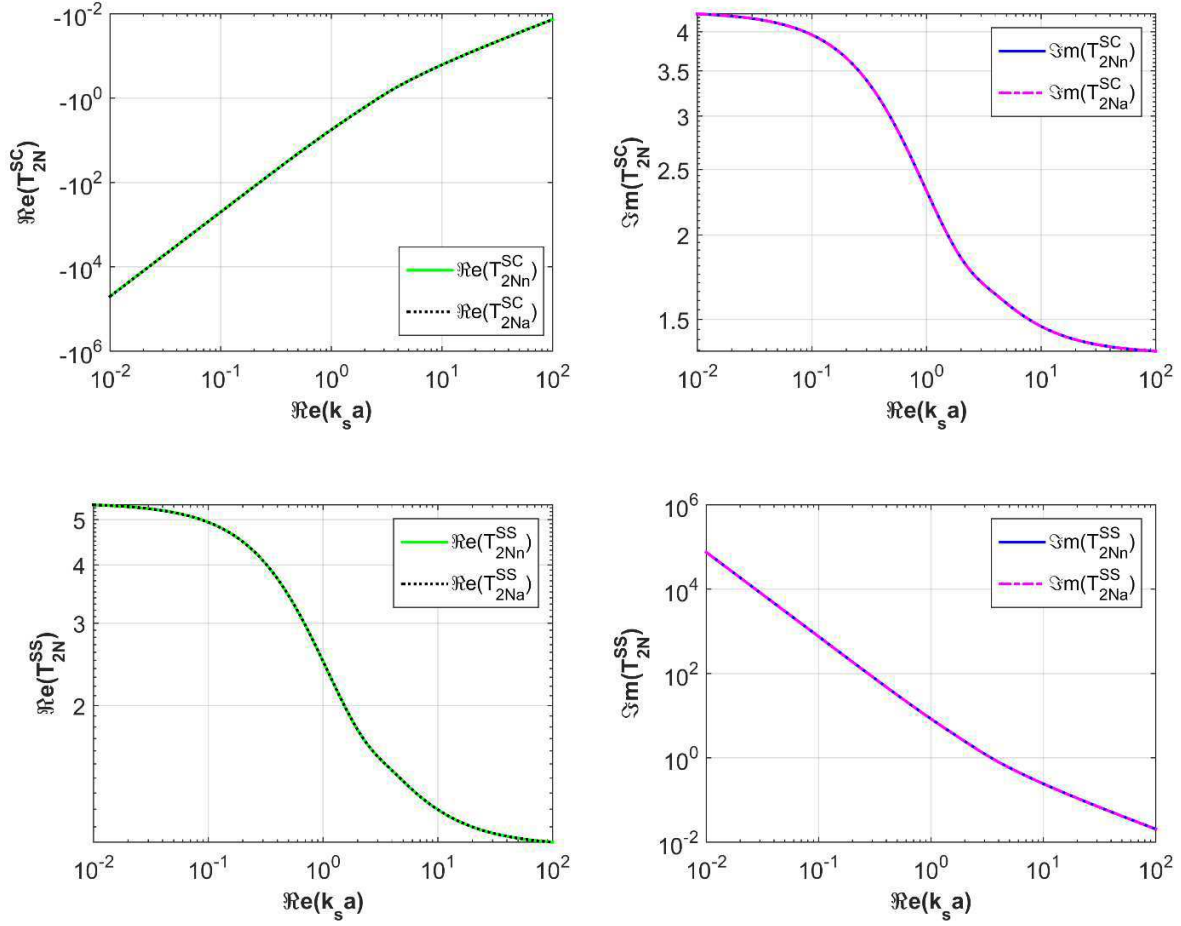


Figure 2.3: (b) shows the variation of the real and imaginary parts of normalised shear-acoustic quadrupole coefficients T_{2N}^{SC} and T_{2N}^{SS} with the real part of non-dimensional shear wavenumber.

Figure 2.3 shows how the normalised quadrupole scattering coefficients vary with the real part $\Re(y_s)$ of the dimensionless shear wavenumber. T_{2N}^{CC} and T_{2N}^{CS} look very alike. For the case of T_{2N}^{SC} and T_{2N}^{SS} , their imaginary parts are similar and exhibit a sharp drop in magnitude with an increase in $\Re(y_s)$, whereas their real parts, albeit a downward trend, are somewhat different in that the $\Re(T_{2N}^{CS})$ has a longer viscous regime than the $\Re(T_{2N}^{SS})$ does. The imaginary parts of T_{2N}^{CC} and T_{2N}^{CS} resemble the real part of T_{2N}^{SS} ; as $\Re(y_s)$ is on the increase, they all show a smooth decline and asymptote to zero.

2.5.3 Dependence of Coefficients on Orders

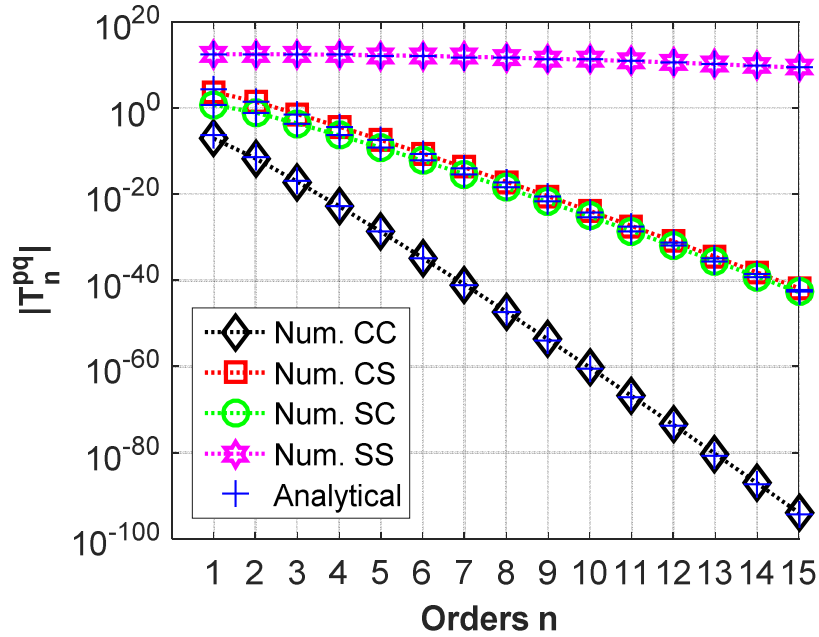


Figure 2.4 depicts the variation of moduli of n^{th} order scattering coefficients with their orders for $|y_c| = 0.1$ and $\text{Re}(y_s) = 14.7$.

Figure 2.4 shows how T_n^{cc} , T_n^{cs} , T_n^{sc} and T_n^{ss} varies with their scattering orders for $|y_c| = 0.1$. The variation of a scattering coefficient of a wave with its order depends on the dimensionless wavenumber of that wave. T_n^{cc} goes down faster because the magnitude of y_c is smaller than that of y_s . Both T_n^{cc} and T_n^{sc} being scattering coefficients of a compressional wave, T_n^{cc} falls off more slowly than T_n^{sc} because shear-compressional interaction is stronger than that of compressional-shear, and the same is true with T_n^{ss} and T_n^{cs} . T_n^{ss} does not decrease due to the high value of y_s and the strong shear-shear interaction. As can be seen from the y_c dependence of the scattering coefficients found in the previous section, all T_n^{ss} have a larger magnitude than the other coefficients and the magnitude of T_2^{cs} is of the same order as that of T_0^{cc} and T_1^{cc} .

2.6 CONCLUSION

In this chapter we have undertaken a detailed study on the scattering by an elastic spherical scatterer embedded in a viscous fluid of infinite extent and have derived analytical solutions for scattering coefficients for arbitrary partial wave order for both incident compressional and shear waves by taking account the viscosity of the surrounding fluid through the wave mode conversion phenomenon. The solutions obtained presents a generalisation of the results of a previous study of the dipole scattering coefficients conducted by Pinfield and Forrester. Although the compressional wavelength is assumed to stay within the Rayleigh scattering limit, no assumption has been made about the shear wavelength in the fluid and hence the solutions are general in terms of the shear wave. The analytical solutions are shown to reduce to prior known results in the case of dipole scattering. The validity of the approximated solutions is numerically checked by comparing with their exact numerical solution of the boundary equations and found to agree well. The analytical approximations of the monopole and dipole scattering coefficients will be used in the next chapter to study the effective bulk modulus and mass density. The higher order scattering coefficients may be useful in studying multi-mode multiple scattering models analytically, especially in the case of the incident shear wave. The quadrupole scattering coefficients might also be required to calculate the effective viscosity of a suspension using a core-shell effective medium model.

REFERENCES

- [1] J. W. Strutt, “Investigation of the Disturbance produced by a Spherical Obstacle on the Waves of Sound,” *Proc. London Math. Soc.*, vol. s1-4, no. 1, pp. 253–283, 1871.
- [2] P. S. Epstein and R. R. Carhart, “The Absorption of Sound in Suspensions and Emulsions. I. Water Fog in Air,” *J. Acoust. Soc. Am.*, vol. 25, no. 3, pp. 553–565, 2005.
- [3] J. R. Allegra and S. A. Hawley, “Attenuation of Sound in Suspensions and Emulsions: Theory and Experiments,” *J. Acoust. Soc. Am.*, vol. 51, no. 5B, pp. 1545–1564, 2005.
- [4] P. C. Waterman and R. Truell, “Multiple scattering of waves,” *J. Math. Phys.*, vol. 2, no. 4, pp. 512–537, 1961.
- [5] J. G. Fikioris and P. C. Waterman, “Multiple scattering of waves. II. ‘Hole corrections’ in the scalar case,” *J. Math. Phys.*, vol. 5, no. 10, pp. 1413–1420, 1964.
- [6] A. K. Hipp, G. Storti, and M. Morbidelli, “Acoustic characterization of concentrated suspensions and emulsions. 2. Experimental validation,” *Langmuir*, vol. 18, no. 2, pp. 405–412, 2002.
- [7] J. Mei, Z. Liu, W. Wen, and P. Sheng, “Effective dynamic mass density of composites,” *Phys. Rev. B - Condens. Matter Mater. Phys.*, vol. 76, no. 13, 2007.
- [8] V. J. Pinfield, “Thermo-elastic multiple scattering in random dispersions of spherical scatterers,” *J. Acoust. Soc. Am.*, vol. 136, no. 6, pp. 3008–3017, 2014.
- [9] D. M. Forrester, J. Huang, V. J. Pinfield, and F. Luppé, “Experimental verification of nanofluid shear-wave reconversion in ultrasonic fields,” *Nanoscale*, vol. 8, no. 10, pp. 5497–5506, 2016.
- [10] V. J. Pinfield and D. M. Forrester, “Multiple scattering in random dispersions of spherical scatterers: Effects of shear-acoustic interactions,” *J. Acoust. Soc. Am.*, vol. 141, no. 1, pp. 649–660, 2017.
- [11] T. Valier-Brasier and J.-M. Conoir, “Propagation of coherent transverse waves: Influence of the translational and rotational subwavelength resonances,” *J. Acoust. Soc. Am.*, vol. 142, no. 2, pp. 512–522, 2017.
- [12] G. T. Kuster and M. N. Toksöz, “Velocity and Attenuation of Seismic Waves in Two-Phase Media: Part I. Theoretical Formulations,” *Geophysics*, vol. 39, no. 5, pp. 587–606, 2002.
- [13] R. L. Kligman, W. M. Madigosky, and J. R. Barlow, “Effective dynamic properties of composite viscoelastic materials,” *J. Acoust. Soc. Am.*, vol. 70, no. 5, pp. 1437–1444, 2005.
- [14] G. C. Gaunaurd and H. Überall, “Resonance theory of the effective properties of perforated solids,” *J. Acoust. Soc. Am.*, vol. 71, no. 2, pp. 282–295, 2005.
- [15] M. M. Alam, V. J. Pinfield, F. Luppé, and P. Maréchal, “Effective dynamic properties of random complex media with spherical particles,” *J. Acoust. Soc. Am.*, vol. 145, no. 6, pp. 3727–3740, Jun. 2019.
- [16] W. S. Rayleigh, “Theory of Sound,” *London Macmillan, Repr. 1945, New York Dover*, 1896.
- [17] K. F. Herzfeld, “LXIX. The scattering of sound-waves by small elastic spheres,” *London, Edinburgh, Dublin Philos. Mag. J. Sci.*, vol. 9, no. 59, pp. 741–751, 2014.

- [18] J. J. Faran, “Sound Scattering by Solid Cylinders and Spheres,” *J. Acoust. Soc. Am.*, vol. 23, no. 4, pp. 405–418, 1951.
- [19] V. C. Anderson, “Sound Scattering from a Fluid Sphere,” *J. Acoust. Soc. Am.*, vol. 22, no. 4, pp. 426–431, 1950.
- [20] R. W. Hart, “Sound Scattering of a Plane Wave from a Nonabsorbing Sphere,” *J. Acoust. Soc. Am.*, vol. 23, no. 3, pp. 323–329, 2005.
- [21] C. F. Ying and R. Truell, “Scattering of a plane longitudinal wave by a spherical obstacle in an isotropically elastic solid,” *J. Appl. Phys.*, vol. 27, no. 9, pp. 1086–1097, 1956.
- [22] Y. H. Pao and C. C. Mow, “Scattering of plane compressional waves by a spherical obstacle,” *J. Appl. Phys.*, vol. 34, no. 3, pp. 493–499, 1963.
- [23] N. G. Einspruch and R. Truell, “Scattering of a Plane Longitudinal Wave by a Spherical Fluid Obstacle in an Elastic Medium,” *J. Acoust. Soc. Am.*, vol. 32, no. 2, pp. 214–220, 2005.
- [24] L. Knopoff, “Scattering of compression waves by spherical obstacles,” *Geophysics*, vol. 24, no. 1, pp. 30–39, 2002.
- [25] L. Knopoff, “Scattering of Shear Waves By Spherical Obstacles,” *Geophysics*, vol. 24, no. 2, pp. 209–219, 2002.
- [26] N. G. Einspruch, E. J. Witterholt, and R. Truell, “Scattering of a plane transverse wave by a spherical obstacle in an elastic medium,” *J. Appl. Phys.*, no. 5, pp. 806–818, 1960.
- [27] D. W. Kraft and M. C. Franzblau, “Scattering of elastic waves from a spherical cavity in a solid medium,” *J. Appl. Phys.*, vol. 42, no. 8, pp. 3019–3024, 1971.
- [28] R. J. McBride and D. W. Kraft, “Scattering of a transverse elastic wave by an elastic sphere in a solid medium,” *J. Appl. Phys.*, vol. 43, no. 12, pp. 4853–4861, 1972.
- [29] Y. Iwashimizu, “Scattering of elastic waves by a movable rigid sphere embedded in an infinite elastic solid,” *J. Sound Vib.*, vol. 21, no. 4, pp. 463–469, 1972.
- [30] P. C. Waterman, “Matrix theory of elastic wave scattering,” *J. Acoust. Soc. Am.*, vol. 60, no. 3, pp. 567–580, 2005.
- [31] V. Varatharajulu and Y. Pao, “Scattering matrix for elastic waves. I. Theory,” *J. Acoust. Soc. Am.*, vol. 60, no. 3, pp. 556–566, 2005.
- [32] M. K. Hinders, “Plane-elastic-wave scattering from an elastic sphere,” *Nuovo Cim. B Ser. 11*, vol. 106, no. 7, pp. 799–818, 1991.
- [33] J.-P. Sessarego, J. Sageloli, R. Guillermin, and H. Überall, “Scattering by an elastic sphere embedded in an elastic isotropic medium,” *J. Acoust. Soc. Am.*, vol. 104, no. 5, pp. 2836–2844, 2002.
- [34] C. J. T. Sewell, “The Extinction of Sound in a Viscous Atmosphere by Small Obstacles of Cylindrical and Spherical Form,” *Philos. Trans. R. Soc. A Math. Phys. Eng. Sci.*, vol. 210, no. 459–470, pp. 239–270, 2006.
- [35] V. J. Pinfield and R. E. Challis, “Acoustic scattering by a spherical obstacle: Modification to the analytical long-wavelength solution for the zero-order coefficient,” *J. Acoust. Soc. Am.*, vol. 129, no. 4, pp. 1851–1856, 2011.

- [36] D. Brill and G. Gaunaurd, “Resonance theory of elastic waves ultrasonically scattered from an elastic sphere,” *J. Acoust. Soc. Am.*, vol. 81, no. 1, pp. 1–21, 2005.
- [37] G. B. Arfken, H. J. Weber, and F. E. Harris, *Mathematical Methods for Physicists*. 2013.
- [38] P. M. Morse, H. Feshbach, and E. L. Hill, “Methods of Theoretical Physics,” *Am. J. Phys.*, vol. 22, no. 6, pp. 410–413, 2005.
- [39] C. G. Gray, “Multipole expansions of electromagnetic fields using Debye potentials,” *Am. J. Phys.*, vol. 46, no. 2, pp. 169–179, 2005.
- [40] C. Wilcox, “Debye Potentials,” *Indiana Univ. Math. J.*, vol. 6, no. 2, pp. 167–201, 2013.
- [41] D. Brill, G. Gaunaurd, and H. Überall, “Resonance theory of elastic shear-wave scattering from spherical fluid obstacles in solids,” *J. Acoust. Soc. Am.*, vol. 67, no. 2, pp. 414–424, 2005.
- [42] V. J. Pinfield, “Acoustic scattering in dispersions: Improvements in the calculation of single particle scattering coefficients,” *J. Acoust. Soc. Am.*, vol. 122, no. 1, pp. 205–221, 2007.
- [43] L. W. Anson and R. C. Chivers, “Ultrasonic scattering from spherical shells including viscous and thermal effects,” *J. Acoust. Soc. Am.*, vol. 93, no. 4, pp. 1687–1699, 1993.

CHAPTER THREE

EFFECTIVE DYNAMIC PROPERTIES WITH SPHERES

3.1 INTRODUCTION

This chapter addresses the problem of the determination of effective dynamic properties in a shear-acoustic system of spherical particles in a viscous fluid at high concentrations, a problem requiring full account of both acoustic and shear wave modes and the impact of particle interactions due to shear boundary layer overlap. The Generalised Self-Consistent Model (GSCM) as applied in Refs. [1–3], not being restricted to low concentration, has been adopted and applied to a system where wave mode conversion is taken into account, under a large compressional wavelength assumption, in order to obtain analytical expressions for the effective *dynamic* parameters. Although use of the GSCM restricts the validity of the model in terms of the long compressional wavelength, it permits a full investigation of effective properties without limit on concentration, whereas multiple scattering models are suitable to low concentrations. An effective bulk modulus is obtained from the monopole mode, and an effective density from the dipole mode; for the first time, an effective density of a discrete random medium, taking the viscosity of the host fluid into account through wave mode conversion using scattering theory, is presented. The long compressional wavelength assumption applies with respect to both the particle size and the average inter-particle distance. Contrary to the case of a solid (or visco-elastic) host, the shear wavelength in a viscous fluid is not the same order of magnitude as the compressional one, and the frequency dependence of the effective parameters is thus investigated by varying the dimensionless shear wavenumber over a wide range of values, while confining the dimensionless compressional wavenumber to the long wavelength limit. Whilst the effective bulk modulus is found to be quasi-static with only limited frequency-dependence, the effective mass density is frequency-dependent and hence its behaviour is investigated numerically. In this chapter, the model and its principal results are presented in Sec. 3.2. In section 3.3, numerical predictions of the model are presented, and their physical interpretation discussed.

3.2 MODEL

3.2.1 Core-Shell System for Effective Medium

The system consists of a small-amplitude (linear) acoustic wave propagating through a medium consisting of identical spherical inclusions (particles) of radius a , randomly dispersed in an infinitely extended homogenous isotropic matrix medium with a given concentration c . Using the principles of the GSCM, an equivalent problem is constructed by embedding a single particle coated with shell of the host medium (a viscous fluid) within a homogeneous medium which has the well-defined effective properties of the whole system (Fig 3.1). Effective properties may be obtained in cases where the (effective) acoustic wavelength is much larger than both the particle (core-shell inclusion) size and the average inter-particle separation [2, 4]. The radius of the shell, b , is fixed such that the concentration within the shell is equivalent to that in the medium as a whole, thus $b = ac^{-1/3}$.

The *self-consistency* condition or equivalently the Coherent Potential Approximation (CPA), requires the scattering from the core-shell inclusion to vanish when embedded in the effective medium [1, 4-5]. Here both acoustic (compressional and shear) wave modes are included in all three phases. Thus, mode conversions are accounted for in the model. The self-consistency condition is applied independently to the Rayleigh partial wave orders, namely the monopole and dipole modes, and to both compressional and shear scattered waves, consistent with the requirement for minimum scattering. Although the method is limited to long compressional wavelength, no assumption regarding the shear wavelength has been made, thereby allowing us to investigate a wide range of shear wavelengths for incident compressional waves to determine the frequency-dependence of the effective dynamic density.

The GSCM we have employed is similar to that in Refs. [1, 3] in two respects: firstly, the authors seek a self-consistent solution by invoking the CPA to ensure that the core-shell system embedded within the effective medium produces no scattered waves in the lowest orders of scattering coefficients; and secondly, they directly work on the shell boundary conditions with no scattered waves in the effective medium, since the expressions for scattering coefficients of the core particle are known.

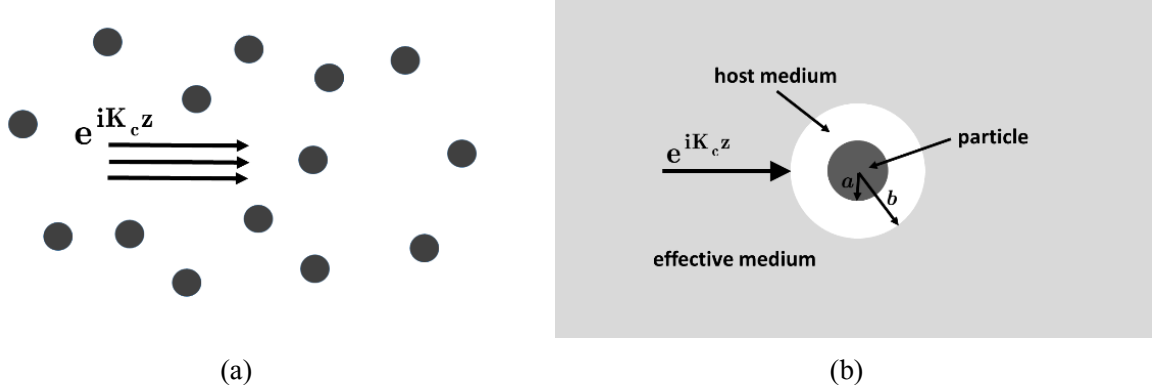


Figure 3.1: Illustration of the Generalised Self-Consistent Method adopted in this work. The acoustic wave field in the complex medium (a) is equivalent to that in the effective medium surrounding a single inclusion embedded within a shell of the host medium (b). Self-consistency requires that the scattering from the core-shell system be zero.

We consider an incident effective compressional wave that propagates in the effective medium and encounters the core-shell inclusion, producing no scattered waves in the effective medium, but two inward-propagating refracted waves (one compressional and one shear with amplitudes C_n^{cc} and C_n^{cs} respectively) in the shell. These two refracted waves are, in turn, scattered by the core particle, each generating an outward-propagating wave of each mode in the shell and two refracted waves inside the core particle. The scattering of waves from the core particle in the host medium is characterised by scattering coefficients T_n^{cc} and T_n^{cs} for an incident compressional wave, and T_n^{sc} and T_n^{ss} for an incident shear wave. These combine with the incident amplitudes of the inward-propagating refracted waves in the shell (C_n^{cc} and C_n^{cs}) to define the amplitude of the outward-propagating waves in the shell.

The solution to determine the effective properties proceeds by the application of the boundary conditions at the interface of the shell and effective medium for each partial wave order independently, considering all wave modes. Rearrangement of the equations and the application of the long-wavelength requirement for the incident compressional wave leads to solutions for the effective bulk modulus and effective density. The validity of the model is not limited to a particular concentration range, but the long wavelength assumption $|X_c| := |K_c b| \ll 1$, and $|x_c| := |k_c b| \ll 1$ imposes a frequency and particle size limit which is

dependent on the concentration. The practical limits imposed by this requirement are explored in the results of section 3.3.

3.2.2 Core-Shell Boundary Equations

In the shell, the wave potentials for an incident compressional wave can be written as:

$$\Phi_{c,shell} = \sum_{n=0}^{\infty} i^n (2n+1) P_n(\cos\theta) \left[C_n^{cc} j_n(x_c) + (C_n^{cc} T_n^{cc} + C_n^{cs} T_n^{sc}) h_n(x_c) \right] \quad (3.1)$$

$$\psi_{s,shell} = \sum_{n=0}^{\infty} i^n (2n+1) P_n(\cos\theta) \left[C_n^{cs} j_n(x_s) + (C_n^{cc} T_n^{cs} + C_n^{cs} T_n^{ss}) h_n(x_s) \right] \quad (3.2)$$

The effective properties are obtained by applying the same boundary equations as in the single sphere case to the outer boundary, $r=b$ of the core-shell system of the effective medium model. The continuity of the displacements at the interface between the effective medium and the shell gives:

$$\begin{aligned} X_c j'_n(X_c) + t_n^{cc} Y_c h'_n(X_c) + t_n^{cs} n(n+1) h_n(X_s) &= C_n^{cc} x_c j'_n(x_c) \\ + T_n^{cc} C_n^{cc} x_c h'_n(x_c) + C_n^{cc} T_n^{cs} n(n+1) h_n(x_s) + C_n^{cs} n(n+1) j_n(x_s) & \quad (3.3) \\ + C_n^{cs} T_n^{ss} n(n+1) h_n(x_s) + C_n^{cs} T_n^{sc} y_c h'_n(x_c) \end{aligned}$$

and

$$\begin{aligned} j_n(X_c) + t_n^{cc} h_n(X_c) + t_n^{cs} [X_s h'_n(X_s) + h_n(X_s)] &= C_n^{cc} j_n(x_c) + \\ T_n^{cc} C_n^{cc} h_n(x_c) + C_n^{cc} T_n^{cs} [x_s h'_n(x_s) + h_n(x_s)] + C_n^{cs} [y_s j'_n(x_s) + j_n(x_s)] & \quad (3.4) \\ + C_n^{cs} T_n^{ss} [x_s h'_n(x_s) + h_n(x_s)] + C_n^{cs} T_n^{sc} h_n(x_c) \end{aligned}$$

Continuity of stress produces:

$$\begin{aligned}
& \frac{\rho_{\text{eff}}}{X_s^2} \left\{ [X_s^2 - 2n(n+1)] j_n(X_c) + 4X_c j'_n(X_c) \right\} \\
& + t_n^{\text{cc}} \frac{\rho_{\text{eff}}}{X_s^2} \left\{ [X_s^2 - 2n(n+1)] h_n(X_c) + 4X_c h'_n(X_c) \right\} \\
& - 2t_n^{\text{cs}} \frac{\rho_{\text{eff}}}{X_s^2} n(n+1) [X_s h'_n(X_s) - h_n(X_s)] \\
& = C_n^{\text{cc}} \frac{\rho}{X_s^2} \left\{ [X_s^2 - 2n(n+1)] j_n(x_c) + 4x_c j'_n(x_c) \right\} \\
& + C_n^{\text{cc}r} T_n^{\text{cc}} \frac{\rho}{X_s^2} \left\{ [X_s^2 - 2n(n+1)] h_n(x_c) + 4x_c h'_n(x_c) \right\} \\
& + 2C_n^{\text{cc}r} T_n^{\text{cs}} \frac{\rho}{X_s^2} n(n+1) [h_n(x_s) - x_s h'_n(x_s)] \\
& + 2C_n^{\text{cs}} \frac{\rho}{X_s^2} n(n+1) [j_n(x_s) - x_s j'_n(x_s)] \\
& + 2C_n^{\text{cs}} T_n^{\text{ss}} \frac{\rho}{X_s^2} n(n+1) [h_n(x_s) - x_s h'_n(x_s)] \\
& + C_n^{\text{cs}} T_n^{\text{sc}} \frac{\rho}{X_s^2} \left\{ [X_s^2 - 2n(n+1)] h_n(x_c) + 4x_c h'_n(x_c) \right\}
\end{aligned} \tag{3.5}$$

and

$$\begin{aligned}
& 2 \frac{\rho_{\text{eff}}}{X_s^2} [j_n(X_c) - X_c j'_n(X_c)] + 2t_n^{\text{cc}} \frac{\rho_{\text{eff}}}{X_s^2} [h_n(X_c) - X_c h'_n(X_c)] \\
& + t_n^{\text{cs}} \frac{\rho_{\text{eff}}}{X_s^2} \left\{ 2X_s h'_n(X_s) + [X_s^2 - 2n(n+1) + 2] h_n(X_s) \right\} \\
& = 2C_n^{\text{cc}} \frac{\rho}{X_s^2} [j_n(x_c) - x_c j'_n(x_c)] + 2C_n^{\text{cc}r} T_n^{\text{cc}} \frac{\rho}{X_s^2} \left\{ h_n(x_c) - x_c h'_n(x_c) \right\} \\
& + C_n^{\text{cc}r} T_n^{\text{cs}} \frac{\rho}{X_s^2} \left\{ 2x_s h'_n(x_s) + [x_s^2 - 2n(n+1) + 2] h_n(x_s) \right\} \\
& + C_n^{\text{cs}} \frac{\rho}{X_s^2} \left\{ 2x_s j'_n(x_s) + [x_s^2 - 2n(n+1) + 2] j_n(x_s) \right\} \\
& + C_n^{\text{cs}} T_n^{\text{ss}} \frac{\rho}{X_s^2} \left\{ 2x_s h'_n(x_s) + [x_s^2 - 2n(n+1) + 2] h_n(x_s) \right\} \\
& + 2C_n^{\text{cs}} T_n^{\text{sc}} \frac{\rho}{X_s^2} [h_n(x_c) - x_c h'_n(x_c)]
\end{aligned} \tag{3.6}$$

3.2.3 Effective Bulk Modulus

In order to derive an expression for the effective bulk modulus, the monopole mode (Rayleigh partial wave with $n=0$) with an incident compressional wave is considered. Owing to the spherical symmetry of this mode, the expansions and contractions of the particle and shell act as a source of spherical compressional waves and the motion relates closely to the difference in bulk modulus (inverse of compressibility) of the media. No shear waves exist in the monopole mode (all shear wave amplitudes are therefore zero), and the tangential displacement and stress boundary equations are identically satisfied and therefore not applied. The viscous nature of the fluid host is retained in the radial stress component and within the compressional wavenumber. The system reduces to the two following boundary equations:

$$Y_c j'_0(Y_c) + t_0 Y_c h'_0(Y_c) = C_0^{cc} y_c j'_0(y_c) + T_0^{cc} C_0^{cc} y_c h'_0(y_c) \quad (3.7)$$

$$\begin{aligned} & (\lambda_{\text{eff}} + 2\mu_{\text{eff}}) Y_c^2 j_0(Y_c) + 4\mu_{\text{eff}} Y_c j'_0(Y_c) \\ & - t_0^{cc} \left[-(\lambda_{\text{eff}} + 2\mu_{\text{eff}}) Y_c^2 h_0(Y_c) - 4\mu_{\text{eff}} Y_c h'_0(Y_c) \right] \\ & = C_0^{cc} \left[(\lambda + 2\mu) y_c^2 j_0(y_c) + 4\mu y_c j'_0(y_c) \right] \\ & + T_0^{cc} C_0^{cc} \left[(\lambda + 2\mu) y_c^2 h_0(y_c) + 4\mu y_c h'_0(y_c) \right] \end{aligned} \quad (3.8)$$

The equations are written in terms of the Lamé parameters λ , μ , in order to relate to the bulk modulus $B = \lambda + (2/3)\mu$. The parameters can take complex values in order to represent a lossy material, in particular $\mu = -i\omega\eta_s$ for a viscous liquid. The imaginary part of the bulk modulus similarly relates to the bulk viscosity $\Im m(B) = -\omega\eta_B$ and its real part is the inverse of the compressibility. Primed properties are used for the particle and unprimed for the host medium in the following as well as in the appendices.

The use of the *self-consistency* condition $t_0^{cc} = 0$ gives:

$$Y_c j'_0(Y_c) = C_0^{cc} y_c j'_0(y_c) + C_0^{cc} T_0^{cc} y_c h'_0(y_c) \quad (3.9)$$

$$\begin{aligned}
& (\lambda_{\text{eff}} + 2\mu_{\text{eff}}) Y_c^2 j_0(Y_c) + 4\mu_{\text{eff}} Y_c j_0'(Y_c) \\
& = C_0^{\text{cc}} \left[(\lambda + 2\mu) y_c^2 j_0(y_c) + 4\mu y_c j_0'(y_c) \right] \\
& + C_0^{\text{cc}} T_0^{\text{cc}} \left[(\lambda + 2\mu) y_c^2 h_0(y_c) + 4\mu y_c h_0'(y_c) \right]
\end{aligned} \tag{3.10}$$

By taking only the dominant term of the spherical Bessel function for the incident wave, given the smallness of its argument, since the compressional wavelength in the effective medium is assumed to be much larger than the shell radius, we have:

$$B_{\text{eff}} = \frac{(\lambda + 2\mu) y_c^2 j_0(y_c) + 4\mu y_c j_0'(y_c) + T_0^{\text{cc}} \left[(\lambda + 2\mu) y_c^2 h_0(y_c) + 4\mu y_c h_0'(y_c) \right]}{-3 \left[y_c j_0'(y_c) + T_0^{\text{cc}} y_c h_0'(y_c) \right]} \tag{3.11}$$

where $B_{\text{eff}} = \lambda_{\text{eff}} + \frac{2}{3}\mu_{\text{eff}}$ is the effective bulk modulus.

Expanding the Bessel and Hankel functions for small arguments in both dimensionless compressional wavenumbers leads to:

$$B_{\text{eff}} = \frac{B y_c^3 + 4i\mu T_0^{\text{cc}}}{y_c^3 - 3iT_0^{\text{cc}}} \tag{3.12}$$

$$\frac{B_{\text{eff}} - B}{3B_{\text{eff}} + 4\mu} = \frac{iT_0^{\text{cc}}}{y_c^3} \tag{3.13}$$

To get an expression in the low frequency limit, we use the following low frequency expression of the scattering coefficient T_0^{cc} (derived in the previous chapter):

$$T_0^{\text{cc}} = ic \frac{(B - B')}{4\mu + 3B'} y_c^3 \tag{3.14}$$

which results in:

$$B_{\text{eff}} = \frac{4B\mu(1 - c) + B'(3B + 4\mu c)}{3B'(1 - c) + 4\mu + 3cB} \tag{3.15}$$

which can be rearranged as:

$$\frac{B - B_{\text{eff}}}{3B_{\text{eff}} + 4\mu} = c \frac{B - B'}{4\mu + 3B'} \quad (3.16)$$

Equation (3.16) is the same as that obtained by Kuster and Toksöz for solid-in-solid systems [6]. For an elastic solid host medium, Eqn. (3.15) shows that the effective bulk modulus B_{eff} does not vary with frequency. Similarly, considering an inviscid liquid as the host medium, $\mu \rightarrow 0$, $B \rightarrow \lambda$, and the effective bulk modulus is again independent of frequency and reduces to the harmonic mean of the component phases weighted by concentration, as found by Mei and Aristegui for cylindrical [1] and spherical [7] scatterers, respectively:

$$\frac{1}{B_{\text{eff}}} = \frac{(1 - c)}{B} + \frac{c}{B'} \quad (3.17)$$

This bulk modulus expression appears in the Wood's formula for sound velocity [8].

For a viscous liquid host medium with elastic solid particles, taking the complex shear modulus $\mu = -i\omega\eta_s$ results in a scattering coefficient such that T_0^{cc}/y_c^3 is again weak frequency-dependent (consistent with that presented by Allegra and Hawley [9]) and hence Eqn. (3.12) shows that the ratio of the effective bulk modulus to that of the host is quasi-static.

To conclude, while there is no difference between the dynamic and static effective bulk moduli in case of an inviscid host medium, a weak frequency-dependence of the ratio of the effective bulk modulus to that of the host is introduced in case of a viscous liquid host.

3.2.4 Effective Dynamic Mass Density

The effective dynamic mass density has been investigated extensively over a number of years, with many researchers finding its value to differ appreciably from the volume average mass density [1], [6], [7], [10]–[15] even in the zero frequency limit, unless studying solid-in-solid composites. The difference in inertia between the particles and the background medium causes the particles to move relative to the host matrix; due to this periodic oscillation, the particles mostly radiate in the forward and backward directions, known as dipole radiation. The difference in the relative motion caused by the restoring force in the elastic or viscous fluid host medium implies that the effective dynamic mass density is in general a complex quantity.

The effective dynamic mass density can be determined from the dipole mode $n=1$ by considering a compressional wave mode incident on the single core-shell system embedded within the effective medium. Both compressional and shear wave modes exist in all regions for the dipole partial wave order, except the scattered ones in the effective outer medium, where their amplitudes are set to zero. Four boundary conditions are applied at the shell surface; in this case, these are expressed in terms of wavenumbers and densities, rather than the Lamé parameters as were used for the monopole mode. Again, simplification is achieved by applying the long compressional wavelength condition. Frequency dependence appears through the variation of the shear wavelength relative to the particle size through the parameter y_s which is not restricted to small values. Four sets of results are derived here:

- (i) by rearrangement of the boundary equations and applying an assumption on the amplitudes of the waves in the shell (an assumption validated in the next section) to derive a frequency-dependent effective density;
- (ii) by analytical solution of the boundary equations using series expansions for all functions of compressional wave modes and retaining the leading order term for the scattering coefficients. This proves the assumption made in (i) and results in an effective density expression which is the leading order in $|x_s|$;

(iii) by expanding the expression for the effective density obtained in (ii) using series expansions in the shear wavenumbers in the liquid host, to obtain the low frequency expression of the effective density when $|y_s|$ is small;

(iv) by using the large argument asymptotic expansion of the Bessel and Hankel functions related to shear waves in the viscous liquid host in order to recover Ament's formula for the effective mass density in the case of an inviscid fluid, corresponding to infinitely large $|y_s|$.

Each of these is presented in the following sections with fuller details.

3.2.4.1 General expression for the effective density

For the monopole scattering, setting t_1^{cc} and t_1^{cs} equal to zero, as required by CPA, in Eqns. (3.3) to (3.6), yield the following set of equations:

$$X_c j_1'(X_c) = C_1^{cc} \left[x_c j_1'(x_c) + T_1^{cc} x_c h_1'(x_c) + 2T_1^{cs} h_1(x_s) \right] + C_1^{cs} \left[2j_1(x_s) + T_1^{sc} x_c h_1'(x_c) + 2T_1^{ss} h_1(x_s) \right] \quad (3.18)$$

$$j_1(X_c) = C_1^{cc} \left\{ j_1(x_c) + T_1^{cc} h_1(x_c) + T_1^{cs} \left[x_s h_1'(y_s) + h_1(x_s) \right] \right\} + C_1^{cs} \left\{ \left[x_s j_1'(x_s) + j_1(x_s) \right] + T_1^{sc} h_1(x_c) + T_1^{ss} \left[x_s h_1'(x_s) + h_1(x_s) \right] \right\} \quad (3.19)$$

$$\begin{aligned} \frac{\rho_{\text{eff}}}{X_s^2} \left\{ \left[X_s^2 - 4 \right] j_1(X_c) + 4 X_c j_1'(X_c) \right\} &= C_1^{cc} \frac{\rho}{X_s^2} \left\{ \left[x_s^2 - 4 \right] j_1(x_c) + 4 x_c j_1'(x_c) \right\} \\ &+ C_1^{cc} T_1^{cc} \frac{\rho}{X_s^2} \left\{ \left[x_s^2 - 4 \right] h_1(x_c) + 4 x_c h_1'(x_c) \right\} + 4 C_1^{cc} T_1^{cs} \frac{\rho}{X_s^2} \left[h_1(x_s) - x_s h_1'(x_s) \right] \\ &+ 4 C_1^{cs} \frac{\rho}{X_s^2} \left[j_1(x_s) - x_s j_1'(x_s) \right] + C_1^{cs} T_1^{sc} \frac{\rho}{X_s^2} \left\{ \left[x_s^2 - 4 \right] h_1(x_c) + 4 x_c h_1'(x_c) \right\} \\ &+ 4 C_1^{cs} T_1^{ss} \frac{\rho}{X_s^2} \left[h_1(x_s) - x_s h_1'(x_s) \right] \end{aligned} \quad (3.20)$$

$$\begin{aligned}
2 \frac{\rho_{\text{eff}}}{X_s^2} [j_1(X_c) - X_c j_1'(X_c)] &= 2C_1^{\text{cc}} \frac{\rho}{X_s^2} [j_1(x_c) - x_c j_1'(x_c)] \\
+ 2C_1^{\text{cc}} T_1^{\text{cc}} \frac{\rho}{X_s^2} \{h_1(x_c) - x_c h_1'(x_c)\} &+ C_1^{\text{cc}} T_1^{\text{cs}} \frac{\rho}{X_s^2} \{2x_s h_1' + [x_s^2 - 2]h_1(x_s)\} \\
+ C_1^{\text{cs}} \frac{\rho}{X_s^2} \{2x_s j_1' + [x_s^2 - 2]j_1(x_s)\} &+ 2C_1^{\text{cs}} T_1^{\text{sc}} \frac{\rho}{X_s^2} [h_1(x_c) - x_c h_1'(x_c)] \\
+ C_1^{\text{cs}} T_1^{\text{ss}} \frac{\rho}{X_s^2} [2x_s h_1'(x_s) + [x_s^2 - 2]h_1(x_s)] &
\end{aligned} \tag{3.21}$$

Multiplying Eqn. (3.21) by 2 and adding it to Eqn. (3.20) gives:

$$\begin{aligned}
\frac{\rho_{\text{eff}}}{\rho} j_1(X_c) &= C_1^{\text{cc}} [j_1(x_c) + T_1^{\text{cc}} h_1(x_c) + 2T_1^{\text{cs}} h_1(x_s)] \\
&+ C_1^{\text{cs}} [2j_1(x_s) + 2T_1^{\text{ss}} h_1(x_s) + T_1^{\text{sc}} h_1(x_c)]
\end{aligned} \tag{3.22}$$

The effective density expression can be obtained by dividing Eqn. (3.22) either by the radial [Eqn. (3.18)] or the polar displacement equation [Eqn. (3.19)]. Here we divide Eqn. (3.22) by Eqn. (3.18) and obtain:

$$\frac{\rho_{\text{eff}}}{\rho} = \frac{D [j_1(x_c) + T_1^{\text{cc}} h_1(x_c) + 2T_1^{\text{cs}} h_1(x_s)] + [2j_1(x_s) + T_1^{\text{sc}} h_1(x_c) + 2T_1^{\text{ss}} h_1(x_s)]}{D [x_c j_1'(x_c) + T_1^{\text{cc}} x_c h_1'(x_c) + 2T_1^{\text{cs}} h_1(x_s)] + [2j_1(x_s) + T_1^{\text{sc}} y_1 h_1'(x_c) + 2T_1^{\text{ss}} h_1(x_s)]} \tag{3.23}$$

The ratio of amplitudes:

$$D = \frac{C_1^{\text{cc}}}{C_1^{\text{cs}}} \tag{3.24}$$

can be expressed, under assumptions based on the large compressional wavelength conditions as validated in the next section, as:

$$D = \frac{[x_s j_1'(x_s) - j_1(x_s)] - T_1^{\text{sc}} [x_c h_1'(x_c) - h_1(x_c)] + T_1^{\text{ss}} [x_s h_1'(x_s) - h_1(x_s)]}{[x_c j_1'(x_c) - j_1(x_c)] + T_1^{\text{cc}} [x_c h_1'(x_c) - h_1(x_c)] - T_1^{\text{cs}} [x_s h_1'(x_s) - h_1(x_s)]} \tag{3.25}$$

The ratio of the scattering coefficients, D , as given in Eqn. (3.25), is obtained from the subtraction of Eqn. (3.19) from Eqn. (3.18) and the neglect of terms of the order X_c^3 on the left hand side, under the condition that C_1^{cc} is of order less than or equal to 1 (i.e. $O(x_c)^1$) and C_1^{cs} is of order less than or equal to 2 (i.e. $O(x_c)^2$). In order to validate those assumptions, Maple (Maplesoft) software has been used to carry out analytical expansions under the large compressional wavelength assumptions, $|x_c| \ll 1$, $|X_c| \ll 1$. First, Eqns. (3.18)-(3.19) have been solved to obtain C_1^{cc} and C_1^{cs} . Using then the expansions of the Bessel and Hankel functions associated with compressional waves in series of powers of their argument, and taking into account the dependency of the scattering coefficients (derived in the previous chapter) on x_c , their respective leading order terms are found to be respectively $O(x_c)^0$ and $O(x_c)^1$.

3.2.4.2 Leading order in compressional wavenumber

x_c being small compared to x_s , we make the following approximations for the Bessel and Hankel functions with argument x_c :

$$j_1(x_c) \simeq \frac{x_c}{3}, \quad h_1(x_c) \simeq -\frac{i}{x_c^2}, \quad h_1'(x_c) \simeq \frac{2i}{x_c^3}, \quad \text{so } x_c h_1'(x_c) - h_1(x_c) \simeq \frac{3i}{x_c^2}.$$

With the aid of these expressions, Eqns. (3.23) and (3.25) simplify to:

$$\frac{\rho_{\text{eff}}}{\rho} = \frac{D \left[\frac{x_c}{3} - T_1^{cc} \frac{i}{x_c^2} + 2T_1^{cs} h_1(x_s) \right] + \left[2j_1(x_s) - T_1^{sc} \frac{i}{x_c^2} + 2T_1^{ss} h_1(x_s) \right]}{D \left[\frac{x_c}{3} + T_1^{cc} \frac{2i}{x_c^2} + 2T_1^{cs} h_1(x_s) \right] + \left[2j_1(x_s) + 2T_1^{ss} h_1(x_s) + T_1^{sc} \frac{2i}{x_c^2} \right]} \quad (3.26)$$

and
$$D = \frac{ix_c^2 \left[x_s j_1'(x_s) - j_1(x_s) \right] + 3T_1^{sc} + ix_c^2 T_1^{ss} \left[x_s h_1'(x_s) - h_1(x_s) \right]}{-3T_1^{cc} - iT_1^{cs} x_c^2 \left[x_s h_1'(x_s) - h_1(x_s) \right]} \quad (3.27)$$

Inserting Eqn. (3.27) into Eqn. (3.26), and after performing some algebra, we obtain:

$$\frac{\rho_{\text{eff}}}{\rho} = \frac{E}{F} \quad (3.28)$$

with

$$\begin{aligned} E = & 3 \left(T_1^{\text{cs}} T_1^{\text{sc}} - T_1^{\text{cc}} T_1^{\text{ss}} \right) \left[x_s h_1'(x_s) - 7h_1(x_s) \right] \\ & - 3T_1^{\text{cc}} \left[x_s j_1'(x_s) - 7j_1(x_s) \right] - 3x_c T_1^{\text{sc}} - 6T_1^{\text{cs}} \frac{x_c^2}{x_s} \\ & + ix_c^3 T_1^{\text{ss}} \left[h_1(x_s) - x_s h_1'(x_s) \right] + ix_c^3 \left[j_1(x_s) - x_s j_1'(x_s) \right] \end{aligned} \quad (3.29)$$

and

$$\begin{aligned} F = & 6 \left(T_1^{\text{cc}} T_1^{\text{ss}} - T_1^{\text{cs}} T_1^{\text{sc}} \right) \left[x_s h_1'(x_s) + 2h_1(x_s) \right] \\ & + 6T_1^{\text{cc}} \left[x_s j_1'(x_s) + 2j_1(x_s) \right] - 3x_c T_1^{\text{sc}} - 6T_1^{\text{cs}} \frac{x_c^2}{x_s} \\ & + ix_c^3 T_1^{\text{ss}} \left[h_1(x_s) - x_s h_1'(x_s) \right] + ix_c^3 \left[j_1(x_s) - x_s j_1'(x_s) \right] \end{aligned} \quad (3.30)$$

Equation (3.28) is exactly the same equation as that derived in the Ref. [16] [Eqn. 8] which was obtained from the division of Eqn. (3.22) by Eqn. (3.19). Equations (3.28)-(3.30) have been obtained with no restriction as to the magnitude of the dimensionless shear wavenumber x_s .

Two solutions have now been presented for the dynamic effective density, accounting for mode conversions between compressional and shear wave modes: the general equation (3.23) and its leading order in x_c , equation (3.28). Both are limited to small compressional wavenumber x_c , but no assumption has yet been made on the magnitude of the dimensionless shear wavenumber x_s , which, in a fluid host medium, can range from small to large values within the long compressional wavelength region. The frequency-dependent behaviour of the effective density will be explored in section 3.3, but consideration is first given explicitly to the low frequency region where the shear wavelength is large compared

with the particle size, as well as the converse case of an inviscid host fluid where the shear wavelength tends to zero.

3.2.4.3 Low frequency expansion in shear wavenumber

Starting from equation (3.28) all Bessel and Hankel functions with argument $x_s = y_s c^{-1/3}$ are expanded as series in the dimensionless shear wavenumber y_s which is now taken to be small. With these low-frequency approximations, one can show that the effective mass density reduces to the following expression:

$$\frac{\rho_{\text{effL}}}{\rho}(y_s) = (1 - c) + c\hat{\rho} + J(c)y_s^2 + K(c)y_s^4 + O(y_s^6) \quad (3.31)$$

where

$$J(c) = -\frac{c}{18} \frac{(\hat{\rho} - 1)^2}{\left(c^{\frac{5}{3}} - 1\right)^2} \left[4c^{\frac{11}{3}} - 9c^{\frac{10}{3}} + 10c^{\frac{8}{3}} - 13c^2 + 13c^{\frac{5}{3}} - 10c + 9c^{\frac{1}{3}} - 4 \right] \quad (3.32)$$

and

$$K(c) = \frac{1}{2268} \frac{(\hat{\rho} - 1)^2}{\left(c^{\frac{5}{3}} - 1\right)^3} \left[\begin{aligned} & -81c^{2/3} + (-112\hat{\rho} + 448)c + (504\hat{\rho} - 909)c^{4/3} \\ & + (-567\hat{\rho} + 567)c^{5/3} + (-560\hat{\rho} + 605)c^2 \\ & + (1260\hat{\rho} - 612)c^{7/3} + (616\hat{\rho} - 1519)c^{8/3} \\ & + (-2562\hat{\rho} + 2922)c^3 + (1071\hat{\rho} - 1071)c^{10/3} \\ & + (1820\hat{\rho} - 1460)c^{11/3} + (-1820\hat{\rho} + 917)c^4 \\ & + (-1071\hat{\rho} + 1719)c^{13/3} + (2562\hat{\rho} - 2517)c^{14/3} \\ & + (-616\hat{\rho} + 616)c^5 + (-1260\hat{\rho} + 855)c^{16/3} \\ & + (560\hat{\rho} - 224)c^{17/3} + (567\hat{\rho} - 648)c^6 \\ & + (-504\hat{\rho} + 504)c^{19/3} + (112\hat{\rho} - 112)c^{20/3} \end{aligned} \right] \quad (3.33)$$

The expansion of the effective mass density in powers of y_s , equation (3.31), has been obtained after using expansions of all the Bessel and Hankel functions related to shear waves, including those in the scattering coefficients, up to relatively large orders, because

a large number of terms cancel each other. Since y_s^2 is purely imaginary for a viscous fluid, it is necessary to retain the first two leading order terms in the effective density in order to obtain both the real and imaginary part of the frequency-dependent effective density.

As expected [10-11], equation (3.31) provides the static limit of the effective density as the volume averaged density,

$$\lim_{\substack{x_c \rightarrow 0 \\ y_s \rightarrow 0}} \frac{\rho_{\text{eff}}}{\rho} = (1 - c) + c \hat{\rho} \quad (3.34)$$

which is indeed the addition law of densities. Since y_s^2 is purely imaginary for a viscous liquid, the leading-order frequency dependence in Eqn. (3.31) provides only the imaginary part of the effective density; the real part varies only as y_s^4 . The concentration dependence, Eqns. (3.32)-(3.33), is complicated, and features terms in one-third powers of the concentration, which is typical for such core-shell self-consistent models. This is in contrast to the multiple scattering models that usually provide effective properties at low concentration and are often expressed as series in integer orders of the latter.

Having determined the effective density in the long-shear-wavelength limit (small y_s), the case of an inviscid host fluid, for which y_s tends to infinity, is now examined.

3.2.4.4 The limit of an inviscid liquid host

In order to obtain the limit of effective density for an inviscid medium, $|y_s|$, $|x_s|$ are taken to be large, using the asymptotic expansions of the Bessel and Hankel functions in Eqn. (3.28), along with the scattering coefficients for large $|x_s|$ [Eqns. (2.53), (2.54), (2.65), (2.66) of the previous chapter]. Considering a viscous liquid host, with large $|y_s|$, while still meeting the long compressional wavelength requirement, the dimensionless shear wavenumber in the viscous host fluid, $y_s = (1 + i) \sqrt{\rho\omega / (2\eta_s)} a$, is written in the form:

$$y_s = (1 + i)\beta \quad (3.35)$$

with $\beta \gg 1$. Using the asymptotic expansions of the spherical Bessel and Hankel functions, in Eqns. (2.53), (2.54), (2.65), (2.66) derived in the previous chapter for large β , leads to:

$$T_1^{cc} \sim \frac{i}{3} y_c^3 \frac{\hat{\rho} - 1}{2\hat{\rho} + 1} \quad (3.36)$$

$$T_1^{cs} \sim -ie^{-iy_s} y_c \frac{\hat{\rho} - 1}{2\hat{\rho} + 1} \quad (3.37)$$

$$T_1^{sc} \sim -2i \frac{e^{-iy_s}}{y_s} y_c^2 \frac{\hat{\rho} - 1}{2\hat{\rho} + 1} \quad (3.38)$$

$$T_1^{ss} \sim -ie^{-iy_s} \sin(y_s) \quad (3.39)$$

Equation (3.36) is identical to that obtained for a single sphere in an inviscid host liquid which does not support shear waves.

The numerator of the fraction in Eqn. (3.28) thus behaves as:

$$i \frac{c}{3} y_c^3 e^{-iy_s} \sin(y_s - x_c) \frac{\hat{\rho} - 1}{2\hat{\rho} + 1} \quad (3.40)$$

and the denominator as:

$$y_c^3 e^{-iy_s} \sin(y_s - x_c) \frac{2(c-1)\hat{\rho} - 1 - 2c}{2\hat{\rho} + 1} \quad (3.41)$$

Hence, in the limit of large $|y_s|$ and $|x_s|$, equation (3.28) becomes:

$$\frac{\rho_{\text{eff}}}{\rho} \sim 1 - 9ic \frac{T_1^{cc}}{y_c^3 + 6icT_1^{cc}} \quad (3.42)$$

The effective density is now considered in the limit as $|y_s|$ tends to infinity, *i.e.* the reduction of Eqn. (3.28) to Eqn. (3.42) in the limit of large $|y_s|$ is physically equivalent to a host liquid tending to an inviscid liquid.

Taking the limiting form of the scattering coefficient T_1^{cc} for large $|y_s|$, Eqn. (3.42) reduces to:

$$\frac{\rho_{\text{eff}}}{\rho} = \frac{(\rho + 2\rho') + c(\rho' - \rho)}{(\rho + 2\rho') - 2c(\rho' - \rho)} \quad (3.43)$$

which is identical to Ament's formula (for spherical particles) for an inviscid fluid host [10]. The same results for effective density as Eqns. (3.42)-(3.43) are obtained by applying the self-consistent scheme directly in the case of an inviscid fluid host as shown in the following. Hence our expression for effective density tends to the expected static limit for an inviscid fluid host when $|y_s|$ tends to infinity (still obeying $|y_c| \ll 1$).

For an inviscid liquid host which does not support shear waves (rather than the limit of a viscous liquid host at large $|y_s|$), the boundary equations at $r=b$ are greatly simplified, resulting in:

$$\begin{cases} X_c j'_n(X_c) = x_c C_n^{cc} [j'_n(x_c) + T_n^{cc} h'_n(x_c)] \\ \frac{\rho_{\text{eff}}}{\rho} j_n(X_c) = C_n^{cc} [j_n(x_c) + T_n^{cc} h_n(x_c)] \end{cases} \quad (3.44)$$

This leads to Eqn. (3.17) for the monopole mode $n = 0$ and to equation (3.43), for the dipole mode $n = 1$, which is the limit of large $|x_s|$ in a viscous liquid host.

3.3 RESULTS OF NUMERICAL CALCULATIONS

Numerical calculations were carried out in Matlab for silica particles in water at 25°C. The material properties of silica and water used are shown in Table 3.1. Only the effective density is investigated numerically since the ratio of the effective bulk modulus to that of the host is found to be quasi-static. The two expressions obtained for the effective density, Eqn. (3.28), and the low frequency expansion for small $|y_s|$, Eqn. (3.31), are compared. Both frequency and concentration dependence are investigated.

The effective mass density, derived under the large compressional wavelength assumption, depends on concentration and on the ratios, to the particles size, of both the compressional

and the shear wavelengths in the host. In order to demonstrate the effect of this condition on the range of validity of the model in terms of particle size, frequency and concentration, we write the condition as $|x_c| < |x_c|_{\max}$ with $|x_c|_{\max} = 0.1$. Since the imaginary part of k_c is small, compared to its real part, we thus obtain a validity condition:

$$\text{a.f} < |x_c|_{\max} \frac{v}{2\pi} c^{1/3} \quad (3.45)$$

Table 3.1: Physical properties of silica and water at 25°C (298.15 K). Data for water are from Ref. [17] and for silica from Ref. [18] with a modified silica density, based on experimental measurement [19].

Physical parameters	Water	Silica
Sound velocity (m.s ⁻¹)	1497	5968
Density (kg.m ⁻³)	997	2100
Shear viscosity (Pa.s)	0.000891	0
Shear modulus (GPa)	0	30.9
Attenuation coefficient (Np.m ⁻¹ .MHz ⁻²)	0.023	2.6×10 ⁻¹⁰

The ranges of particle size and frequency over which the model is therefore valid are shown in Fig. 3.2 indicating a useful and workable range of validity, which improves at higher concentration (as the shell becomes smaller with fixed particle size).

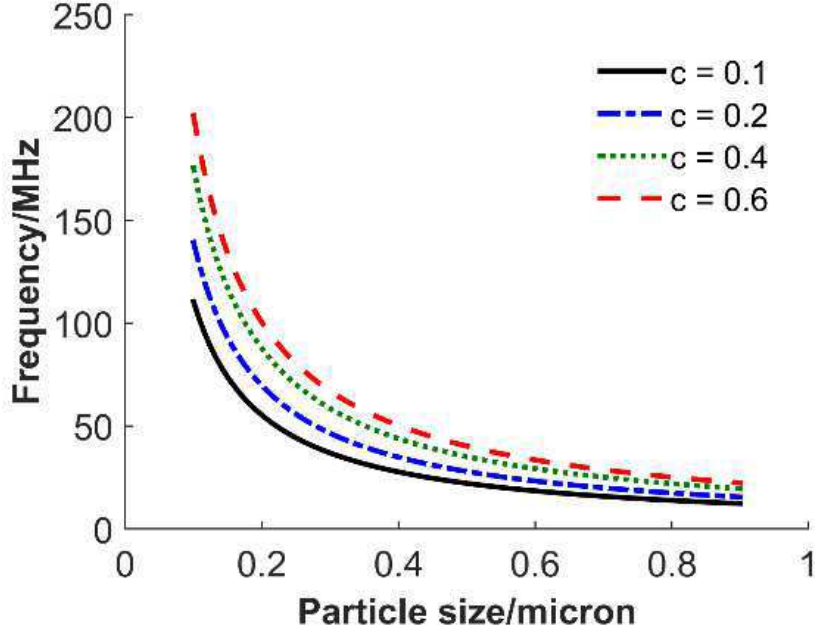


Figure 3.2: Range of validity of the model in terms of particle size and frequency at different concentrations, satisfying the condition $|x_c| \leq 0.1$. The condition is satisfied below the curves.

While the shear wavelength in an elastic particle is the same order of magnitude as the compressional wavelength, this is not the case in a viscous fluid, and we want to investigate a large range of y_s values (as encountered in experimental conditions). However, investigating small shear and large compressional wavelengths is possible only for sufficiently large particles. Applying the validity condition above implies that for a fixed particle size a_0 , the maximum value that $\Re(y_c)$ can attain is approximately given by:

$$\left[\Re(y_s) \right]_{\max}^2 = \frac{1}{2} |x_c|_{\max} \frac{|k_s^2|}{|k_c|} c^{1/3} a_0 \quad (3.46)$$

Conversely, setting both $|x_c|_{\max}$ and the maximum value of $\Re(y_s)$ one is interested with, Eqn. (3.46) provides the minimum value a_0 that the particle radius can take.

3.3.1 Dependence on Frequency at Different Particle Sizes

First the frequency dependence of the effective density at fixed concentration is investigated. Setting $[\Re(y_s)]_{\max}$ to 100, $|x_c|_{\max}$ to 0.1 and concentration c to 0.4, Eqn. (3.46) provides a minimum value for the particle radius a approximately equal to 160 μm . Figure 3.3 shows the effective mass density variation with the real part of y_s , up to 100, for smaller values of radius, ranging from 50 nm to 100 μm along with the maximum values that $\Re(y_s)$ can reach in each case, according to Eqn. (3.46). While the curves of the effective mass density depend only on the dimensionless wavenumbers and, thus, not on the particular elastic and viscous fluid media we are dealing with, the maximum values of $\Re(y_s)$ that can be reached for different values of a_0 depend on those, through the $|k_s^2|/|k_c|$ ratio in Eqn. (3.46).

Eqns. (3.23) and (3.28) agree over the full range, until the limit of $|y_c| \leq 0.1$ is reached (not shown on the plot). Figure 3.3 shows that the low frequency expansion, Eq. (3.31), provides quite accurate results even up to values of $\Re(y_s)$ slightly larger than unity. The effective density is seen to tend to the volume averaged mass density [Eq. (3.34)] at small $|y_s|$, and to that of Ament's formula for the inviscid fluid host, Eq. (3.43), at large $|y_s|$. While the smaller the particles the smaller the range of y_s where the results are valid, one can see the evolution of the effective density from its static value to the dynamic range with the increase of y_s , even for nanoparticles such that $a \leq 100 \text{ nm}$.

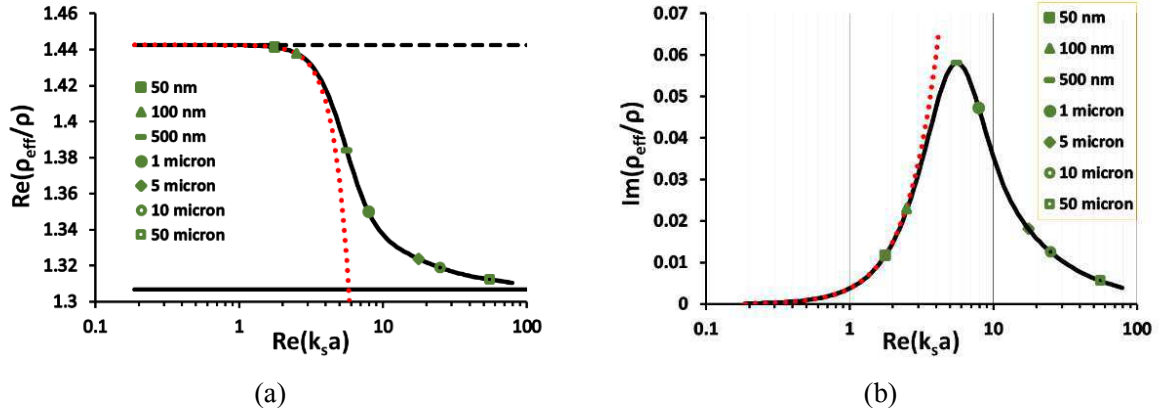


Figure 3.3: The real (a) and imaginary (b) parts of the normalised effective density for silica particles in water at 40%v/v concentration, as a function of the dimensionless shear wavenumber y_s . The solid curve shows the result of Eq. (3.28); the dotted line shows the low frequency expansion in Eq. (3.31). The dashed line shows the static limit [from Eq. (3.34)], the solid (constant) black line Ament's static limit, Eq. (3.43), for the inviscid fluid. The curves were calculated using a particle radius of 100 μm ; the symbols show the upper limit of y_s for particles of different radii satisfying the condition $|x_c| \leq 0.1$.

The intermediate parts of the curves (Fig. 3.3) show a peak in the imaginary part of the effective density corresponding to an inflection point in the real part, for $\Re(y_s)$ slightly larger than unity. Single particle scattering theory shows that the scattering coefficients involving a shear wave undergo a resonance-like behaviour against frequency at $\Re(y_s) \simeq 1$ [9]. The effect of such a behaviour has been observed on the compressional coherent wave properties predicted both by multiple scattering models that consider only multiple scattering of the acoustic mode, such as Lloyd and Berry's model [20], and by the multi-mode scattering model of Luppé *et al.* [21] (see discussions in Ref. [18]). The same kind of effect is seen here on the effective mass density.

3.3.2 Dependence on Frequency at Different Concentrations

Having investigated the frequency dependence of the effective mass density at fixed concentration, Figure 3.4 now shows how this frequency dependence is influenced by a change in the particle concentration. Two observations can be made as the concentration increases (i) the change of magnitude in the real and imaginary parts of the mass density

occurs at higher values of $\Re(x_s)$ (i.e. higher frequency at fixed particle size), and (ii) the amplitude of the peak in the imaginary part increases, as well as the difference between static and inviscid limits on the real part.

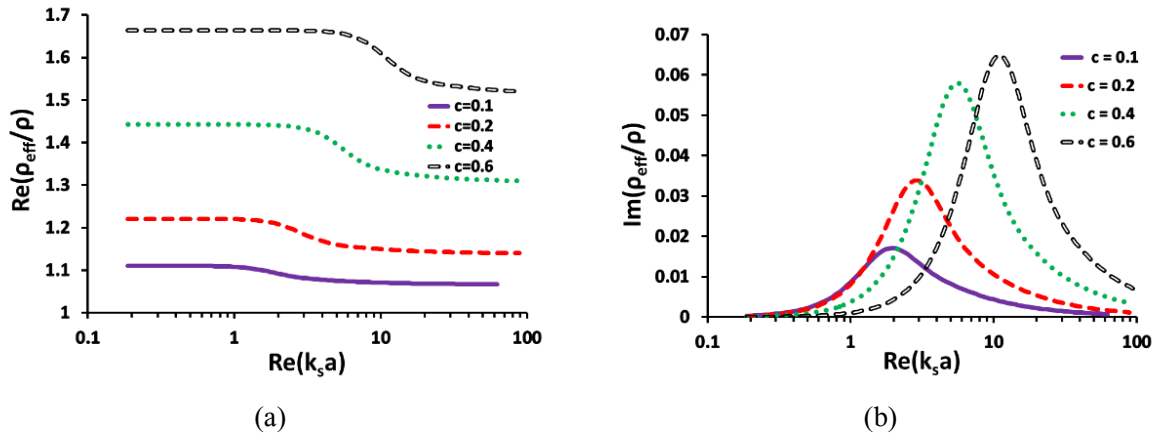


Figure 3.4: The real (a) and imaginary (b) parts of the normalised effective density given by Eq. (3.28) for silica particles in water at different concentrations, as a function of the dimensionless shear wavenumber y_s . The curves were calculated using a particle radius of $100 \mu\text{m}$; smaller particles have a different upper limit of validity in $\Re(y_s)$ in order to satisfy the condition $|x_c| \leq 0.1$, as shown in Fig. (2).

Recent numerical investigation [22] and experimental validation (on acoustic attenuation) [19], [23] have demonstrated that the resonance peak observed in the attenuation against frequency curve for the coherent compressional wave also shifts to higher $\Re(x_s)$ as the concentration increases. This is consistent with the findings here on the effect of concentration on the effective density, which influences the effective compressional wavenumber. Physically, the effect relates to the effective stiffening of the medium due to the increase in viscous drag caused by the presence of a higher density of particles in the medium. This increased drag has been observed in a concentrated particle suspension and the corresponding viscosity increase, modelled by many workers including Happel and others (see review in Ref.[18]). The shift to higher $\Re(y_s)$ of the resonance peak of both the properties of the coherent compressional wave and the effective density as the concentration increases indicates that the resonance frequency is driven by the wavelength to particle size ratio of the shear wave in the effective medium rather than that in the host medium.

3.3.3 Dependence on Concentration at Fixed y_s

In order to explore the concentration dependence further, different regions around the resonance condition are investigated, selecting fixed values of $\Re(y_s)$ either side of the resonance peak, near the static limit, near the inviscid limit and near the resonance condition. Since the long compressional wavelength condition must be satisfied with $|x_c| \leq 0.1$, and the shell radius becomes larger as the concentration decreases, the condition becomes more stringent on particle size and frequency at low concentrations. Thus, particle sizes and frequencies have been selected (for a given value of $\Re(y_s)$) such that the $|x_c| \leq 0.1$ condition is satisfied for concentrations greater than $c_{\min} = 0.05$ (5%v/v). The long compressional wavelength condition is satisfied by Eq. (3.45) with $c = c_{\min}$.

A particle radius is selected to satisfy this condition for each value of $\Re(y_s)$; the frequency is then deduced from a and $\Re(y_s)$. Thus the data presented all satisfy the long compressional wavelength condition $|x_c| \leq 0.1$ for concentrations above 5%v/v and some for smaller concentrations. Table 3.2 shows the set of values of particle radius and frequency that were used for the calculations shown in Figure 3.5, along with the corresponding minimum concentration satisfying the $|x_c| \leq 0.1$ condition.

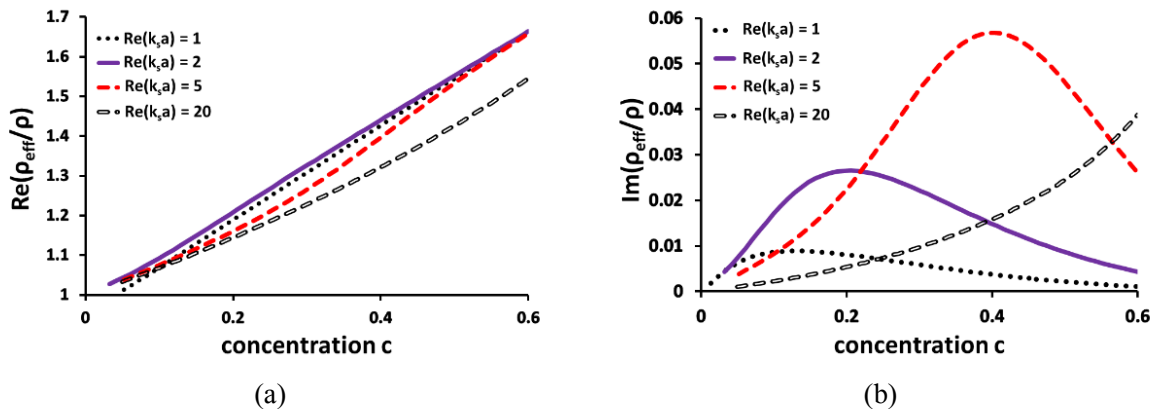


Figure 3.5: The real (a) and imaginary (b) parts of the normalised effective density from Eq. (3.28) for silica particles in water as a function of concentration, at fixed values of the dimensionless shear wavenumber $\Re(k_s a)$.

The real and imaginary parts of the effective density are shown in Figure 3.5 as a function of concentration for several values of the dimensionless shear wavenumber. At small and intermediate values of $\Re(y_s)$, the real part of the effective density is almost linear, and is determined largely by the linear variation of the static limit of Eq. (3.34). The rather weak frequency-dependence is manifested only at larger $\Re(y_s)$, where some curvature is seen and the real part of the effective density is observed to deviate significantly from the static value. The imaginary part of the effective density shows a peak in all but the highest $\Re(y_s)$ curves. As already observed in figure 2b, the magnitude of the peaks increases with concentration. The peaks occur for pairs of $[\Re(y_s), c]$ values roughly the same as in Figure 3.2b. For example, at $\Re(y_s) = 5$, the peak in the imaginary part of the effective density curve with concentration occurs at $c=0.4$ in figure 4b. At this concentration, it occurred in the curve of Figure 3.3b against $\Re(y_s)$ at $\Re(y_s) = 5.6$. At the largest particle size, all physically-realistic concentration conditions occur to the inviscid limit side of the resonance peak in $\Re(y_s)$ and the concentration dependence is therefore monotonically increasing with concentration.

Table 3.2: System parameters for investigation of concentration-dependence of the effective density at fixed $\Re(y_s)$.

$\Re(y_s)$	a (nm)	f (MHz)	c_{\min} (%v/v)
1	50	113.9	1.4
2	150	50.6	3.2
5	800	11.1	5.2
20	13,000	0.67	5.0

3.3.4 Dependence on Frequency with Different Viscosities

In order to show how the effective density may be affected by changes in viscosity of the fluid host medium, we show its dependence as a function of frequency in Fig. 3.6 for a particle size of 3 μm , concentration 25% and with different host fluids (properties shown in Table 3.3). The density contrast between particles and fluid is different in each case, hence the static and inviscid limits are also different. As viscosity of the fluid medium increases, the inflection of the real part of the normalised effective viscosity moves to higher frequency (but corresponds to the same value of $\Re(y_s)$).

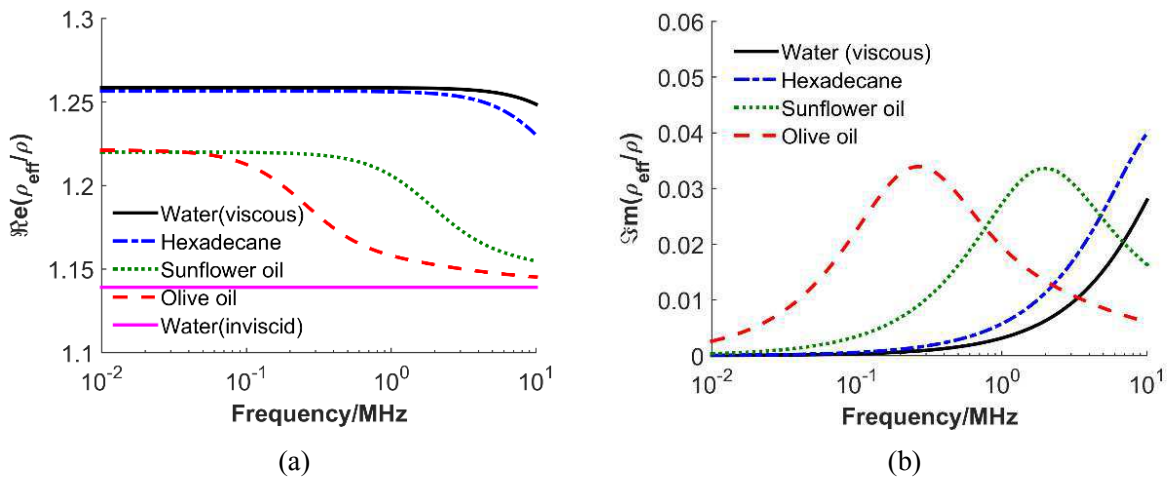


Figure 3.6: The real (a) and imaginary (b) parts of the normalised effective density as a function of frequency from Eq. (3.28) for silica particles in various viscous fluids, for a particle radius of 3 μm and 25% concentration. at fixed values of the dimensionless shear wavenumber $\Re(y_s)$.

Table 3.3: Host fluid properties for investigation of viscosity-dependence of the effective density.

Host fluid	Water ^[18]	Hexadecane ^[18]	Sunflower oil ^[17]	Olive oil ^[24]
Sound velocity (m.s^{-1})	1497	1299	1470	1464
Density (kg.m^{-3})	997	1000	920.6	915.8
Shear viscosity (Pa.s)	0.000891	0.00663	0.054	0.092
Attenuation coefficient ($\text{Np.m}^{-1}.\text{MHz}^{-p}$)	0.023	0.145	1.15	1.625
Attenuation exponent p	2	2	1.77	2

3.4 CONCLUSION

An effective medium core-shell model has been utilised, taking wave mode conversions into account, to study the case of spherical solid particles in a viscous liquid host, deriving the effective bulk modulus and mass density for the system. Approximate explicit formulas for both effective properties have been derived under the condition of large compressional wavelengths in the particles, the host, and the effective medium, with respect to the particle size. No assumption was made on the shear wavelength in the host, allowing the study of the transition of the effective mass density from its volume averaged value at large shear wavelength to Ament's formula for an inviscid fluid at small ones. The effective density is both frequency and concentration dependent within the long compressional wavelength region, given by Eqs. (3.23), (3.28) and (3.31), representing respectively the general dependence, the leading order dependence in compressional wavenumber, and a low frequency expansion in the shear wavenumber.

Numerical calculations for silica in water systems show that the frequency and concentration dependence of the effective density in a viscous liquid host medium is complex and complicated. It exhibits a resonance behaviour that occurs at increasing values of $\Re(y_s)$ as the concentration increases. This is consistent with previous observations of a similar behaviour of the coherent wave effective properties made during the comparison of a multi-mode multiple scattering model with experimental data [19], [23].

The analytical results presented account for viscous effects in modelling the dynamics of nanoparticle systems. We chose to follow the same procedure as the authors of Ref. [1], working directly on the boundary conditions at the shell outer surface with zero amplitude scattered waves. In Ref. [1], the authors were able to derive not only the effective mass density and bulk modulus, but also the shear modulus, which allows the reconstruction of the effective wavenumbers of the coherent waves. In our, apparently more complicated, case, work is still in progress to obtain the wavenumbers, and it may be that a criterion for large shear wavelength may be required in order to do so. We hope that way, not only to recover the same attenuation of the coherent compressional wave as from the MST model [21] for small concentrations, as validated by experiments [19], but also to be able to predict that attenuation for higher concentrations than the MST-based model can account for.

REFERENCES

- [1] J. Mei, Z. Liu, W. Wen, and P. Sheng, “Effective dynamic mass density of composites,” *Phys. Rev. B - Condens. Matter Mater. Phys.*, vol. 76, no. 13, 2007.
- [2] P. Sheng, X. Jing, and M. Zhou, “Beyond the effective medium: quasi modes in disordered media,” *Phys. A Stat. Mech. its Appl.*, vol. 207, no. 1–3, pp. 37–45, 1994.
- [3] Y. Wu, Y. Lai, and Z. Q. Zhang, “Effective medium theory for elastic metamaterials in two dimensions,” *Phys. Rev. B - Condens. Matter Mater. Phys.*, vol. 76, no. 20, 2007.
- [4] X. Jing, P. Sheng, and M. Zhou, “Acoustic and electromagnetic quasimodes in dispersed random media,” *Phys. Rev. A*, vol. 46, no. 10, pp. 6513–6534, 1992.
- [5] J. Kim, J. Ih, and B. Lee, “Dispersion of elastic waves in random particulate composites,” *J. Acoust. Soc. Am.*, vol. 97, no. 3, pp. 1380–1388, 2005.
- [6] G. T. Kuster and M. N. Toksöz, “Velocity and Attenuation of Seismic Waves in Two-Phase Media: Part I. Theoretical Formulations,” *Geophysics*, vol. 39, no. 5, pp. 587–606, 2002.
- [7] C. Aristégui and Y. C. Angel, “Effective mass density and stiffness derived from P-wave multiple scattering,” *Wave Motion*, vol. 44, no. 3, pp. 153–164, 2007.
- [8] A. B. Wood, “A Textbook of Sound,” *Nature*, 1956.
- [9] J. R. Allegra and S. A. Hawley, “Attenuation of Sound in Suspensions and Emulsions: Theory and Experiments,” *J. Acoust. Soc. Am.*, vol. 51, no. 5B, pp. 1545–1564, 2005.
- [10] W. S. Ament, “Sound Propagation in Gross Mixtures,” *J. Acoust. Soc. Am.*, vol. 25, no. 4, pp. 638–641, 2005.
- [11] J. G. Berryman, “Long-wavelength propagation in composite elastic media I. Spherical inclusions,” *J. Acoust. Soc. Am.*, vol. 68, no. 6, pp. 1809–1819, 1980.
- [12] J. G. Berryman, “Long-wavelength propagation in composite elastic media II. Ellipsoidal inclusions,” *J. Acoust. Soc. Am.*, vol. 68, no. 6, pp. 1820–1831, 1980.
- [13] J. Mei, Z. Liu, W. Wen, and P. Sheng, “Effective mass density of fluid-solid composites,” *Phys. Rev. Lett.*, vol. 96, no. 2, pp. 1–4, 2006.
- [14] P. A. Martin, A. Maurel, and W. J. Parnell, “Estimating the dynamic effective mass density of random composites,” *J. Acoust. Soc. Am.*, vol. 128, no. 2, pp. 571–577, 2010.
- [15] C. Jin, “On the estimation of dynamic mass density of random composites,” *J. Acoust. Soc. Am.*, vol. 132, no. 2, pp. 615–620, 2012.
- [16] M. M. Alam, V. J. Pinfield, F. Luppé, and P. Maréchal, “Effective dynamic properties of random complex media with spherical particles,” *J. Acoust. Soc. Am.*, vol. 145, no. 6, pp. 3727–3740, Jun. 2019.
- [17] D. J. McClements and M. J. W. Povey, “Scattering of ultrasound by emulsions,” *J. Phys. D. Appl. Phys.*, vol. 22, no. 1, pp. 38–47, 1989.
- [18] R. E. Challis, M. J. W. Povey, M. L. Mather, and A. K. Holmes, “Ultrasound techniques for characterizing colloidal dispersions,” *Reports Prog. Phys.*, vol. 68, no. 7, pp. 1541–1637, 2005.

- [19] D. M. Forrester, J. Huang, V. J. Pinfield, and F. Luppé, “Experimental verification of nanofluid shear-wave reconversion in ultrasonic fields,” *Nanoscale*, vol. 8, no. 10, pp. 5497–5506, 2016.
- [20] P. Lloyd and M. V. Berry, “Wave propagation through an assembly of spheres: IV. Relations between different multiple scattering theories,” *Proc. Phys. Soc.*, vol. 91, no. 3, pp. 678–688, 1967.
- [21] F. Luppé, J.-M. Conoir, and A. N. Norris, “Effective wave numbers for thermo-viscoelastic media containing random configurations of spherical scatterers,” *J. Acoust. Soc. Am.*, vol. 131, no. 2, pp. 1113–1120, 2012.
- [22] V. J. Pinfield and D. M. Forrester, “Multiple scattering in random dispersions of spherical scatterers: Effects of shear-acoustic interactions,” *J. Acoust. Soc. Am.*, vol. 141, no. 1, pp. 649–660, 2017.
- [23] D. M. Forrester, J. Huang, and V. J. Pinfield, “Characterisation of colloidal dispersions using ultrasound spectroscopy and multiple-scattering theory inclusive of shear-wave effects,” *Chem. Eng. Res. Des.*, vol. 114, pp. 69–78, Oct. 2016.
- [24] J. N. Coupland and D. J. McClements, “Physical properties of liquid edible oils,” *JAACS, J. Am. Oil Chem. Soc.*, vol. 74, no. 12, pp. 1559–1564, 1997.

CHAPTER FOUR

EFFECTIVE DENSITY WITH SPHEROIDS

4.1 INTRODUCTION

In this chapter, we attach importance to the effect of particle shape on the effective dynamic mass density. We obtain analytical expressions for the effective mass density for a random dispersion of spheroidal particles by taking the viscosity of the background fluid into consideration. To this end, we, however, do not need to resort to any scattering theory. Instead, we employ Ament's method and extend it from spherical particles to spheroidal ones. In 1953, Ament, using an elegant approach, derived an expression for the effective dynamic mass density for a system of spherical particles by taking account of the viscosity of the host fluid through drag force [1]. Since particle shape is one of the factors that affects viscous drag [2-4], it stands to reason that particle geometry can have some amount of influence on effective dynamic properties of a suspension of particles in a viscous fluid.

There is not much literature on the effective properties of a random composite for particles with shapes other than spherical particles in three dimensional case. This is the reason why it is important to shed new light on the effect of particle shape on the effective properties of a suspension.

Berryman obtained analytical expressions for the effective elastic parameters for a system of elastic ellipsoidal particles embedded in an elastic solid matrix using a self-consistent effective medium method in the long-wavelength limit; his approach, however, was quasi-static [5]. Although there were some studies on the effective properties of solid-in-solid composites composed of ellipsoidal particles, they were mainly based on static approach [6-7]. To the best of our knowledge, no study on the dynamics of effective parameters for acoustic wave propagation regarding the particle shape except spherical particles has been reported to date.

In the following, we first rederive the Ament's effective density formulas for a monodisperse system consisting of spherical particles in a viscous fluid in order to facilitate the derivation of effective density formulas for spheroidal particles, and also because Ament's paper suffers from some typographical errors.

4.2 SPHERICAL PARTICLES

Ament's method is based on a hypothetical experiment, consisting of two rigid, weightless, infinite parallel planes separated by a distance δ . Let us consider a suspension which contains N number of particles per unit volume, each having volume V and experiencing a drag D . Suppose that the planes oscillate according to $\bar{v}e^{-i\omega t}$, with δ and $\delta\omega/\bar{v}$ so small that average fluid and particle velocities are independent of distance from the walls.

Placing a sample of the suspension in the space between the planes mentioned above, one can obtain a momentum density:

$$\rho_{\text{eff}}\bar{v} = (1 - c)\rho v + \rho'c v_p \quad (4.1)$$

with

$$\bar{v} = (1 - c)v + c v_p \quad (4.2)$$

where \bar{v} is the effective velocity of the suspension, v is the velocity of the host fluid, and v_p is the velocity of the particle.

4.2.1 Drag force

The equilibrium condition between the drag and the buoyant forces can be written as:

$$D(v_p - v) = i\omega V(\rho'v_p - \rho v) \quad (4.3)$$

Defining $\Delta := \rho' - \rho$ and solving equations (4.1) and (4.2) for v and v_p , and inserting them into equation (4.3) eliminates \bar{v} , v and v_p :

$$\frac{D}{V} \frac{\rho_{\text{eff}} - (1-c)\rho - c\rho'}{(1-c)\Delta} = i\omega \frac{(1-c)\rho'(\rho_{\text{eff}} - \rho) - c\rho(\rho' - \rho_{\text{eff}})}{(1-c)\Delta}$$

Noting that the static density is $\rho_s = (1-c)\rho + c\rho'$, we get:

$$\begin{aligned} \frac{D}{V} &= i\omega \frac{\rho_{\text{eff}} [(1-c)\rho' + c\rho] - \rho\rho'}{\rho_{\text{eff}} - \rho_s} \\ \therefore \frac{D}{V} &= i\omega \frac{\rho_{\text{eff}} [(1-c)\rho' + c\rho] - \rho\rho' - \rho(\rho_{\text{eff}} - \rho_s) + \rho(\rho_{\text{eff}} - \rho_s)}{\rho_{\text{eff}} - \rho_s} \\ \therefore \frac{D}{V} - i\omega\rho &= i\omega \frac{\rho_{\text{eff}} [(1-c)\rho' + c\rho] - \rho\rho' - \rho(\rho_{\text{eff}} - \rho_s)}{\rho_{\text{eff}} - \rho_s} \end{aligned} \quad (4.4)$$

Noting that the numerator can be written as:

$$\rho_{\text{eff}} [(1-c)\rho' + c\rho] - \rho\rho' - \rho(\rho_{\text{eff}} - \rho_s) = (1-c)\Delta(\rho_{\text{eff}} - \rho),$$

then equation (4.4) becomes:

$$\rho_{\text{eff}} - \rho_s = \frac{i\omega(1-c)\Delta(\rho_{\text{eff}} - \rho)}{\frac{D}{V} - i\omega\rho} = G(\rho_{\text{eff}} - \rho) \quad (4.5)$$

with

$$G = \frac{i\omega(1-c)\Delta}{\frac{D}{V} - i\omega\rho} \quad (4.6)$$

4.2.2 Effective Mass Density

After some manipulation, the equation (4.5) can be cast into the following form:

$$\rho_{\text{eff}} = \rho_s + \frac{G}{1-G}(\rho_s - \rho) = \rho_s + \frac{G}{1-G}c\Delta \quad (4.7)$$

It is important to note that equations (4.5) and (4.7) are just the rearrangements of equations (5) and (6) of the Ament paper.

The dynamic drag on a rigid spherical particle of radius a in oscillatory motion can be written in the form, in the time harmonic regime [8,9]:

$$D = 6\pi\eta a \left[1 + \beta a - i\beta a \left(1 + \frac{2}{9}\beta a \right) \right] \quad (4.8)$$

where $\beta = \sqrt{\frac{\rho\omega}{2\eta}}$ is the real part of the shear wavenumber k_s .

The first term of the equation is steady Stokes drag which dominates at very low ω , i.e. in the viscous regime, while the last term is the inertial drag which is manifested in the added mass term $i(2/9)(\beta a)^2$; it dominates at very high frequencies, i.e. in the inertial regime.

The inertial drag, being independent of η , does not contribute to any losses, and is therefore a conservative force. At high frequencies, the loss is caused by the Basset force/history terms βa and $-i\beta a$. A particle, submerged in a viscous fluid, experiences the Basset (history) force when it accelerates or decelerates with respect to the fluid. The Basset force can be many times as large as the steady Stokes drag when the particle is accelerated or decelerated at a high rate.

Dividing equation (4.8) by $V = \frac{4}{3}\pi a^3$ and noting that $\frac{6\pi\eta a}{V} = \frac{9}{4}\frac{1}{\beta^2 a^2}\rho\omega$, we get:

$$\frac{D}{V} = \frac{9}{4} \frac{1}{\beta^2 a^2} \rho \omega \left[1 + \beta a - i \beta a \left(1 + \frac{2}{9} \beta a \right) \right]$$

$$\therefore \frac{D}{V} - i \omega \rho = \frac{9}{4} \frac{1}{(\beta a)^2} \rho \omega (1 + \beta a) - i \omega \rho \frac{9}{4} \frac{1}{\beta a} - \frac{3}{2} i \omega \rho \quad (4.9)$$

Therefore, equation (4.6) becomes:

$$G = \frac{-2(1-c)\Delta}{\frac{9}{2} \frac{1}{\beta a} \rho + 3\rho + iZ} \quad (4.10)$$

with

$$Z = \frac{9}{2} \left(\frac{1}{\beta a} + \frac{1}{(\beta a)^2} \right) \rho \quad (4.11)$$

$$1 - G = 1 + \frac{2(1-c)\Delta}{\frac{9}{2} \frac{1}{\beta a} \rho + 3\rho + iZ} = \frac{2(1-c)\Delta + \frac{9}{2} \frac{1}{\beta a} \rho + 3\rho + iZ}{\frac{9}{2} \frac{1}{\beta a} \rho + 3\rho + iZ} \quad (4.12)$$

Using the ratio between equations (4.10) and (4.12), we obtain:

$$\frac{G}{1-G} = \frac{-2(1-c)\Delta}{2(1-c)\Delta + \frac{9}{2} \frac{1}{\beta a} \rho + 3\rho + iZ}$$

$$\therefore \frac{G}{1-G} = \frac{-2(1-c)\Delta}{W + iZ} \quad (4.13)$$

$$\text{with } W = 2(1-c)\Delta + \frac{9}{2} \frac{1}{\beta a} \rho + 3\rho \quad (4.14)$$

Therefore, equation (4.6) becomes:

$$\rho_{\text{eff}} = \rho_s - \frac{2c(1-c)\Delta^2}{W+iZ} = \rho_{\text{effR}} + i\rho_{\text{effI}} \quad (4.15)$$

$$\text{with } \begin{cases} \rho_{\text{effR}} = \rho_s - \frac{2c(1-c)\Delta^2 W}{W^2 + Z^2} \\ \rho_{\text{effI}} = \frac{2c(1-c)\Delta^2 Z}{W^2 + Z^2} \end{cases} \quad (4.16)$$

Equation (4.15) agrees with the Eqn. (27) of the Ref. [11] and Eqns. (4.16) with Eqn. (1.5) of the Ref. [12].

4.2.3 Inviscid Limit

At high frequency: $\beta a \gg 1$

$$Z = \frac{9}{2} \left[\frac{1}{\beta a} + \frac{1}{(\beta a)^2} \right] \rho \xrightarrow{\beta a \gg 1} 0$$

$$\text{and } W \xrightarrow{\beta r \gg 1} 2\Delta(1-c) + 3\rho$$

$$\rho_{\text{eff}} = c\Delta + \rho - \frac{2c(1-c)\Delta^2}{2(1-c)\Delta + 3\rho}$$

$$\therefore \frac{\rho_{\text{eff}}}{\rho} = \frac{(\rho + 2\rho') + c\Delta}{(\rho + 2\rho') - 2c\Delta} \quad (4.17)$$

which is what was referred to as Ament's formula for an inviscid fluid in chapter 3.

4.3 SPHEROIDAL PARTICLES

Equation (4.5) is valid for a system of particles of arbitrary shape, therefore replacing the drag D with that on a spheroid will produce an expression for the effective mass density for a suspension of spheroidal particles. We use the analytical results of Lai and Mockros derived for viscous drag on both a prolate and an oblate spheroid [4].

Let us consider a spheroidal particle of equatorial radius a_{eq} and polar radius a_p , obeying the following equation:

$$\left(\frac{x}{a_{\text{eq}}}\right)^2 + \left(\frac{y}{a_{\text{eq}}}\right)^2 + \left(\frac{z}{a_p}\right)^2 = 1 \quad , \quad (4.18)$$

as illustrated in Fig. 4.1, and define:

$$\varepsilon = \frac{\sqrt{(\max(a_p, a_{\text{eq}}))^2 - (\min(a_p, a_{\text{eq}}))^2}}{a_p} \quad (4.19)$$

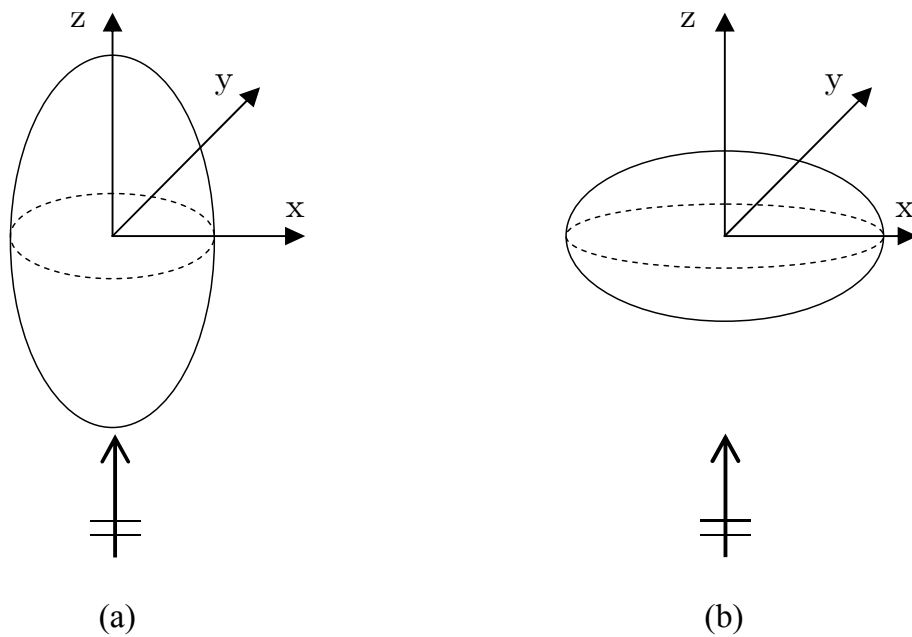


Figure 4.1: (a) Prolate spheroid particle with $a_{\text{eq}} < a_p$. (b) Oblate spheroid particle with $a_{\text{eq}} > a_p$.

If the inclusion is not a sphere, its direction of motion, in that case that of the incident wave, must be specified. In the following, we consider that direction to be along the axis of symmetry of the spheroids.

4.3.1 Prolate Spheroids

A prolate spheroid corresponds to the case where the polar radius is larger than the equatorial one. The drag on a prolate spheroid executing translatory oscillations along its axis of symmetry in an infinite, incompressible, viscous fluid can be written in our notation as [4]:

$$D_p = 8\pi\eta a_p \frac{\varepsilon}{\kappa} + \frac{32\pi\eta a_p^2 \varepsilon^2}{3 \kappa^2} \sqrt{\frac{\rho\omega}{2\eta}} - i\omega \left[\frac{4}{3} \pi a_{eq}^2 a_p \rho \frac{\left(\frac{1}{\varepsilon^2} - 1\right) Q_1\left(\frac{1}{\varepsilon}\right)}{1 - \left(\frac{1}{\varepsilon^2} - 1\right) Q_1\left(\frac{1}{\varepsilon}\right)} + \frac{32\pi\eta a_p^2 \varepsilon^2}{3 \kappa^2} \sqrt{\frac{\rho}{2\omega\eta}} \right] \quad (4.20)$$

with

$$\kappa = \frac{1}{2} \left(\frac{1}{\varepsilon^2} + 1 \right) \log \left(\frac{1 + \varepsilon}{1 - \varepsilon} \right) - \frac{1}{\varepsilon} \quad (4.21)$$

and Q_1 the Legendre function of the second kind,

$$Q_1(x) = \frac{x}{2} \log \left(\frac{x+1}{x-1} \right) - 1, \quad (4.22)$$

The drag expression is obtained from an expansion of spheroidal wave functions in a power series of h and is correct to the first order in h [4], defined from:

$$h^2 = \frac{i \left| a_p^2 - a_{eq}^2 \right| \rho \omega}{\eta} = 2i\beta^2 \left| a_p^2 - a_{eq}^2 \right|,$$

so that we shall restrict h to values obeying Eqn. (4.23):

$$h = |k_s| \sqrt{a_p^2 - a_{eq}^2} \ll 1, \quad (4.23)$$

even though it is said, in Lai and Mockros's work [4], that it may go up to 10.

Equation (4.20), normalized relatively to the spheroid volume V_p produces:

$$\frac{D_p}{V_p} = \rho\omega \left(\frac{3}{\beta^2 a_{eq}^2} \frac{\varepsilon}{\kappa} + \frac{4}{\beta a_{eq}} \frac{a_p}{a_{eq}} \frac{\varepsilon^2}{\kappa^2} \right) - i\rho\omega \left[\frac{\left(\frac{1}{\varepsilon^2} - 1 \right) Q_1 \left(\frac{1}{\varepsilon} \right)}{1 - \left(\frac{1}{\varepsilon^2} - 1 \right) Q_1 \left(\frac{1}{\varepsilon} \right)} + \frac{4}{\beta a_{eq}} \frac{a_p}{a_{eq}} \frac{\varepsilon^2}{\kappa^2} \right] \quad (4.24)$$

$$\therefore \frac{D_p}{V_p} - i\rho\omega = \rho\omega(F_p + R_p) - i\rho\omega(E_p + R_p) \quad (4.25)$$

$$\text{with } F_p = \frac{3}{\beta^2 a_{eq}^2} \frac{\varepsilon}{\kappa}, R_p = \frac{4}{\beta a_{eq}} \frac{a_p}{a_{eq}} \frac{\varepsilon^2}{\kappa^2} \text{ and } E_p = \frac{1}{1 - \left(\frac{1}{\varepsilon^2} - 1 \right) Q_1 \left(\frac{1}{\varepsilon} \right)} \quad (4.26)$$

Inserting equation (4.25) into equation (4.6), where the subscript p added to G , D , V stands for prolate spheroids, yields:

$$G_p = \frac{-\Delta(1-c)}{\rho(E_p + R_p) + i\rho(F_p + R_p)}$$

$$\therefore \frac{G_p}{1-G_p} = \frac{-\Delta(1-c)}{\rho(E_p + R_p) + \Delta(1-c) + i\rho(F_p + R_p)} \quad (4.27)$$

With the aid of equation (4.27), equation (4.7) yields an expression for the dynamic effective mass density:

$$\rho_{\text{eff}p} = \rho_s - \frac{c(1-c)\Delta^2}{W_p + iZ_p} \quad (4.28)$$

with

$$W_p = \rho(E_p + R_p) + \Delta(1 - c) \quad (4.29)$$

and

$$Z_p = \rho(F_p + R_p) \quad (4.30)$$

Separating the real and imaginary parts, we get:

$$\rho_{\text{eff}} = \rho_s - \frac{\Delta^2(1 - c)cW_p}{(W_p^2 + Z_p^2)} + i \frac{\Delta^2(1 - c)cZ_p}{(W_p^2 + Z_p^2)}. \quad (4.31)$$

We now investigate all the important limiting behaviors of the effective density expression.

4.3.1.1 Ament

Since the drag on a prolate spheroid reduces to that on a sphere in the limit $\varepsilon \ll 1$, i.e. when $a_p \rightarrow a_{\text{eq}}, a_{\text{eq}} \rightarrow a$, equation (4.28) must tend to the Ament's equation. To show that, it is important that the limit be evaluated carefully using asymptotic series of logarithms.

With the aid of an asymptotic series development around $\varepsilon = 0$:

$$\frac{1}{2} \log \left(\frac{1 + \varepsilon}{1 - \varepsilon} \right) = \sum_{k=0}^{\infty} \frac{\varepsilon^{2k+1}}{(2k + 1)}$$

Thus, equation (4.21) becomes:

$$\kappa = \sum_{k=0}^{\infty} \left(\frac{\varepsilon^{2k+1}}{(2k + 3)} + \frac{\varepsilon^{2k+1}}{(2k + 1)} \right),$$

i.e.

$$\frac{\kappa}{\varepsilon} = \sum_{k=0}^{\infty} \left(\frac{\varepsilon^{2k}}{(2k+3)} + \frac{\varepsilon^{2k}}{(2k+1)} \right) = \sum_{k=0}^{\infty} \frac{\varepsilon^{2k}}{(k+1) - \frac{1}{4(k+1)}},$$

and

$$\lim_{\varepsilon \rightarrow 0} \frac{\varepsilon}{\kappa} = \frac{3}{4}$$

Then, comparing equation (4.30) to equation (4.11), we get:

$$\lim_{\varepsilon \rightarrow 0} Z_p = \frac{9}{4} \rho \left(\frac{1}{\beta^2 a^2} + \frac{1}{\beta a} \right) = \frac{Z}{2}$$

$$Q_1 \left(\frac{1}{\varepsilon} \right) = \frac{1}{2\varepsilon} \log \left(\frac{1+\varepsilon}{1-\varepsilon} \right) - 1 = \sum_{k=1}^{\infty} \frac{\varepsilon^{2k}}{2k+1}$$

$$\therefore 1 - \left(\frac{1}{\varepsilon^2} - 1 \right) Q_1 \left(\frac{1}{\varepsilon} \right) = 1 - \sum_{k=1}^{\infty} \frac{\varepsilon^{2k-2}}{2k+1} + \sum_{k=1}^{\infty} \frac{\varepsilon^{2k}}{2k+1}$$

and

$$\lim_{\varepsilon \rightarrow 0} \left[1 - \left(\frac{1}{\varepsilon^2} - 1 \right) Q_1 \left(\frac{1}{\varepsilon} \right) \right] = \lim_{\varepsilon \rightarrow 0} \left[1 - \sum_{k=1}^{\infty} \frac{\varepsilon^{2k-2}}{2k+1} + \sum_{k=1}^{\infty} \frac{\varepsilon^{2k}}{2k+1} \right] = 1 - \frac{1}{3} = \frac{2}{3}$$

Finally, by comparing equation (4.29) to equation (4.14), we obtain:

$$\lim_{\varepsilon \rightarrow 0} W_p = 3\rho \left(\frac{1}{2} + \frac{3}{\beta a} \right) + \Delta(1-c) = \frac{W}{2}$$

Therefore, equation (4.28) does reduce to the Ament equation (4.15) in the limit of a sphere.

4.3.1.2 Static limit

In the static limit, i.e. when $\omega \rightarrow 0$ and $1/\beta \rightarrow \infty$, this equation tends to $\rho_{\text{eff}} \rightarrow \rho_s$:

$$\lim_{(1/\beta) \rightarrow \infty} W_p = \rho \left[\frac{1}{1 - \left(\frac{1}{\varepsilon^2} - 1 \right) Q_1 \left(\frac{1}{\varepsilon} \right)} + \frac{4}{\beta a_{\text{eq}}} \frac{a_p}{a_{\text{eq}}} \frac{\varepsilon^2}{\kappa^2} \right] + \Delta(1 - c) \rightarrow \infty$$

$$\lim_{(1/\beta) \rightarrow \infty} Z_p^2 / W_p \rightarrow \infty$$

$$\lim_{(1/\beta) \rightarrow \infty} \frac{\Delta^2 c (1 - c)}{W_p + Z_p^2 / W_p} \rightarrow 0$$

and similarly,

$$\lim_{(1/\beta) \rightarrow \infty} \frac{\Delta^2 c (1 - c) Z_p}{W_p^2 + Z_p^2} \rightarrow 0$$

Therefore equation (4.31) tends to:

$$\lim_{\omega \rightarrow \infty} \rho_{\text{eff}} = \lim_{(1/\beta) \rightarrow \infty} \rho_{\text{eff}} = \rho_s \quad (4.32)$$

Equation (4.32) shows that the static limit of the effective mass density is the same for spheres as for oblate and prolate rigid spheroids submitted to a compressional plane wave propagating parallel to their axis of revolution.

4.3.1.3 Inviscid limit

Strictly speaking, the inviscid limit, i.e. when $\beta \rightarrow \infty$, should not be considered here for spheroids other than spheres, due to equation (4.23), but we shall nonetheless study it at constant value of ε , in order to be able to evaluate the influence of the viscosity on the effective mass density. The following equation (4.33) will be, though somehow inaccurately, referred to as the inviscid limit case in the numerical section.

$$\lim_{(1/\beta) \rightarrow 0} W_p = \rho E_p + \Delta(1 - c)$$

and

$$\lim_{(1/\beta) \rightarrow 0} Z_p = 0$$

So that equation (4.28) provides:

$$\begin{aligned} \rho_{\text{effp}} &= \rho_s - \frac{c(1-c)\Delta^2}{\rho E_p + \Delta(1-c)} \\ \therefore \frac{\rho_{\text{effp}}}{\rho} &= \frac{E_p(\rho + c\Delta) + (1-c)\Delta}{E_p\rho + (1-c)\Delta} \end{aligned} \quad (4.33)$$

4.3.2 Oblate Spheroids

An oblate spheroid corresponds to the case where the polar radius is smaller than the equatorial one. The drag on an oblate spheroid executing translatory oscillations along its axis of symmetry in an incompressible viscous fluid in our notations can be written, under the condition that Eqn. (4.23) is fulfilled, as [4]:

$$\begin{aligned} D_o &= 8\pi\eta a_p \frac{\varepsilon'}{\kappa'} + \frac{32\pi\eta a_p^2 \varepsilon'^2}{3 \kappa'^2} \sqrt{\frac{\rho\omega}{2\eta}} \\ &\quad - i\omega \left[\frac{4}{3} \pi a_{\text{eq}}^2 a_p \rho \frac{\left(\frac{1}{\varepsilon'^2} + 1\right) q_1\left(\frac{1}{\varepsilon'}\right)}{1 - \left(\frac{1}{\varepsilon'^2} + 1\right) q_1\left(\frac{1}{\varepsilon'}\right)} + \frac{32\pi\eta a_p^2 \varepsilon'^2}{3 \kappa'^2} \sqrt{\frac{\rho}{2\omega\eta}} \right] \end{aligned} \quad (4.34)$$

with

$$\varepsilon' = \sqrt{\frac{a_p^2 - a_{\text{eq}}^2}{a_p^2}} = i\varepsilon, \quad (4.35)$$

$$q_1(x) = 1 - x \cot^{-1}(x) = -Q_1(ix)$$

so that

$$q_1\left(\frac{1}{\varepsilon'}\right) = -Q_1\left(\frac{1}{\varepsilon}\right) \quad (4.36)$$

and

$$\kappa' = \frac{1}{\varepsilon'} - \left(\frac{1}{\varepsilon'^2} - 1\right) \cot^{-1}\left(\frac{1}{\varepsilon'}\right) \quad (4.37)$$

or, using equation (4.22) and equation (4.21) along with the definition of the ellipsoidal harmonic q_1 in terms of Q_1 :

$$\kappa' = -\frac{i}{\varepsilon} + \frac{1}{2}i\left(\frac{1}{\varepsilon^2} + 1\right) \log\left(\frac{1+\varepsilon}{1-\varepsilon}\right) = i\kappa \quad (4.38)$$

Equation (4.34) thus turns out as:

$$D_o = 8\pi\eta a_p \frac{\varepsilon}{\kappa} + \frac{32\pi\eta a_p^2 \varepsilon^2}{3 \kappa^2} \sqrt{\frac{\rho\omega}{2\eta}} - i\omega \left[\frac{4}{3} \pi a_{eq}^2 a_p \rho \frac{\left(\frac{1}{\varepsilon^2} - 1\right) Q_1\left(\frac{1}{\varepsilon}\right)}{1 - \left(\frac{1}{\varepsilon^2} - 1\right) Q_1\left(\frac{1}{\varepsilon}\right)} + \frac{32\pi\eta a_p^2 \varepsilon^2}{3 \kappa^2} \sqrt{\frac{\rho}{2\omega\eta}} \right] \quad (4.39)$$

which shows that the expression of the drag for oblate spheroids D_o (Eq. (4.39)), in our notations, is the same as for prolate spheroids D_p (Eq. (4.20)). Equations (4.28) to (4.30) for the effective mass density are therefore also valid for both prolate and oblate spheroids as long as equation (4.23) is fulfilled.

4.4 NUMERICAL RESULTS AND DISCUSSION

Numerical calculation has been performed on a monodisperse suspension of silica spheres, of silica prolate spheroids and of silica oblate spheroids in water at 25°C on the same frequency range as in Chapter 3. The physical constants of silica and water are listed in Table 2.1 of Chapter 2.

We first consider spheres and compare Ament's formula with that obtained in Chapter 3 for two different concentrations, $c = 0.1$ in Figs. 4.1 (a) and (b) and $c = 0.4$ in Figs. 4.1 (c) and (d), respectively.

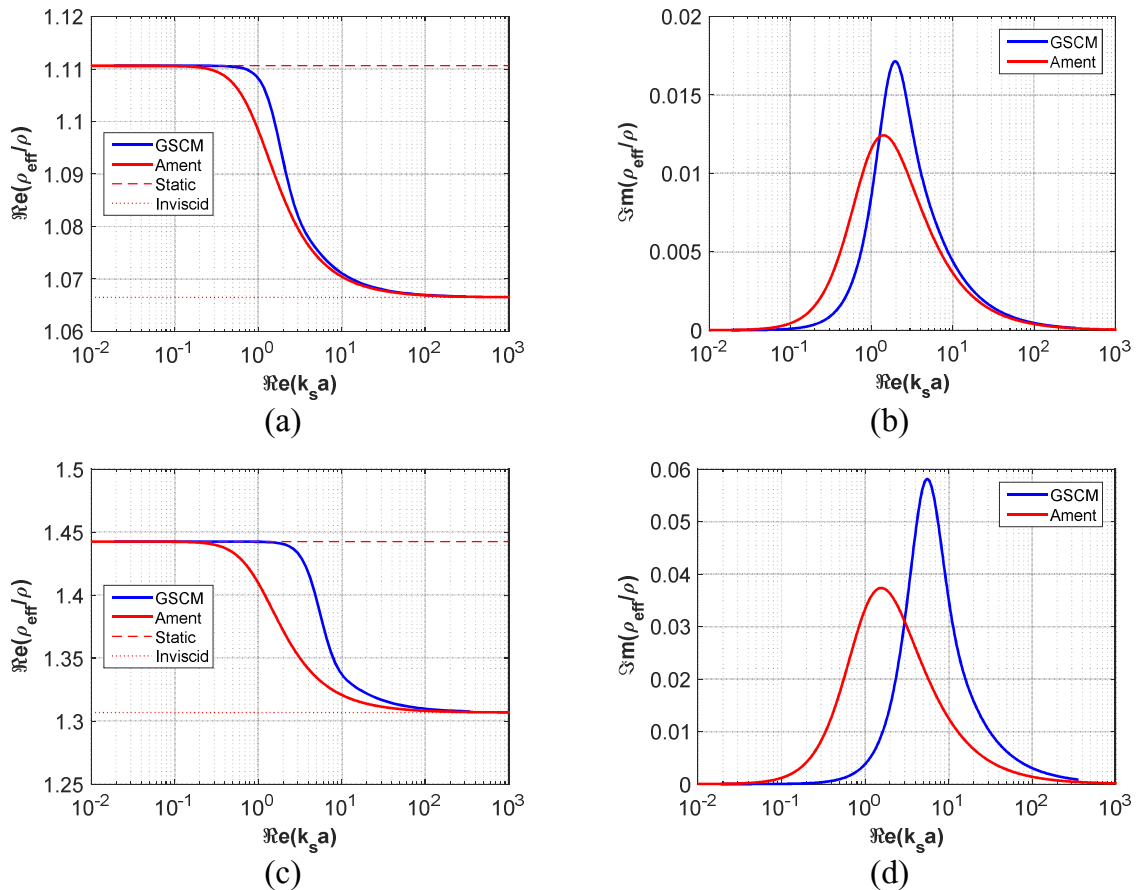


Figure 4.1: Variation of the real (a), (c) and imaginary (b), (d) parts of the normalized effective dynamic mass density as a function of frequency for a suspension of spherical particles at concentration $c = 0.1$ (a), (b) and $c = 0.4$ (c), (d).

The two models do not agree on the frequency range between the static and the inviscid limit, and their difference increases with the concentration. Ament's model considers a constant shear viscosity of the fluid, i.e. not depending on the concentration, in the expression of the drag force. The self-consistent model we used in Chapter 3, on the contrary, takes into account a concentration – dependent effective viscosity, through the use of effective wavenumbers and mass density. We think this is the reason of the observed disagreement.

Now, we compare spheres and spheroids of the same volume, as only then can any deviation in the effective density from the spherical case be attributed to the particle geometry:

$$a^3 = a_{\text{eq}}^2 a_p = 1 \mu\text{m}^3, \quad (4.40)$$

The concentration is kept constant and the ellipticity, defined as:

$$e_{\text{ll}} = \sqrt{1 - \left(\frac{\min(a_p, a_{\text{eq}})}{\max(a_p, a_{\text{eq}})} \right)^2}, \quad (4.41)$$

This ellipticity is set to 0.5 in Figure 4.2 and to 0.9 in Figure 4.3, and the related sphericity is given in the following Table 4.1.

Table 4.1 Geometrical properties of spheroidal particles, keeping the volume constant.

$\left(\frac{x}{a_{\text{eq}}} \right)^2 + \left(\frac{y}{a_{\text{eq}}} \right)^2 + \left(\frac{z}{a_p} \right)^2 = 1$	Sphere	Prolate spheroid		Oblate spheroid	
Sphericity: $s_{\text{ph}} = \frac{a_{\text{eq}}}{a_p}$	1	0.866	0.436	1.155	2.294
Ellipticity: $e_{\text{ll}} = \sqrt{1 - \left(\frac{\min(a_{\text{eq}}, a_p)}{\max(a_{\text{eq}}, a_p)} \right)^2}$	0	0.5	0.9	0.5	0.9

The maximum value of the h parameter as defined in Eqn. (4.23) and corresponding to $(\Re(k_s a))_{\max} = 100$ is less than 2×10^{-4} for $e_{\parallel} = 0.5$ (Figure 4.2) and less than 4×10^{-4} for $e_{\parallel} = 0.9$ (Figure 4.3). The “inviscid” limit for the spheroids corresponds to Eqn. (4.33).

For the small value of ellipticity, $e_{\parallel} = 0.5$, the sphericity (ratio between the equatorial and the polar radius) varies of about 15% around unity. Figure 4.2 illustrates that the difference between spheres and spheroids in this case is quite small on the whole frequency range. In addition, the transition between the static limit and the inviscid one occurs at around the same value for all shapes.

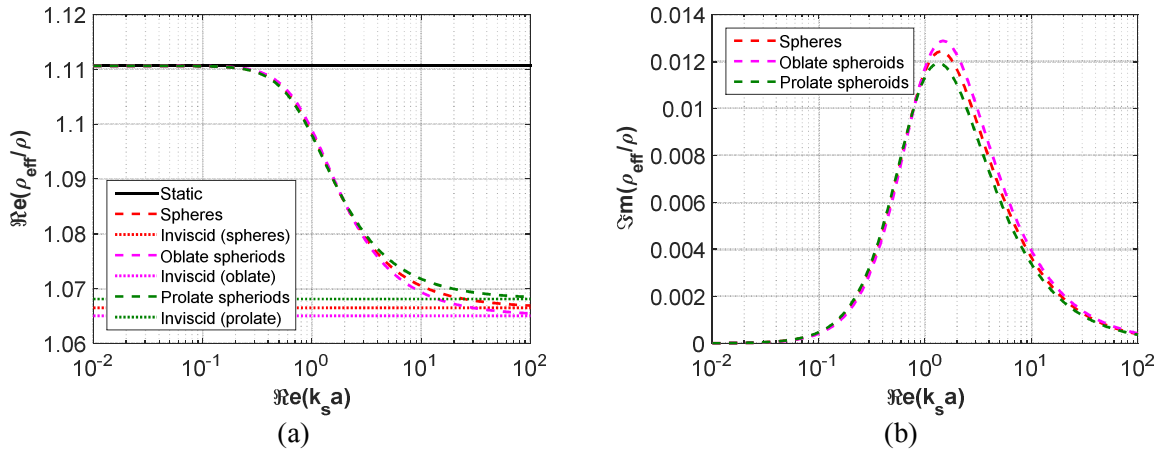


Figure 4.2: Variation of the real (a) and imaginary (b) parts of the effective dynamic mass density as a function of frequency for a suspension of spherical, prolate spheroidal and oblate spheroidal particles of the same volume at concentration $c = 0.1$ and ellipticity $e_{\parallel} = 0.5$.

Figure 4.2 (a) shows that the Stokesian drag, being independent of frequency, is not affected by the particle shape, as could have been expected since the static mass density is the same for all three types of particles of identical volume. As the frequency increases, the Basset force and the inertial drag come into play. At high frequencies, the inertial drag completely dominates over the other drags. Since the added mass/inertial force depends on the particle shape and orientation with respect to the acoustic field, the effective density differs significantly for each type of particle in the inertial regime.

As the ellipticity is increased to $e_{11} = 0.9$, the difference between spheres and spheroids appears more clearly in Figure 4.3.

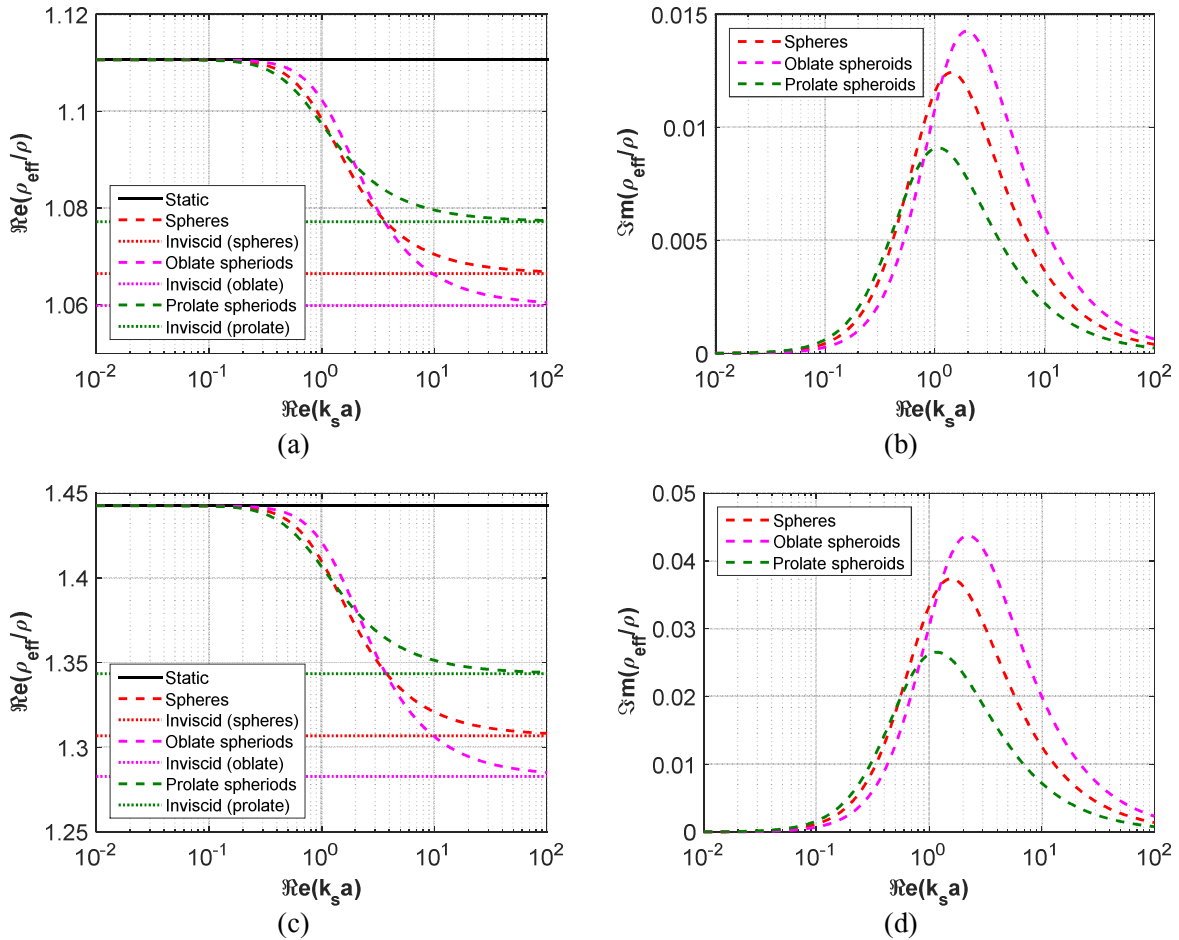


Figure 4.3: Variation of the real (a), (c) and imaginary (b), (d) parts of the effective dynamic mass density as a function of frequency for a suspension of spherical, prolate spheroidal and oblate spheroidal particles of the same volume at concentration $c = 0.1$ (a), (b) and $c = 0.4$ (c), (d), and ellipticity $e_{11} = 0.9$.

The curves corresponding to the spheroids are situated on each side of those corresponding to spheres. At a given frequency, the effective mass density is closer to that in case of an “inviscid” fluid for the prolate spheroids than for the spheres and the oblate spheroids. This corresponds to the fact that the force that opposes the movement of the fluid due to the incident wave is lower for spheroids elongated in the direction of that movement.

4.5 CONCLUSION

In this chapter, we have extended a hydrodynamic model (developed by Ament) from spherical particles to spheroidal ones in order to investigate the effect of particle shape on the effective dynamic density. The extended model has found to agree analytically with all the particular limiting cases. Through the extended model, we have been able to demonstrate that particle shape does affect the effective dynamic mass density, especially in the high frequency region or equivalently for large particle sizes.

REFERENCES

- [1] W. S. Ament, "Sound Propagation in Gross Mixtures," *J. Acoust. Soc. Am.*, vol. 25, no. 4, pp. 638–641, 2005.
- [2] L. E. Payne and W. H. Pell, "The Stokes flow problem for a class of axially symmetric bodies," *J. Fluid Mech.*, vol. 7, no. 4, pp. 529–549, 1960.
- [3] R. P. Kanwal, "Rotatory and longitudinal oscillations of axi-symmetric bodies in a viscous fluid," *Q. J. Mech. Appl. Math.*, vol. 8, no. 2, pp. 146–163, 1955.
- [4] R. Y. S. Lai and L. F. Mockros, "The Stokes-flow drag on prolate and oblate spheroids during axial translatory accelerations," *J. Fluid Mech.*, vol. 52, no. 1, pp. 1–15, Mar. 1972.
- [5] J. G. Berryman, "Long-wavelength propagation in composite elastic media II. Ellipsoidal inclusions," *J. Acoust. Soc. Am.*, vol. 68, no. 6, pp. 1820–1831, 1980.
- [6] S. Nemat-Nasser, M. Lori, and S. K. Datta, "Micromechanics: Overall Properties of Heterogeneous Materials," *J. Appl. Mech.*, vol. 63, no. 2, p. 561, 2008.
- [7] G. W. Milton, *The Theory of Composites*. 2009.
- [8] H. Lamb, *Hydrodynamics*, 6th ed. Cambridge University Press, 1932.
- [9] L. D. (Lev D. Landau and E. M. Lifshitz, *Fluid mechanics*. Elsevier/Butterworth-Heinemann, 2004.
- [10] R. W. Johnson, *Handbook of Fluid Dynamics, Second Edition*. 2016.
- [11] A. S. Ahuja, "Effect of Particle Viscosity on Propagation of Sound in Suspensions and Emulsions," *J. Acoust. Soc. Am.*, vol. 51, no. 1B, pp. 182–191, 2005.
- [12] A. H. Harker and J. A. G. Temple, "Velocity and attenuation of ultrasound in suspensions of particles in fluids," *J. Phys. D. Appl. Phys.*, vol. 21, no. 11, pp. 1576–1588, 1988.

CONCLUSION AND FUTURE PROSPECTS

This thesis has investigated acoustic wave propagation through random dispersions of elastic solid particles in viscous fluids in order to have a better understanding of the viscous mechanism involved in viscous systems that were previously unexplored. Here we summarize our main results, and discuss prospects for future research.

We have derived analytical approximations for scattering coefficients for arbitrary partial wave orders by taking the fluid viscosity into consideration through the wave-mode conversion for both incident compressional and shear waves. Although the solutions are limited to the long compressional wavelength region, no assumption regarding the magnitude of the shear wavelength in the embedding fluid has been made. These solutions for scattering coefficients can be useful in estimating analytical expressions for effective properties of a suspension of solid spherical particles using multi-mode multiple scattering models and effective medium models. Similar to the single-sphere scattering, it might be interesting to derive analytical approximations for scattering coefficients for a single core-shell particle in a viscous fluid, which might be more complicated than the single particle case. Moreover, it may also be interesting to analytically calculate the scattering coefficients of a spheroidal particle in a viscous fluid and then compare the results with those of the single-sphere case to see the effect of particle shape on the wave mode conversion.

In order to investigate the effect of fluid viscosity on the effective properties of a random dispersion of solid spherical particles, we have used a core-shell, self-consistent effective medium model and have derive analytical expressions for the effective bulk modulus and mass density by including the viscosity of the background fluid through the wave mode conversion. The effective bulk modulus is found to be quasi-static, whereas the effective mass density exhibits dynamic behaviours.

The analytical expressions obtained are shown to reduce to prior known results in the limit of both static and inviscid cases. The core-shell effective medium model might be used to calculate the effective compressional and shear wavenumbers. One might also try and use the model to determine the effective viscosity of a suspension.

In most theoretical studies the particles are assumed to be spherical in shape. However, in practice, particles can have different shapes other than sphere, and hence it is of importance to investigate the effect of particle shape on the effective properties of a viscous system. To this end, we have extended a hydrodynamic model (developed by Ament in 1953) from spherical particles to spheroidal ones and have calculated analytical expressions for the effective mass density of a random dispersion of both prolate and oblate spheroidal particles. The analytical expressions have shown to reduce to the particular limiting cases. It has been demonstrated that the particle shape plays a significant role in the dynamic behaviour of the effective mass density, especially when the host fluid tends to be inviscid. The future work might focus on calculating the effective viscosity using the Ament model. This model takes account of the viscosity of the host fluid through the drag on the particles. However, the drag is not related to the particle concentration. It might be interesting to calculate the effective viscosity of a suspension by relating the drag with concentration. In future the author will try and use a hydrodynamic model to calculate the effective compressional wavenumber for both prolate and oblate spheroidal particles in order to investigate the effect of particle shape on the effective velocity and attenuation.

Appendix: Spherical Bessel functions

A1. Definition:

When the Helmholtz equation is solved in spherical coordinates by separation of variables, the radial part, known as the spherical Bessel equation, is of the form:

$$z^2 \frac{d^2 f}{dz^2} + 2z \frac{df}{dz} + [z^2 - n(n+1)]f = 0, \quad n \in \mathbb{Z}, \quad (\text{A1})$$

where z can be arbitrarily complex. Special solutions of this homogeneous differential equation are Bessel, Neumann and Hankel functions $j_n(z)$, $y_n(z)$, $h_n^{(1)}(z)$, $h_n^{(2)}(z)$, respectively. A solution to the equation can be obtained using Forbenius method:

$$j_n(z) = 2^n z^n \sum_{k=0}^{\infty} \frac{(-1)^k (n+k)!}{k!(2n+2k+1)!} z^{2k} = (-z)^n \left(\frac{1}{z} \frac{d}{dz} \right)^n \frac{\sin z}{z} \quad (\text{A2})$$

and $y_n(z) = -(-z)^n \left(\frac{1}{z} \frac{d}{dz} \right)^n \frac{\cos z}{z} \quad (\text{A3})$

$h_n^{(1)}(z)$ and $h_n^{(2)}(z)$ are defined as:

$$h_n^{(1)}(z) = j_n(z) + iy_n(z) \quad (\text{A4})$$

$$h_n^{(2)}(z) = j_n(z) - iy_n(z) \quad (\text{A5})$$

The analytical expressions of the first few Bessel functions are:

$$j_0(z) = \frac{\sin z}{z},$$

$$j_1(z) = \frac{\sin z}{z^2} - \frac{\cos z}{z}, \quad j_1'(z) = \frac{2 \cos z}{z^2} - \frac{2 \sin z}{z^3} + \frac{\sin z}{z}$$

$$j_2(z) = \frac{3 \sin z}{z^3} - \frac{3 \cos z}{z^2} - \frac{\sin z}{z}$$

The general analytical expression for the Hankel function of the first kind of arbitrary order can be written as:

$$h_n(z) = (-i)^{n+1} \sum_{k=0}^n \frac{i^k (n+k)!}{2^k k! (n-k)!} \frac{e^{iz}}{z^{k+1}}. \quad (\text{A6})$$

The first few analytical expressions for the Hankel functions are:

$$h_0(z) = \frac{e^{iz}}{iz}$$

$$h_1(z) = -\frac{e^{iz}}{z} \left(1 + \frac{i}{z}\right), \quad h_1'(z) = \frac{2ie^{iz}}{z^3} + \frac{2e^{iz}}{z^2} - \frac{ie^{iz}}{z}$$

$$h_2(z) = \frac{ie^{iz}}{z} \left(1 + \frac{3i}{z} - \frac{3}{z^2}\right)$$

A2. Recurrence Relations

$$(n+1)f_n(z) + zf_n'(z) = zf_{n-1}(z) \quad (\text{A7})$$

$$nf_n(z) - zf_n'(z) = zf_{n+1}(z) \quad (\text{A8})$$

$$f_{n-1}(z) + f_{n+1}(z) = \frac{2n+1}{z} f_n(z) \quad (\text{A9})$$

$$nf_{n-1}(z) - (n+1)f_{n+1}(z) = (2n+1)f_n'(z) \quad (\text{A10})$$

A3. Wronskian

The Wronskian of two differentiable functions f and g is defined by:

$$W[f, g] \triangleq \begin{vmatrix} f' & g' \\ f & g \end{vmatrix} = f'g - g'f \quad (\text{A11})$$

$$W[j_n(z), h_n(z)] = j_n(z)h_n'(z) - j_n'(z)h_n(z) = \frac{i}{z^2} \quad (\text{A12})$$

A4. Asymptotic Forms

The behaviour of the spherical Bessel functions for small arguments can be deduced from their series expansions, whereas the behaviour for large arguments follow from the asymptotic formulas for $j_n(z)$ and $y_n(z)$. Useful are the specific results:

$$z \rightarrow 0^+ : j_n(z) = \frac{z^n}{(2n+1)!!} \quad (\text{A13})$$

$$j_n'(z) = \frac{nz^{n-1}}{(2n+1)!!} \quad (\text{A14})$$

$$z \rightarrow 0^+ : h_n(z) = -i \frac{(2n-1)!!}{z^{n+1}} \quad (\text{A15})$$

$$h_n'(z) = i \frac{(n+1)(2n-1)!!}{z^{n+2}} \quad (\text{A16})$$

$$z \rightarrow \infty : j_n(z) \sim \frac{1}{z} \sin(z - n\pi/2) \quad (\text{A17})$$

$$z \rightarrow \infty : y_n(z) \sim -\frac{1}{z} \cos(z - n\pi/2) \quad (\text{A18})$$

ABSTRACT

A random dispersion of identical elastic solid particles in a viscous fluid is considered and effective properties, appropriate to the propagation through the medium of an ultrasonic compressional wave of large wavelength compared to the radius of the particles, is investigated. The scattering coefficients of a single spherical particle in a viscous medium are investigated for all combinations of incident and scattered wave types for use in multiple scattering models. Approximate formulae are obtained for the coefficients at n 'th partial wave order in the Rayleigh limit.

For spherical particles, a core-shell self-consistent model is used, in which the medium is modelled by an elastic core of the same material and radius as the particles, surrounded by a shell of the host fluid, and placed in the effective medium. The radius of the shell is such that the ratio of the core/shell volume is equal to the particle concentration. The dynamic properties of the effective medium are sought by minimising the scattering of the shell for different incident compressional partial wave orders (n).

The effective bulk modulus is found from the monopole mode $n=0$ and the effective mass density from the dipole mode $n=1$. When compared to Ament's formula based on local force balance at the particles (assumed rigid), the effective mass density obtained from the core-shell model shows a frequency-dependent effect of concentration similar to that observed in multiple scattering models and experimentally.

Ament's method is then applied to obtain the effective mass density in case of aligned rigid spheroids.

RÉSUMÉ

La propagation d'une onde ultrasonore de compression au travers d'une distribution de particules solides identiques localisées aléatoirement dans un liquide visqueux est étudiée. La longueur d'onde de l'onde de compression est supposée grande devant le rayon des particules, et les propriétés effectives dynamiques du milieu sont recherchées.

Les coefficients de diffusion d'une sphère solide isolée sont étudiés pour différentes polarisations des ondes partielles de mode n incidentes et diffusées. Des expressions approchées en sont données pour tout n dans le régime de diffusion de Rayleigh.

Dans le cas de particules sphériques, le milieu est modélisé par un noyau élastique, de même matériau et rayon que les particules, et entouré d'une coque emplie du fluide hôte. L'ensemble est insoné, dans le milieu effectif, par une onde de compression partielle de mode n . Les propriétés effectives sont recherchées par minimisation de la diffusion pour différentes valeurs de n .

Le module d'élasticité volumique effectif et la masse volumique effective sont obtenus respectivement à partir des modes $n=0$ et $n=1$. Comparée à la formule d'Ament, fondée sur l'équilibre des forces hydrodynamiques et inertielle au niveau de chaque particule supposée rigide, celle obtenue ici fait apparaître un effet de la concentration sur la dépendance fréquentielle de la masse volumique similaire à celui observé, expérimentalement et dans des modèles de diffusion multiple, sur les propriétés effectives des ondes de compression.

La méthode d'Ament est ensuite appliquée pour obtenir la masse volumique effective dans le cas de sphéroïdes rigides alignés.